Integrated 3-D seismic analysis of Atoka Formation sandstone reservoirs, Vacuum Field vicinity, Lea County, New Mexico

by

Soichiro Ota

Submitted in Partial Fulfillment of the Requirements for
the Degree of Master of Science in Geology

New Mexico Institute of Mining and Technology

Socorro, NM

August, 2001

TABLE OF CONTENTS

LIST OF FIGURES

LIST OF TABLES

LIST OF APPENDICES

FIGURES FOR APPENDICES

TABLES FOR APPENDICES

ACKNOWLEDGEMENTS

This project is part of the Permian basin program of oil and gas research currently underway at the New Mexico Bureau of Geology and Mineral Resources, a division of the New Mexico Institute of Mining and Technology. This research was funded in part by a research assistantship under Dr. Brian S. Brister at the New Mexico Bureau of Geology and Mineral Resources, Dr. Peter Scholle, Director. Other funding was provided through a scholarship from the Roswell Geological Society. I would like to thank Marathon Oil Company (Midland, Texas) for providing 3-D seismic and well data. I also would like to thank Roswell Geological Society for providing access to the Petroleum Record Library at Roswell, New Mexico. Stratigraphic and seismic analyses were interpreted on software granted to New Mexico Tech by Landmark Graphics Corporation, Hampson-Russell Software Services Ltd., and GX-Technology Corporation. I would like to thank my committee members Drs. Brian Brister, Peter Mozley, and Harold Tobin. Dr. Bruce Hart is thanked for initial training in seismic analysis. I also would like to thank Dan Leiphart and Robin Pearson for assisting me in understanding the capabilities of the software.

ABSTRACT

Atoka Formation (lower Pennsylvanian) sandstone reservoirs in the Delaware Basin of southeastern New Mexico are generally considered to be very unpredictable targets for natural gas exploration. This study applies an integrated methodology, combining geology, petrophysics and seismic interpretation, to successfully describe and map this problematic formation in the Vacuum Field vicinity, Lea County, New Mexico. The area of interest for this thesis is a four township area (T17-18S, R34-35E). Most Atoka Formation production, cumulatively more than 4 billion cubic feet of natural gas, is from T17S, R35E. This study examined both the larger and the more focused area of interest. The dataset available for this study included cores, petrophysical well logs, and a 109 mi^2 3-D reflection seismic volume. The advantage of studying the well data is to glean key small-scale information that is below seismic resolution, and provide geological constraint to the seismic interpretation through the creation of synthetic seismograms and a geology-based seismic model. Seismic data interpretation yielded information related to geologic structure and tectonic development, stratigraphic subdivisions of the Atoka Formation, and most importantly, the distribution of reservoir-potential sandstone; most of this information could not be derived from the available well data alone.

The Atoka Formation in the area of interest, on the Northwest Shelf of the Delaware Basin, is primarily clastic, sandwiched between overlying Strawn Formation limestone and underlying Morrow Formation limestone. The Atoka Formation can be subdivided into lower Atoka fluvial deposits, and upper Atoka deltaic to marine strata. The upper Atoka Formation is marked by cyclic upward-coarsening, clastic sequences

that represent delta progradation following episodic marine flooding events marked by black, organic shale and limestone. The lower Atoka Formation consists of stacked, vertically-aggraded, fining-upward, fluvial depositional sequences, and can be divided into the "upper sand" and "lower sand". Only the lower sand has demonstrated reservoir characteristics. It was deposited in meandering fluvial channels confined to two incised channel belts, whereas the upper sand's northeast-trending meandering channels were unconfined and free to migrate across a broader floodplain from southeast to northwest, with migration reflecting local tectonic tilting.

The methodology used to understand the Atoka Formation, recommended for wider application in the region, consists of : 1) Understand geologic constraints; use all well data available to build a geologic model for constraining the seismic interpretation, 2) Use synthetic seismograms for correlating log to seismic data; identification of the exact wavelet corresponding to sand bodies is critical for success; 3) Build a seismic model; the seismic model must work from a theoretical sense, from geologic data available and from the seismic volume. In this case, thick sandstone (>20 ft) is vertically resolvable and can be mapped by the presence of an extra trough and related amplitude anomalies according to the bed thickness model, 4) Apply coherency analysis to the seismic volume as the best tool for revealing channels, and 5) Amplitude attribute extraction demonstrates thickness variations within channels/channel belts.

1. INTRODUCTION

1.1 Definition of integrated 3-D seismic analysis

Three-dimensional reflection seismology (3-D seismic) is a multi-dimensional approach to acquiring, processing and interpreting a closely spaced subsurface data volume (Brown, 1999). 3-D seismic interpretation allows visualization of subsurface geological features. When carefully constrained by geological data, 3-D seismic interpretation can reveal a degree of geological detail not possible using conventional well data. The advantage of 3-D seismic over 2-D methods is that through acquisition and processing procedures, geologic features can be correctly placed spatially in the 3-D volume.

An integrated approach to interpreting 3-D seismic data includes combining all methods that can be applied to give geological constraint to the interpretation. Typical geologic information that might be available includes rock samples such as core or cuttings, which can be studied to reveal petrology, petrography, depositional environments, and lithostratigraphy. Indirectly, geophysical well logs can be interpreted to add additional geologic information including lithostratigraphic and sequence stratigraphic correlation, and additional petrologic (mineralogy, porosity, pore-filling media) and depositional environment interpretation. Additionally, well logs can be converted to synthetic seismograms to give ground-truth to features visible in the 3-D seismic volume. Seismic data can yield geologic information between wells, particularly through correlation of well-derived geologic data with seismic attributes. Coherency analysis is useful technique for detecting subtle structural and stratigraphic features such as channel edges. Other attributes (such as amplitude extractions) yield information related to physical properties of reservoirs.

1.2 Problem related to Atoka Formation sandstone reservoirs

The Atoka Formation in southeastern New Mexico consists of problematic natural gas reservoirs in terms of both predictability and economics. In general, the formation is not a primary target for exploration, and instead is discovered while drilling for deeper, more prolific, Morrow Formation reservoirs. The problem with the Atoka Formation is in part due to its complex syndepositional tectonic history. Also, over most of the region, Atoka reservoirs are thin and are thus below seismic resolution. However, in a multi-township area in the vicinity of Vacuum field in Lea County, New Mexico, the lower part of the Atoka Formation includes an unusually thick package of sandstone bodies. The thickness of the sandstone bodies should be sufficient for seismic resolution. If so, an integrated approach to interpreting 3-D seismic data could aid in prediction of the distribution of the potential reservoir sandstones.

In the mid-1990's, Marathon Oil Company and its industry partners acquired a large (multi-township) 3-D seismic volume to study numerous reservoirs in the vicinity of Vacuum field in Lea County, New Mexico (Fig 1.1). Prior to acquisition of the seismic data, Marathon and others had completed prolific gas wells in the Atoka, but had also drilled numerous dry holes. Attempts to improve success using analysis of the 3-D volume were not successful. Marathon provided New Mexico Tech a portion of that dataset along with a proposed problem to solve: to try to gain a better understanding of the Atoka Formation reservoirs from advanced analysis of the seismic data and apply this understanding in a predictive manner.

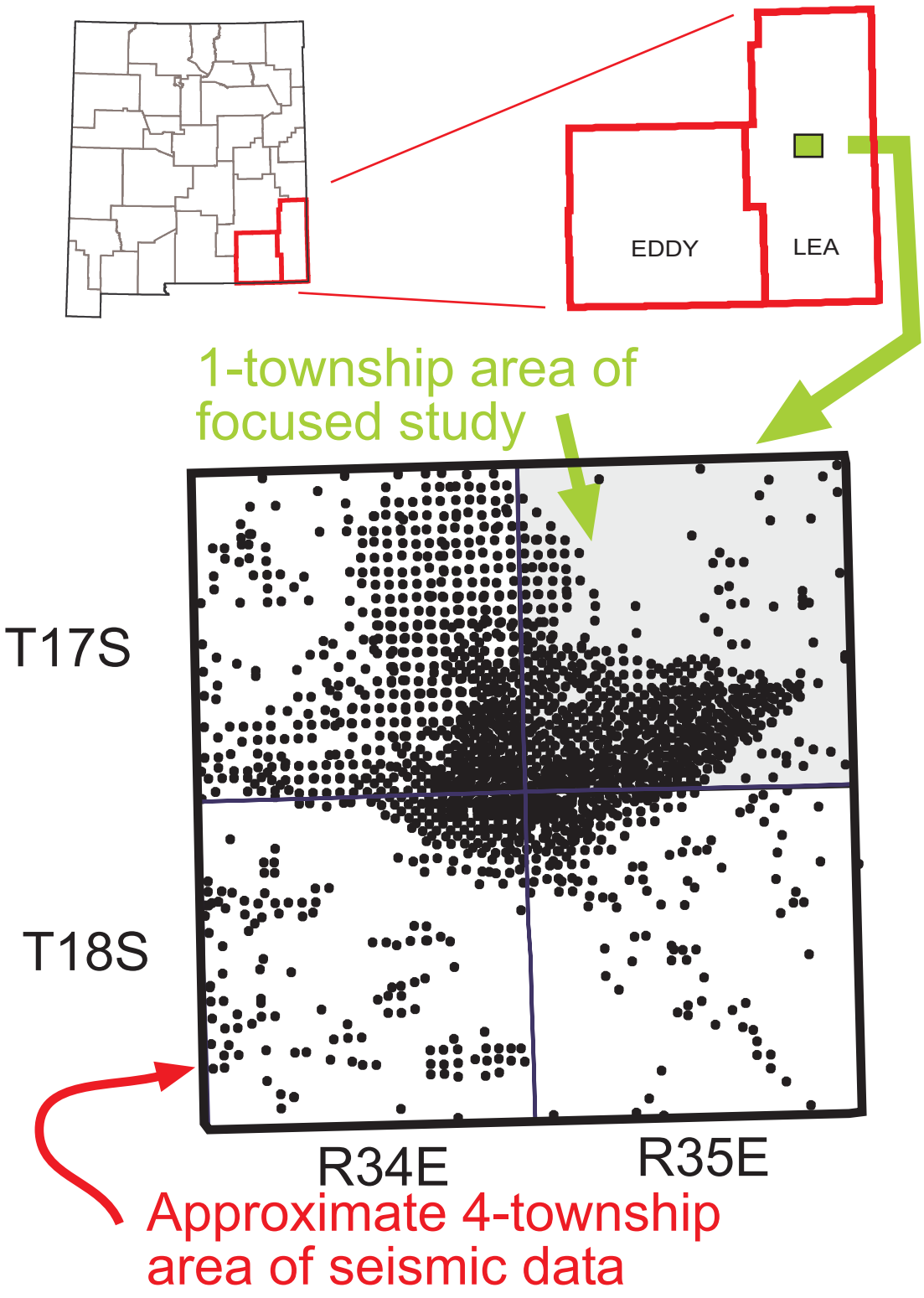

Figure 1.1: The area of study where seismic data was available and the area of focused analysis of Atoka Formation natural gas reservoirs. Dots are well locations.

1.3 Purpose of this research

The purpose of this research is to integrate analyses of a variety of geological, petrophysical, and 3-D seismic analytical and interpretation techniques in order to delineate, predict and explain Atokan Formation sandstone reservoirs and identify successful methods applicable to the solution of the problem. Both the integrated analysis and a recommended method are developed and presented.

2. SETTING AND PREVIOUS WORK

2.1 Geological setting in context of previous work

Relatively little has been published about the Atoka Formation in southeastern New Mexico. This, combined with the fact that the Atoka is generally believed by industry explorationists to be an unpredictable target, yields opportunity for this research to make a significant contribution to the understanding of this field. Perhaps the best references that discuss the Atoka are James (1985) and Speer (1993). Unfortunately, both papers oversimplify or mistake the complex depositional and preservational history of the formation (Mazzullo, 1999a, 2000). For example, James (1985) describes the Atoka Formation sandstone reservoir's depositional environment for the Vacuum field area as being that of an offshore barrier bar system, whereas several geologist who work in that field agree that the productive Atoka sands are actually nonmarine and confined to channels or channel belts (D.M. Rawlins, personal communication, 2000; L. Mazzullo, personal communication, 2001). The following discussion summarizes the general geological setting prevalent during Atoka Formation deposition as commonly described in the literature.

The Pennsylvanian in southeast New Mexico is divided into five series (from oldest to youngest) – Morrowan, Atokan, Des Moinesian, Missourian and Virgilian (Fig 2.1; Cys and Gibson, 1988). Commonly in local industry terminology, these series equate to the following formations: - Morrow Formation, Atoka Formation, Strawn Formation, Canyon Formation and Cisco Formation. For the purposes of this thesis, the formation names will be used in order to better relate to popular usage. The thickness of the Pennsylvanian system is about 2520 ft to 2745 ft (840 m to 915 m) on the Northwest shelf (Meyer, 1966), which is the general location of the study area (Fig 2.2).

SYSTEM	SERIES	DELAWARE BASIN
QUATERNARY	Holocene	Holocene Sand
TERTIARY	Pliocene	Ogallala
CRETACEOUS	Gulfian Comanchean	Limestone, Sandstone
JURASSIC	Absent	
TRAISSIC	Dockum	Dockum
PERMIAN	Ochoa	Dewey Lake
		Rustler
		Salado
		Castile
	Guadalupe	Bell Canyon / Cherry Canyon / Brushy Canyon (Delaware Mt.)
		Victorio Peak
	Leonard	Bone Spring Limestone
	Wolfcamp	Wolfcamp
PENNSYLVANIAN	Virgil	Cisco Formation
	Missouri	Canyon Formation
	Des Moines	Strawn Formation
	Atoka	Atoka Formation
	Morrow	Morrow Formation
MISSISSIPPIAN	Chester	Barnet
	Meramec	Mississippian Limestone
	Osage	
	Kinderhook	
DEVONIAN	Upper Middle	Woodford
		Thirty-one
SILURIAN	Middle	Wristen / Fusselman
ORDOVICIAN	Upper Middle	Montoya
	Lower	Simpson
CAMBRIAN	Upper Middle	
PRECAMBRIAN		Precambrian

Figure 2.1: Geological column of the Delaware Basin (Modified from Hills and Galley, 1988.)

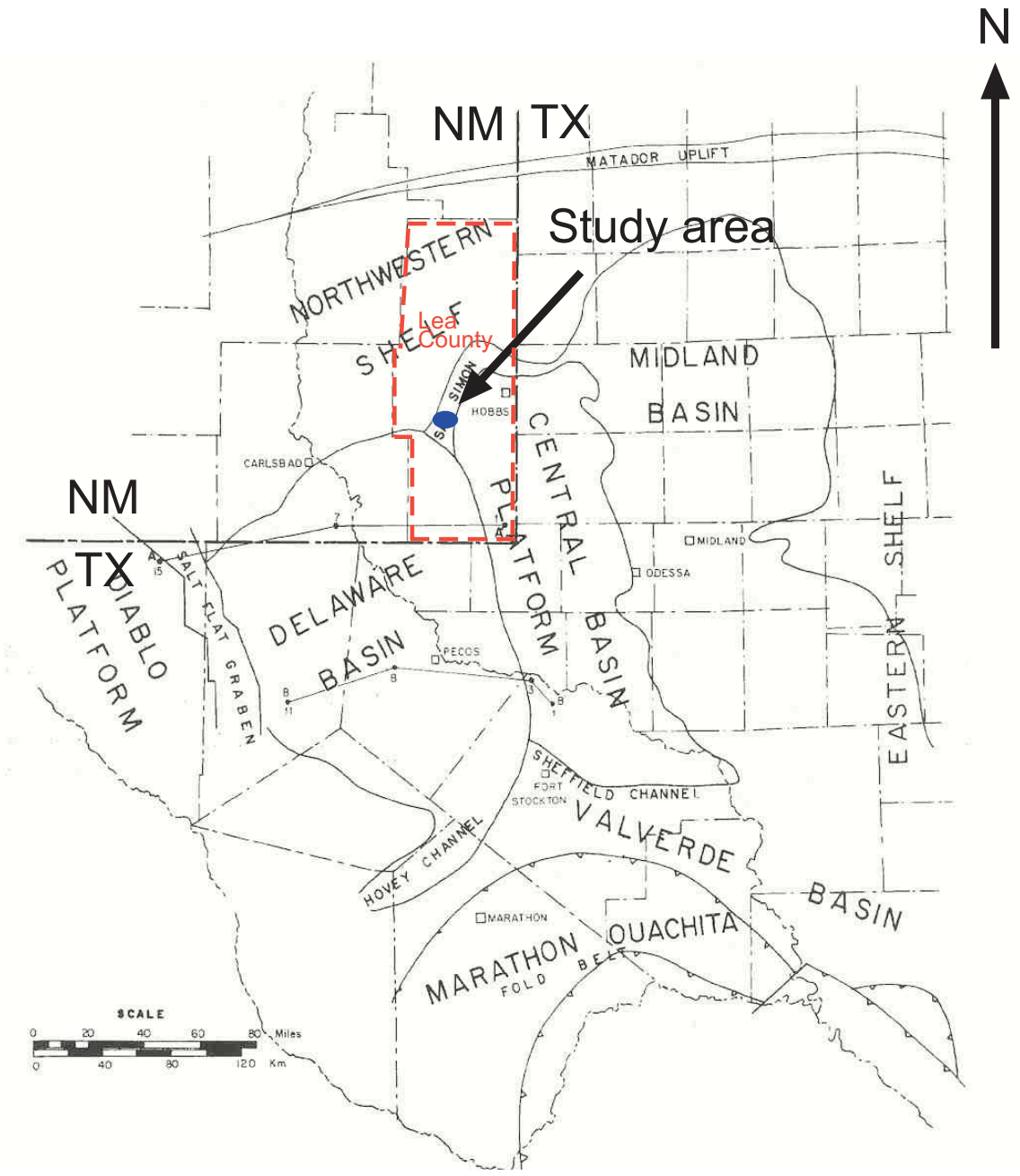

Figure 2.1: Pennsylvanian paleogeography of Permian Basin region in southeast New Mexico and west Texas. (Modified from Hills,1984)

The Pennsylvanian system can be divided into 2 sedimentary packages – the variable marine to non-marine Morrow/Atoka Formations and the marine Strawn/Canyon/Cisco Formations (Cys and Gibson, 1988).

The Atoka Formation was deposited during the early Pennsylvanian in the Delaware Basin, Central Basin Platform and Northwest Shelf areas of southeast New Mexico and west Texas as well as in the Midland Basin in west Texas (Fig 2.3). These tectonic features result from Carboniferous to Permian tectonic activity inboard of the Ouachita-Marathon tectonic belt to the south and east (Hills and Galley, 1988) and south and east of the adjacent and synchronous Pedernal and Matador uplifts of the southern Ancestral Rocky Mountains (Kluth, 1986). Perhaps the most intense episode of tectonic activity associated with this regional period of uplift is recorded by the Morrow and Atoka Formations which are known to have numerous intraformational unconformities (Mazzullo, 1999b). The Atoka, in particular, was deposited during the most intense tectonic activity over a much larger area of the Unites States (Ham and Wilson, 1967).

The Morrow and Atoka Formations are composed of interbedded shale, limestone and sandstone totaling a maximum of 1380 ft (460 m; Meyer, 1966). They were deposited in environments ranging from basinal marine to shallow shelf to non-marine alluvial that migrated several times due to early Pennsylvanian tectonism and sea level fluctuation (Speer, 1993). The clastic Morrow and Atoka Formation sediments deposited on the Northwest Shelf of the Delaware Basin are thought to have been sourced from the Pedernal Uplift which existed to the north and west of the Delaware Basin (James, 1985). At the basin edge of the Northeast shelf during transgressional events, however, cyclic carbonates were deposited (Mazzullo, 1981; Hills, 1984). In the late Pennsylvanian, the

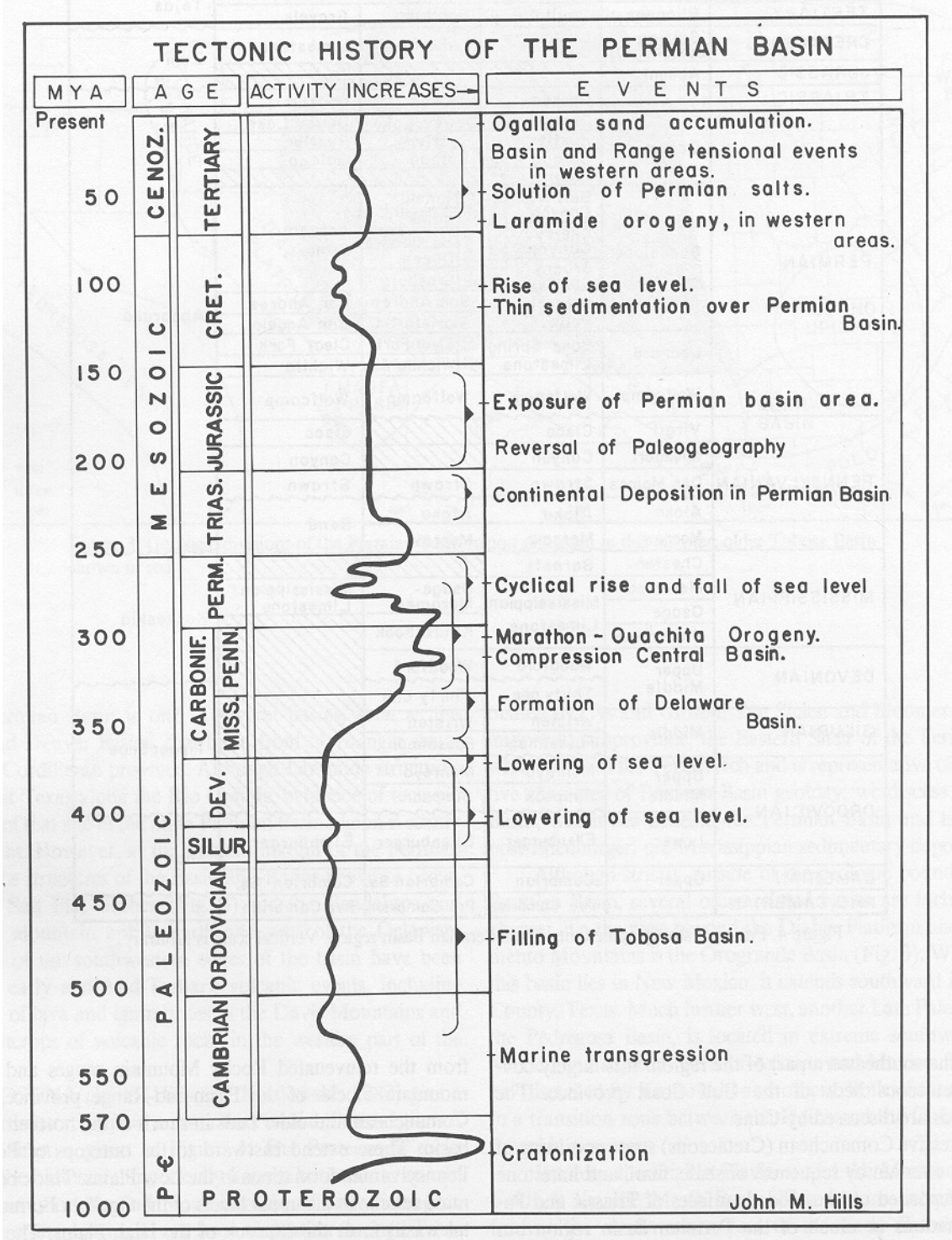

Figure 2.3: Summary of tectonic history in the region of the Permian Basin (Hills and Galley, 1988).

Strawn, Canyon and Cisco formations were deposited as cycles of carbonates (dominant) and shale with a maximum thickness of 1380 ft (460 m; Meyer, 1966).

The Atoka Formation in southeast New Mexico can be generally divided into upper and lower parts. The formation is primarily cyclic deltaic-marine in its upper part, whereas its lower part is nonmarine alluvial in some locations. The formation contains one or more intraformational unconformities, thus the lower part is often not preserved. During deposition of the lower Atoka, the Pedernal uplift shed clastic material that was transported through alluvial systems to deltas in the Delaware Basin. A dramatic sea level change (regression towards low-stand) during the lower Atoka caused channels to be incised into marine shale. The channels were subsequently filled with nonmarine fluvial deposits on the western end of the Northwest Shelf. Buffalo Valley field has been cited as an example (Fig 2.4; James, 1985). Similar and possibly synchronous conditions are interpreted to have existed on the eastern end of the shelf at Vacuum field to explain the postulated nonmarine fluvial channels there (Burnham, 1990). Sandstone bodies enclosed by marine shale, therefore, comprise major stratigraphic traps at Buffalo Valley and Vacuum/Shoebar fields (James 1985; Speer, 1993).

2.2 Setting in terms of regional Atoka Formation gas production

At least 147 major Pennsylvanian reservoirs (85 Morrow, 23 Atoka, 13 Strawn and 26 Canyon and Cisco formations) are known in southeast New Mexico (Table 2.1; Speer, 1993). The most historically important natural gas reservoirs are Morrow and Atoka formation sandstones that are self-sourced by their terrestrial organic content.

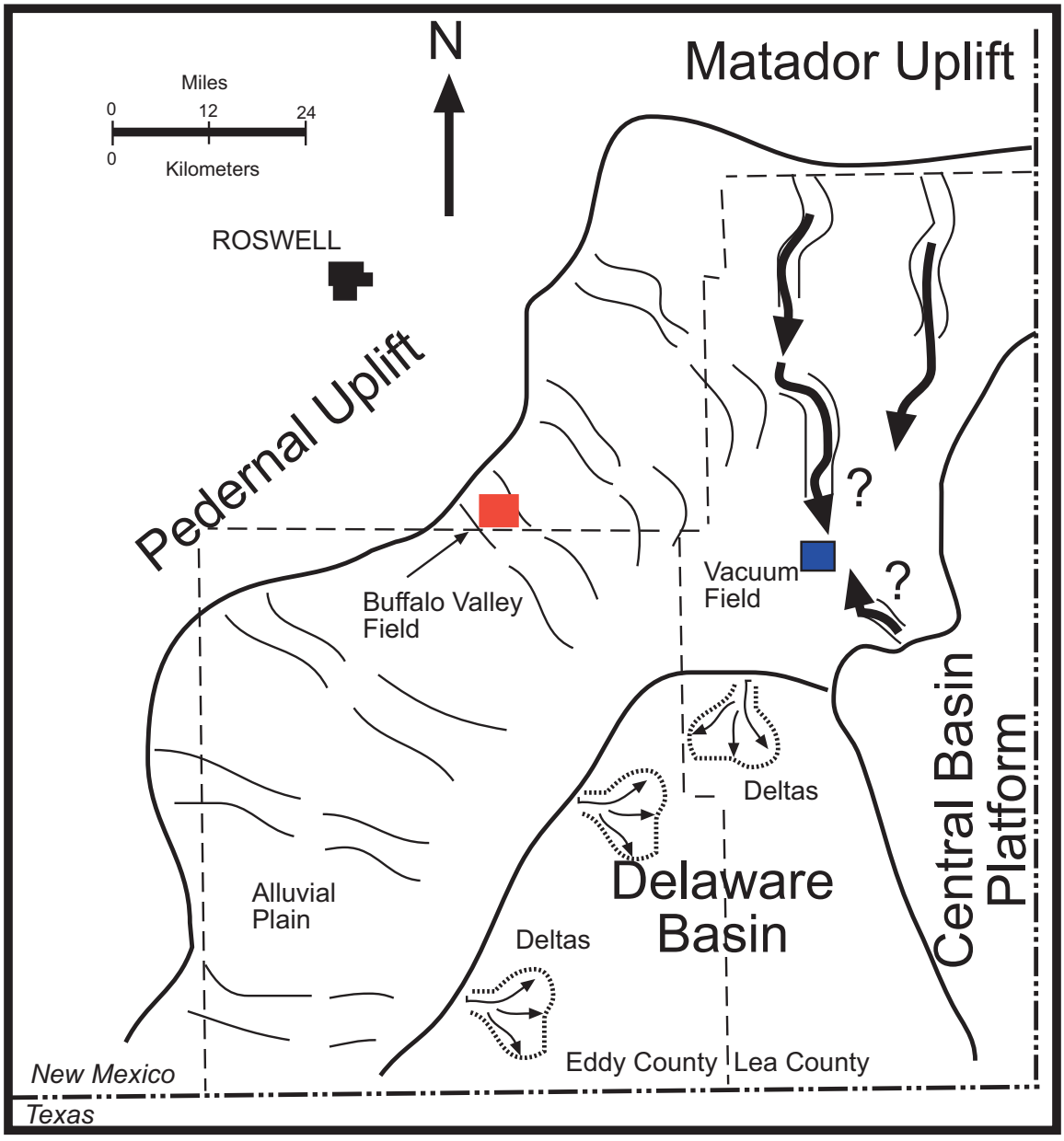

Figure 2.4: Map of depositional environment and hydrocarbon pools in southeastern New Mexcio during lower Atokan time (Modified from James, 1985)

According to Speer (1993), more than 130 gas wells have produced from Atokan rocks, and 23 fields have produced at least 5 billion cubic feet (Bcf). Cumulative production from the Atokan major reservoirs is estimated to be approximately 560.5 Bcf through 1990. Production from the Atokan reservoirs from the Delaware Basin or near its margin on the Northwest Shelf, is all non-associated gas with varying amounts of condensate. Cumulative production from the Atoka wells exceeds 4.4 Bcf in the Vacuum field vicinity.

Play and number of reservoirs	Productive stratigraphic units	Depositional settings	Main reservoir lithology	Main trap	Cumulative production of gas and oil
Upper Penn (26)	Cisco Canyon	Shallow open shelf and shelf margin	Limestone and dolomite	Stratigraphic and combination	1.846 TCF 274 MMBO
Strawn (13)	Strawn	Shallow open shelf ramp	Limestone	Stratigraphic and combination	0.256 TCF 43 MMBO
Atoka (23)	Atoka	Fluvial, strandplian, shelf and shelf edge	Sandstone and limestone	Stratigraphic and combination	0.561 TCF 5MMBO
Morrow (85)	Morrow	Fluvial, deltaic, strandplain and submarine fan	Sandstone	Stratigraphic and combination	2.929 TCF 21 MMBO

Table 2.1: Pennsylvanian plays in the Permian Basin. Numbers apply to major (>5BCF) reservoirs. Modified from Speer, 1993.

3. PROJECT DATA BASE

3.1 Seismic data set

The 3-D seismic data analyzed for this study was provided by Marathon Oil Company. The data was excerpted from a much larger, multi-client, mid-1990's 3-D shoot. The data consists of a 3-D volume underlying approximately 109 square miles in northern Lea County. On the basis of preliminary geological studies, it was determined that only a portion of the 3-D volume would be interpreted in detail to satisfactorily solve the problem posed for this thesis. Therefore, there are two levels of detail in this study, a larger area covering approximately 4 townships for broader-scale structural analysis, and an area of focused study covering approximately 1 township (Fig. 1.1) for stratigraphic and reservoir analysis.

The survey was shot using a Vibroseis source and was recorded as 2 seconds of two-way travel time (TWT) and sampled at 2 millisecond (ms) intervals. The 3-D seismic data grid was laid out with crosslines oriented approximately northwest, and inlines running northeast, perpendicular to crosslines. Other details of the source and receiver pattern and spacing were not provided. The data was processed using dip moveout (DMO) correction, migration, and deconvolution. Processed bin size was approximately 110' x 110'. No other specific information regarding acquisition and processing of 3-D seismic data was made available. Data quality is considered to be sufficient for the purpose of this study; however, it is believed that the data was not processed to zero phase. The implication of non-zero phase data is that synthetic seismogram control does not always compare well to the data. Marathon has apparently

had the data reprocessed to adjust phase (Marathon oil, personal communication), but the reprocessed version was not made available for this study.

3.2 Wireline logs

There are hundreds of wells within the study area. Only a small number of those wells (approximately 50) were drilled deep enough to log the Atoka Formation. Logs were acquired from a variety of public and private sources including the New Mexico Bureau of Geology and Mineral Resources Subsurface Library and the Roswell Petroleum Record Library. Marathon Oil Company provided digital logs for 20 deep wells. As research progressed and the area of investigation was focused, fifteen wells were selected for detailed seismic analysis (see Appendix 2). Several logs from these wells were digitized using Neuralog software made available by the New Mexico Petroleum Recovery Research Center.

The logs that were most useful for this project were sonic, density and gamma ray logs. Sonic/density pairs are preferred for creating synthetic seismograms. Ten of the fifteen key wells had sonic/density pairs, the remaining five wells lacked one or the other log, thus Gardner's rule (Sheriff and Geldart, 1999) was applied to create pseudo-sonic or pseudo-density digital logs (described in Chapter 4, section 4.3). One or more of photoelectric factor (PEF), neutron porosity, SP and resistivity logs were available in the twelve key wells and these were used to aid in correlation and petrophysical characterization. All of the logs are sampled at 2' intervals. All porosity logs were measured assuming default limestone matrix.

3.3 Rock data

Particular effort was applied to find rock samples from wells drilled in the 3-D seismic area. Well cuttings for only one well in the area were available at the New Mexico Bureau of Geology and Mineral Resources Subsurface Library (NMBGMR). Unfortunately, the sandstone reservoir interval of most interest had been removed from the boxes. No cores were found in the area of interest, but two cores from the Northwest Shelf region were found stored at the NMBGMR. They are the Reid "B" #1 (10-10S-31E) and the White Federal #1(13-19S-30E). Although those cores lack the lower Atoka equivalent to the sandstone reservoirs in the Vacuum field vicinity, they were useful to help understand the upper Atoka and are therefore described in Appendix 1. Marathon Oil Company provided core photos (from a core that is not available) for the State 17 Com 3, which is a key well for this study. Observations, interpretations and the core photos are presented in Chapter 4, section 4.2.

4. GEOLOGICAL CHARACTERISTICS OF ATOKA FORMATION

4.1 Overview

3-D seismic data interpretation is a very useful tool for understanding subsurface geology, but it must be carefully constrained geologically in order to gain the greatest benefit. It is important to have as complete an understanding as possible of regional and local geologic characteristics based on whatever data is available. In the oil field, such data is typically limited to well-specific petrologic and stratigraphic information (well samples, logs) and prior studies and interpretations, published and unpublished, including older vintage seismic data. Often studies overlap and build a useful geologic framework over time. This provides the interpreter with the background necessary to recognize the importance of features visible in the seismic and the limitations on the interpretation imposed by the geologic framework. When carrying out the preliminary geological investigation, it is useful to keep in mind the scale of resolution of the seismic data to be interpreted.

As mentioned in Chapter 1, very little has been written about the Atoka Formation in southeast New Mexico. These rocks do not crop out anywhere around the basin, thus only subsurface data is available for analysis. Some anecdotal information was also derived from experienced geologists in the region. The following discussions are based primarily on well log data used in place of rock data, with contributions from observation of a small amount of core.

4.2 Atoka formation stratigraphy

The Atoka Formation is overlain by the Strawn Formation, which consists of mainly limestone with thin shale interbeds. The upper contact with the Strawn is abrupt where massive Strawn limestone rests upon upper Atoka shale. Seismically, due to the fact that the Strawn is one of the strongest reflectors in the seismic volume and masks the top-Atoka reflection, the top of the Atoka Formation yields a weak reflection that is problematic for comparison to synthetic seismograms. The Atoka overlies the upper Morrow Formation, which consists of massive limestone. The basal Atoka contact has Atoka shale lying upon the Morrow limestone. The acoustic impedance contrast is very strong with the high velocity Morrow limestone being recognizable as a very strong reflection. Both the upper and lower contacts are very obvious picks on well logs and easily identified in samples and core, but only the lower contact is unambiguous in the seismic volume.

Figure 4.1 depicts typical gamma ray response of the Atoka Formation. The gamma ray curve is generally a good indicator of lithology, particularly sandstone or limestone (low gamma values) vs. shale (high gamma values). Based on previous studies (Cant, 1982; Wangoner et al, 1990; Miall, 1996; Bridge and Tye, 2000), gamma ray pattern recognition, such as a relative increase or decrease with depth, can be used to estimate sandstone depositional environments. Gamma ray logs from a number of wells were compared to those in previous studies (James, 1985; Speer, 1993; and Worthington, 1999). Based on this work, the top of each formation and important sandstone interval was determined and correlated across the study area. Figure 4.1 is a type log developed

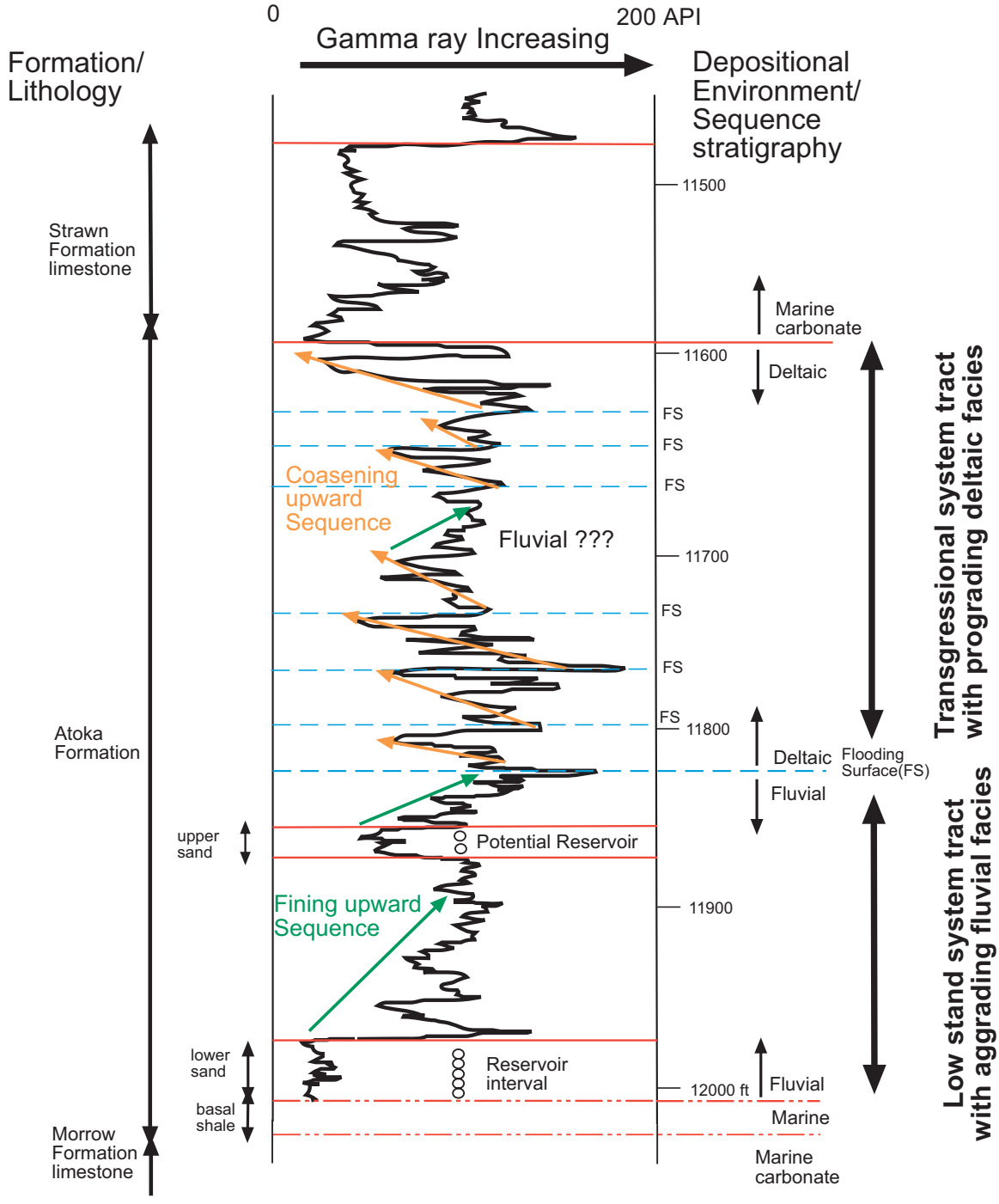

Figure 4.1: Typical gamma ray response of the Atoka Formation with geolgical interpretation. Depth measures from KB by ft.

and used for comparison to other logs and for estimating potential seismic response to changing lithology and depositional (sequence-stratigraphic) trends.

In Figure 4.1, fining upwards parasequences (curve deflects to right) typify the lower Atoka fluvial sandstone depositional environment, whereas coarsening upwards parasequences (curve deflects to left) are interpreted to typify the marine deltaic upper Atoka. The transition from lower to upper Atoka, is not lithologically distinct (not an obvious lithostratigraphic contact) even though it qualifies as a major change from nonmarine fluvial to marine deltaic conditions. In synthetic seismograms, the contact correlates to the base (zero crossing) of a mappable reflection that may result from stacked deltaic sandstone parasequences in the lower part of the upper (marine) Atoka Formation. All production established from the Atoka in the study area has been from the lower, nonmarine, part of the formation, thus the marine-nonmarine mappable transition is the approximate top of the interval of interest for reservoir analysis.

Sequence stratigraphy "systems tract" concepts as applied to the type log suggests that the "classic" systems tract vertical progression in marine basins, due to sea level rise and fall, does not apply exactly to the Atoka Formation. Such a progression is, from base to top: unconformity surface-lowstand systems tract, transgressive systems tract-flooding surface, highstand systems tract-unconformity (Wagoner et al, 1999). This may be due to the fact that the Atoka was deposited during a time of tectonic activity (Mazzullo, 1999). Clearly, there is a lithostratigraphic boundary at the base of the Atoka (shale over limestone). Regional studies generally assume that an erosional unconformity (a sequence boundary) marks the basal Atoka contact (Casavant, 1999) but there is no evidence for or against erosion in the data available for this study.

Presumably, the lower Atoka shale is marine and was cut into by nonmarine channels, perhaps due to sudden relative sea level drop (Burnham, 1990). Following the sea level drop, the remainder of the Atoka sequence, through the lower Strawn, reflects aggradation and an overall transgression. The transgression progressed from erosion and bypass during formation of a broad channel belt, to channel-confined stacked-sand body aggradation (blocky parasequences); (Fig 4.2). As aggradation continued, the system became unconfined and deposition took place in a meander- or braid-plain (fining-upwards parasequences). By the middle of the Atoka, eventual encroachment of marine conditions (relative sea level rise) and development of a deltaic system (coarsening-upwards parasequences) began. As the overall transgression continued, high frequency sea level fluctuations resulted in multiple, stacked, prograding deltaic parasequences to be interbedded with marine-flooding parasequences containing black shale and limestone. The transgression was capped by stable carbonate shelf deposition of the lower Strawn Formation. This would suggest that the Atoka-Strawn contact is lithostratigraphic but not sequence stratigraphic, i.e. there is no sequence boundary unconformity. No data was available for study of this contact. Further work is recommended.

Figures 4.3 and 4.4 are north-south stratigraphic cross-sections through the research area. The reference datum for the cross-sections is the nonmarine-marine contact (lowermost obvious flooding surface). The advantage of these diagrams is that they demonstrate the stratigraphy described above on the scale of seismic resolution. These cross-sections clearly show the distribution of lower Atoka sand sequences. At this scale, they appear to form continuous, sheet-like bodies that cover significant area, but they have lateral boundaries; particularly true for the upper sequences of the lower

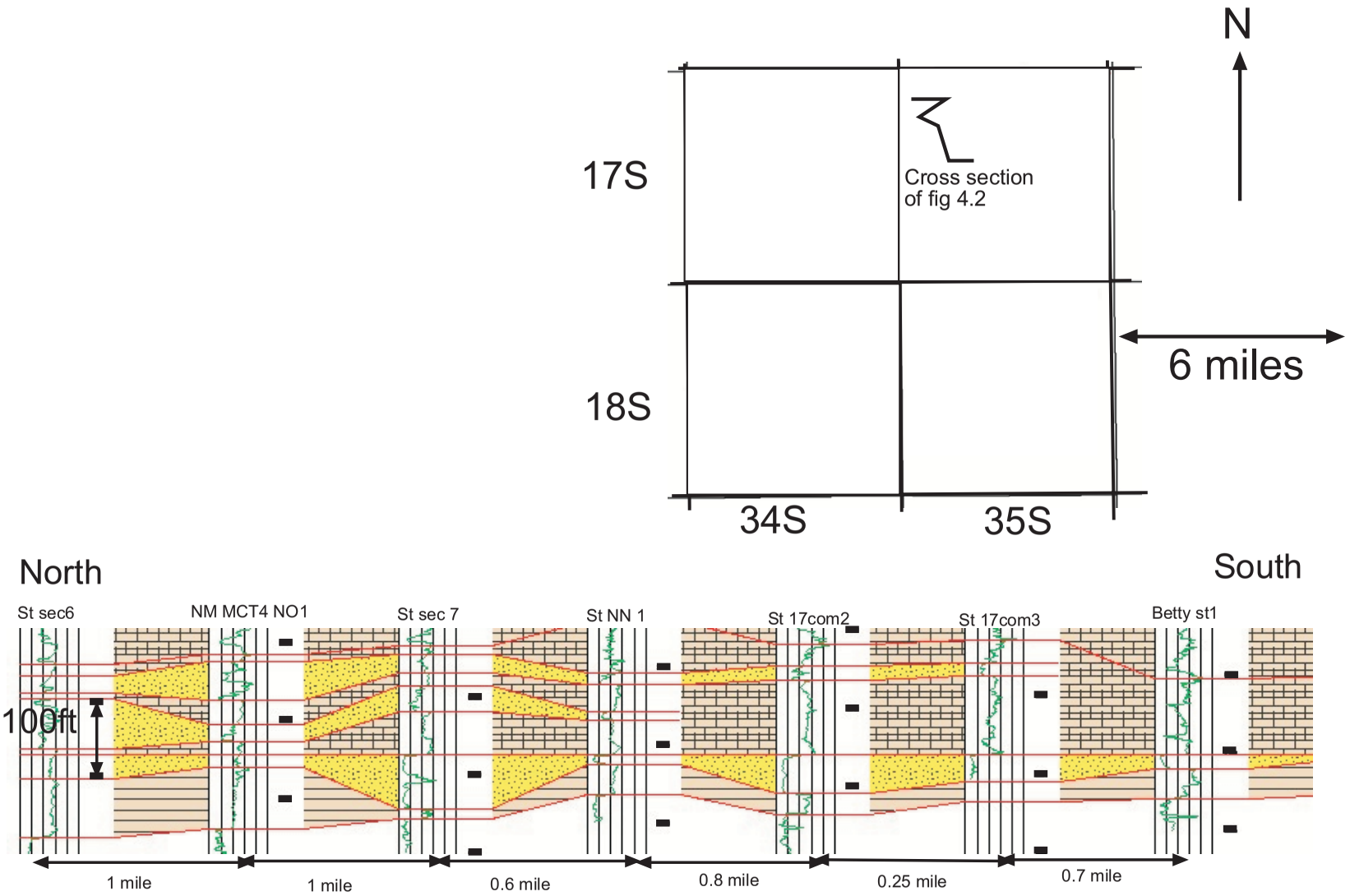

Figure 4.2: Channel Confirmation by gamma ray logs in norht-south the cross section (17S/35E). Datum is top of lower Atoka sand.

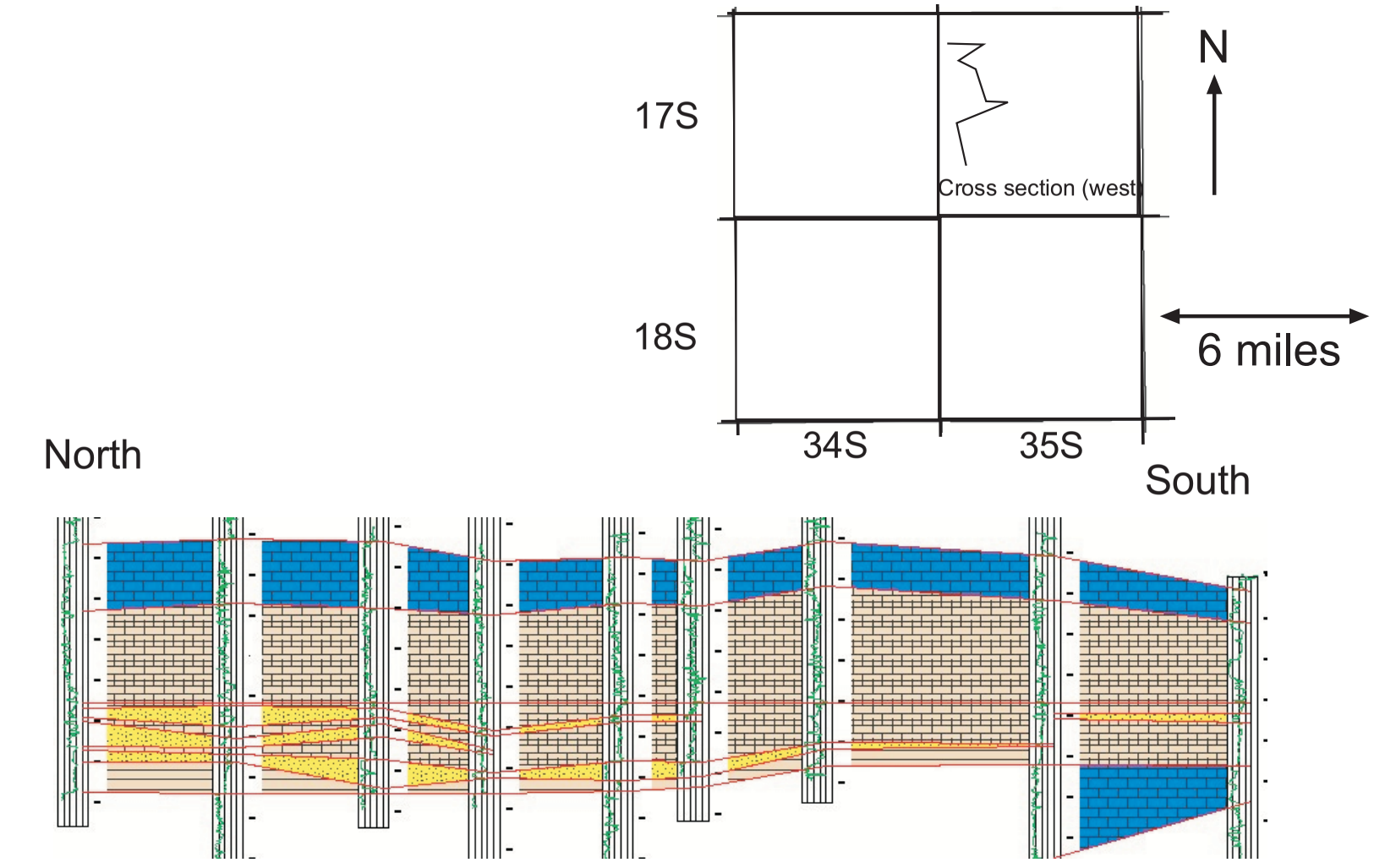

Figure 4.3: North to south cross section (west). In general, sand bodies thin to southward, and distribution of sand bodies represent a vertical sand stacking pattern. Datum is first major flooding surface.

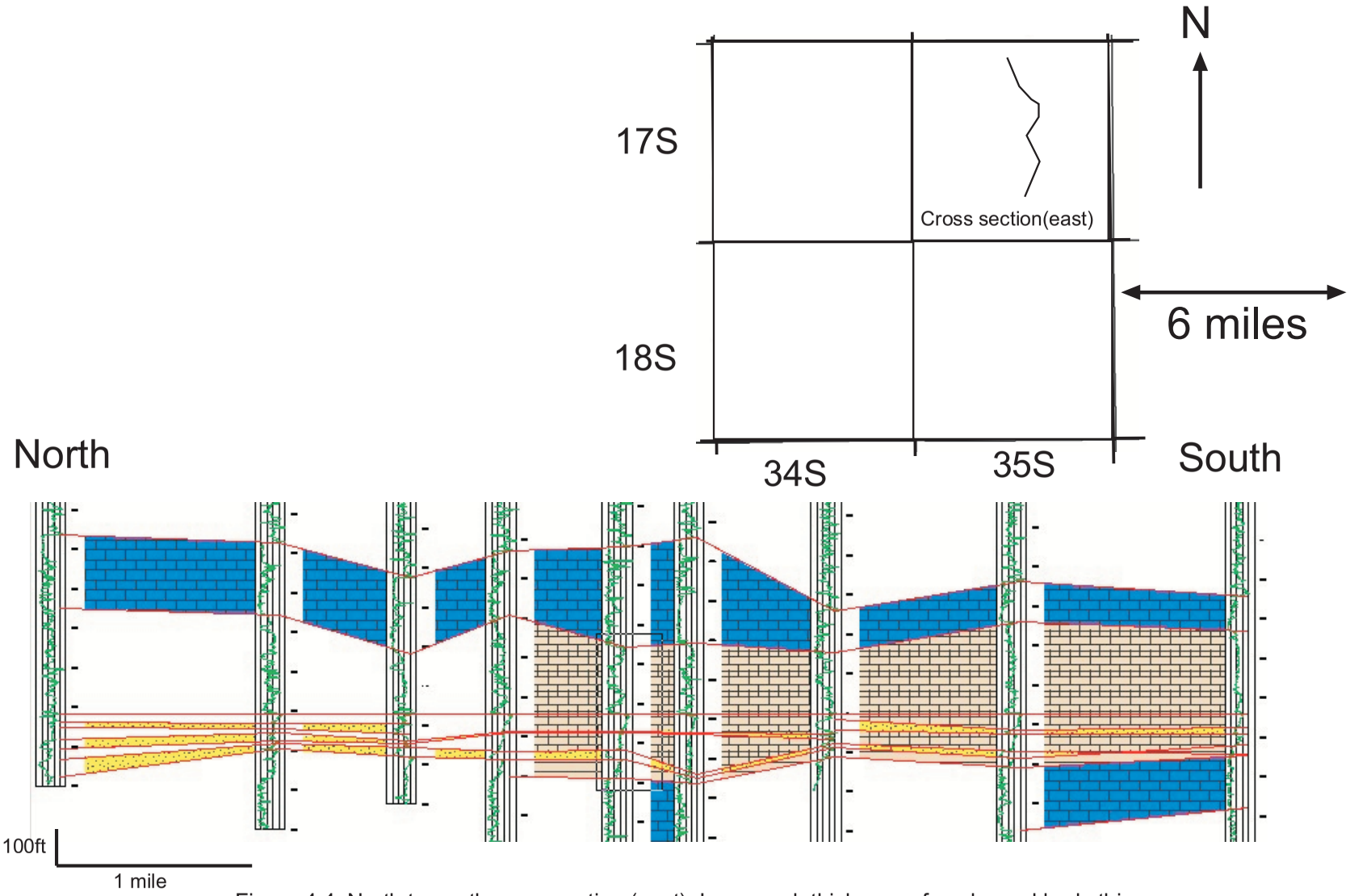

Figure 4.4: North to south cross section (east). In general, thickness of each sand body thins to south. Datum is first major flooding surface.

Atoka. The lower sequence of the lower Atoka appears to thin and thicken more dramatically, reflecting deposition in channels (Fig 4.2). In the lower sand, some wells fall within channels, others near channel edges. From a seismic standpoint, if these sheets are thick enough to be seismically resolvable, their distribution should be mappable. Seismic modeling (Chapter 6) demonstrates that these sand sequences are indeed resolvable.

4.3 Petrology, lithofaces, and reservoir characteristics

Several vertically-accreted sand bodies with cross laminae/cross-beds are observed within the reservoir sandstone bodies in the lowermost Atoka Formation in well State 17 Com 3 (Figs 4.5, 4.6, 4.7, 4.8 and 4.9). At least five stacked channel-fill parasequences are recognized in that well on the basis of fining-upwards beds, or bed sets that in general have coarse to pebbly bases and clay plugs at top. The sandstone bodies tend to have blocky gamma ray curves suggesting channel fill, whereas the clay plugs are readily identified as elevated gamma ray "spikes". The stacked parasequences probably reflect lateral channel migration within a single confining channel belt. An example of depositional sequences in the marine, non-reservoir, upper part of Atoka Formation is summarized in Appendix 1.

Because core availability is rare, logs are very useful for indirect derivation of reservoir properties. Such properties, especially mineral composition and water saturation were determined quantitatively on the basis of petrophysical (quantitative well log) analysis to understand reservoir quality and possible effects on seismic characteristics. Resolution of log data is much higher than that of seismic data.

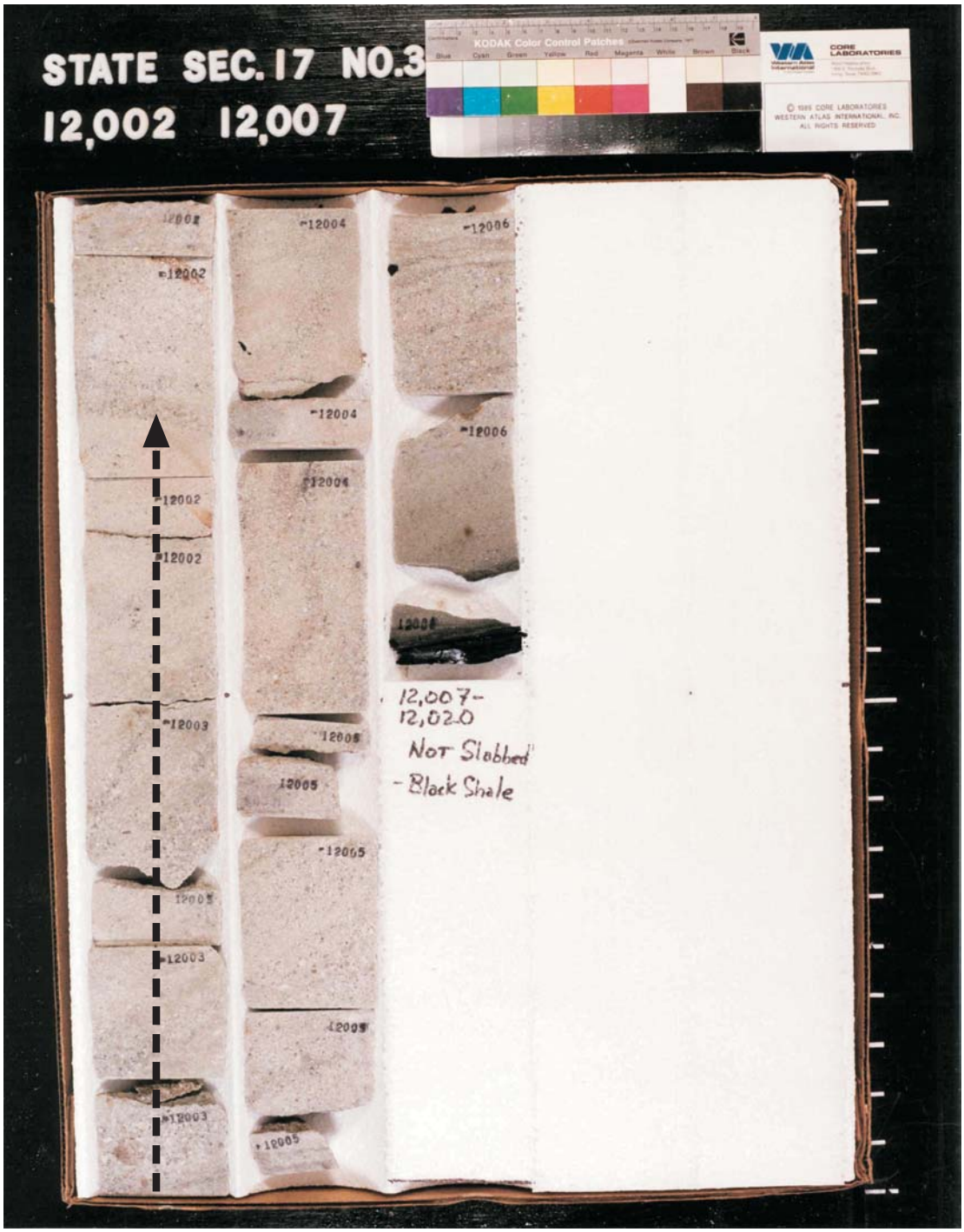

Figure 4.5: Facies analysis of 12007 to 12002 ft depth interval. Arrow describes a fining upward sequence.

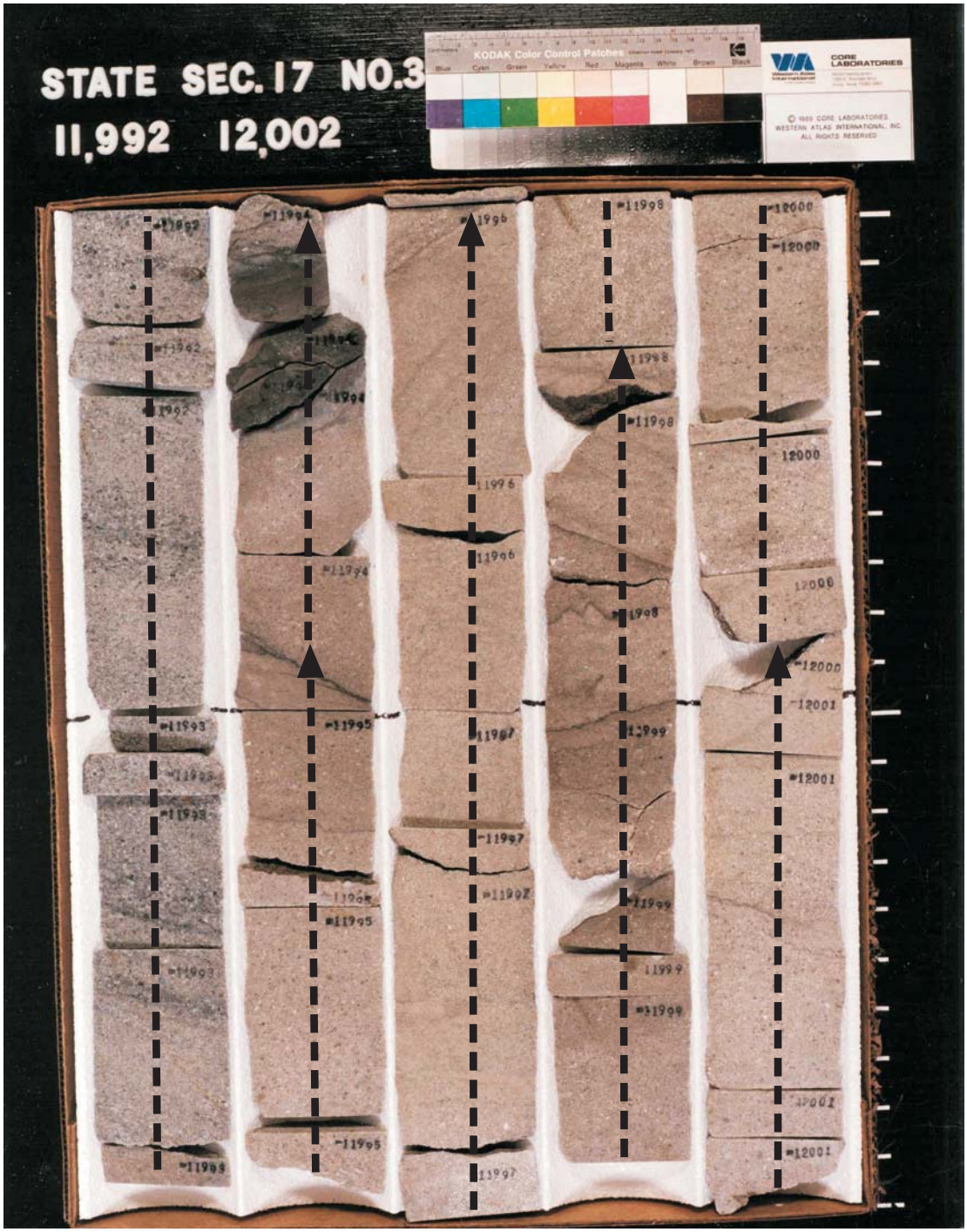

Figure 4.6: Facies analysis of 12002 to 11992 ft depth interval. Arrow describes a fining upward sequence.

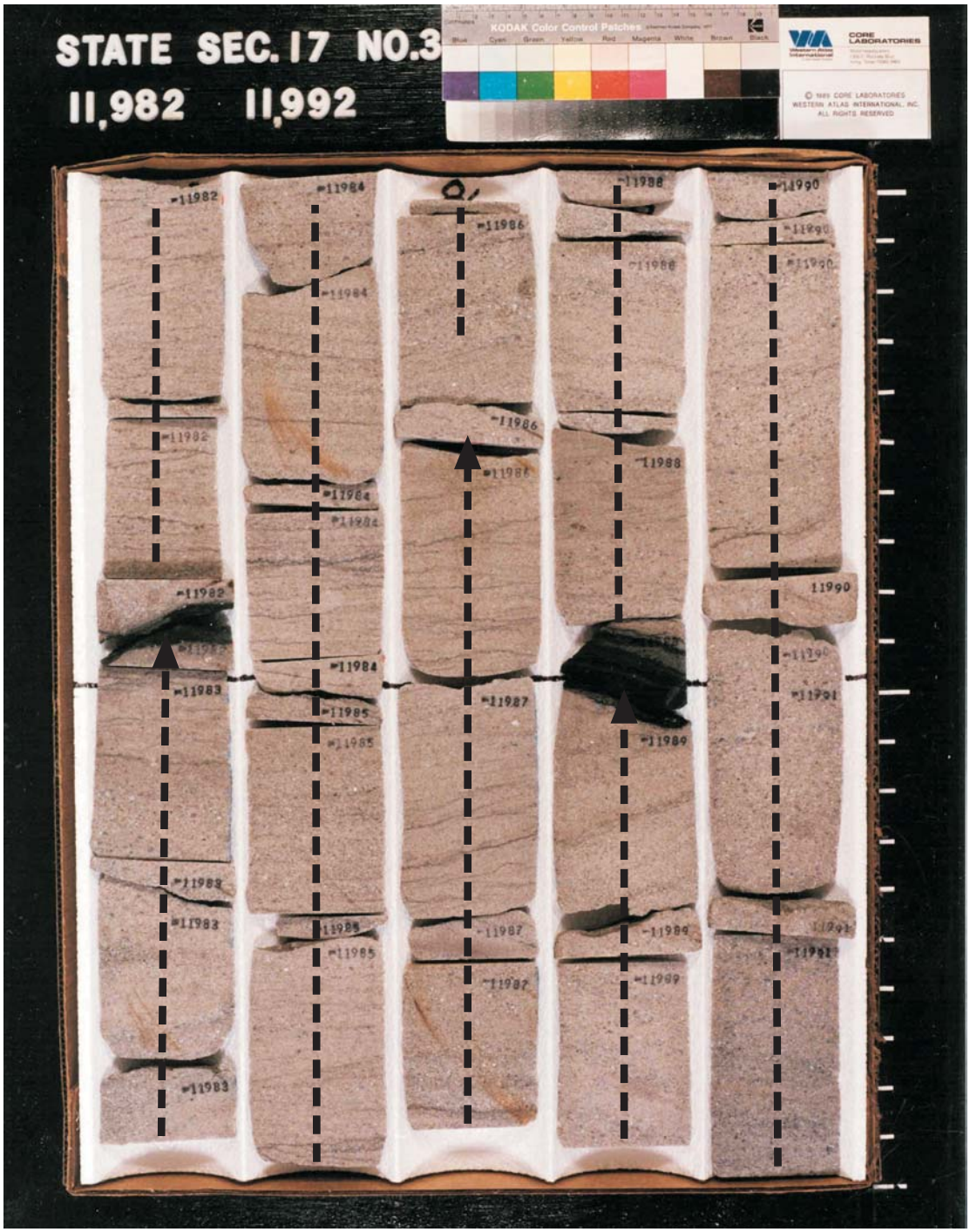

Figure 4.7: Faceis analysis of 11992 to11982 ft depth interval. Arrow describes fining upward sequence.

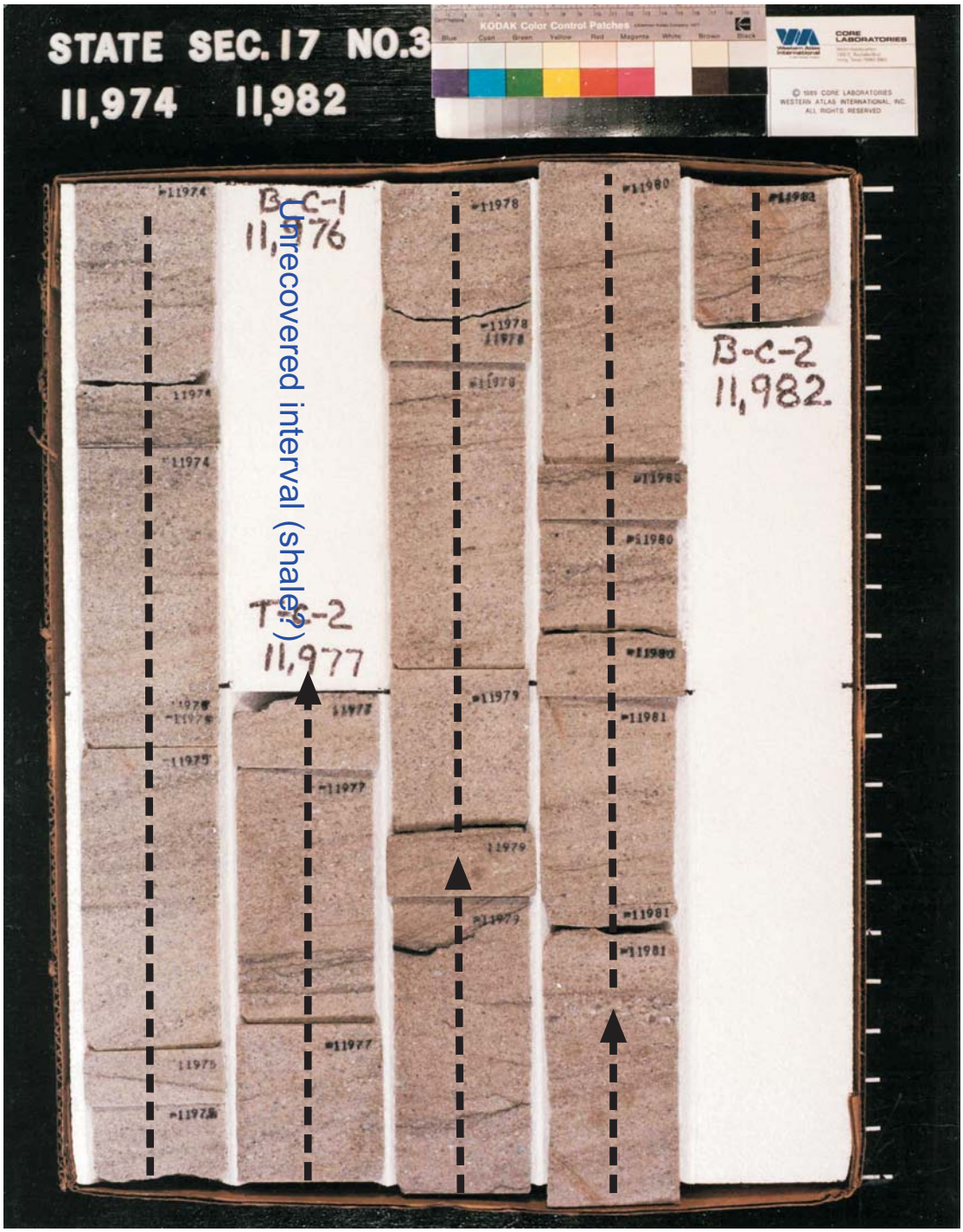

Figure 4.8: Facies analysis of 11982 to 11974 ft depth interval. Arrow decribes a fining upward sequence.

Figure 4.9: Facies analysis of 11974 to 11964 ft depth interval. Arrow describes a fining upward sequence.

Typically vertical resolution of modern logs is two feet or less, depending upon log type (Schlumberger, 1989; Asquith, 1999). On the other hand, resolution of typical seismic data for oil and gas exploration, depending upon depth, is tens of feet at best. One of the goals of this study is to evaluate reservoir quality of the Atoka Formation. Porosity is one of the essential factors to be considered. Because the Atoka Formation is a gas producer, porosity measured by density-porosity and neutron porosity is not always measured accurately due to gas affecting the log response. Neutron-density cross-plot porosity tends to cancel out gas effects, thus it is preferred. Neutron-density cross-plot porosity is not available for all wells in this study. Sonic travel time, which can be converted to porosity, is available for all of the wells. Thus, if a relationship can be demonstrated between neutron-density and sonic porosity in some wells, sonic porosity can be used in the remaining wells. Plotting sonic porosity vs. neutron-density porosity (Fig 4.10) yields results that are reliable for this purpose with a linear regression correlation coefficient more than 90%. Table 4.1 is a summary of average porosity and range of porosity with thickness of productive sand intervals in the study area; data are measured every 2 feet from digital well logs by Petroworks software by Landmark Graphics Corp.

Well name	Thickness(ft)	Minimum porosity	Maximum porosity	Average porosity
STATE SEC 7 COM1	70.1	0.024	0.135	0.094
STATE17 COM2	49	0.058	0.101	0.088
SHOEBAR STATE COM NO1	10	0.026	0.1	0.041
BETTY ST NO1	17	0.028	0.114	0.076
STATE SEC22 COM NO1	15.5	0.033	0.109	0.082
STATE 17 COM NO3	34.5	0.024	0.089	0.072
SOUTH SHOEBAR 15 COM 2	24	0.069	0.134	0.111
AVERAGE POROSITY OF ALL WELLS				0.085

Table 4.1: Summary of porosity information from the Atoka Formation.

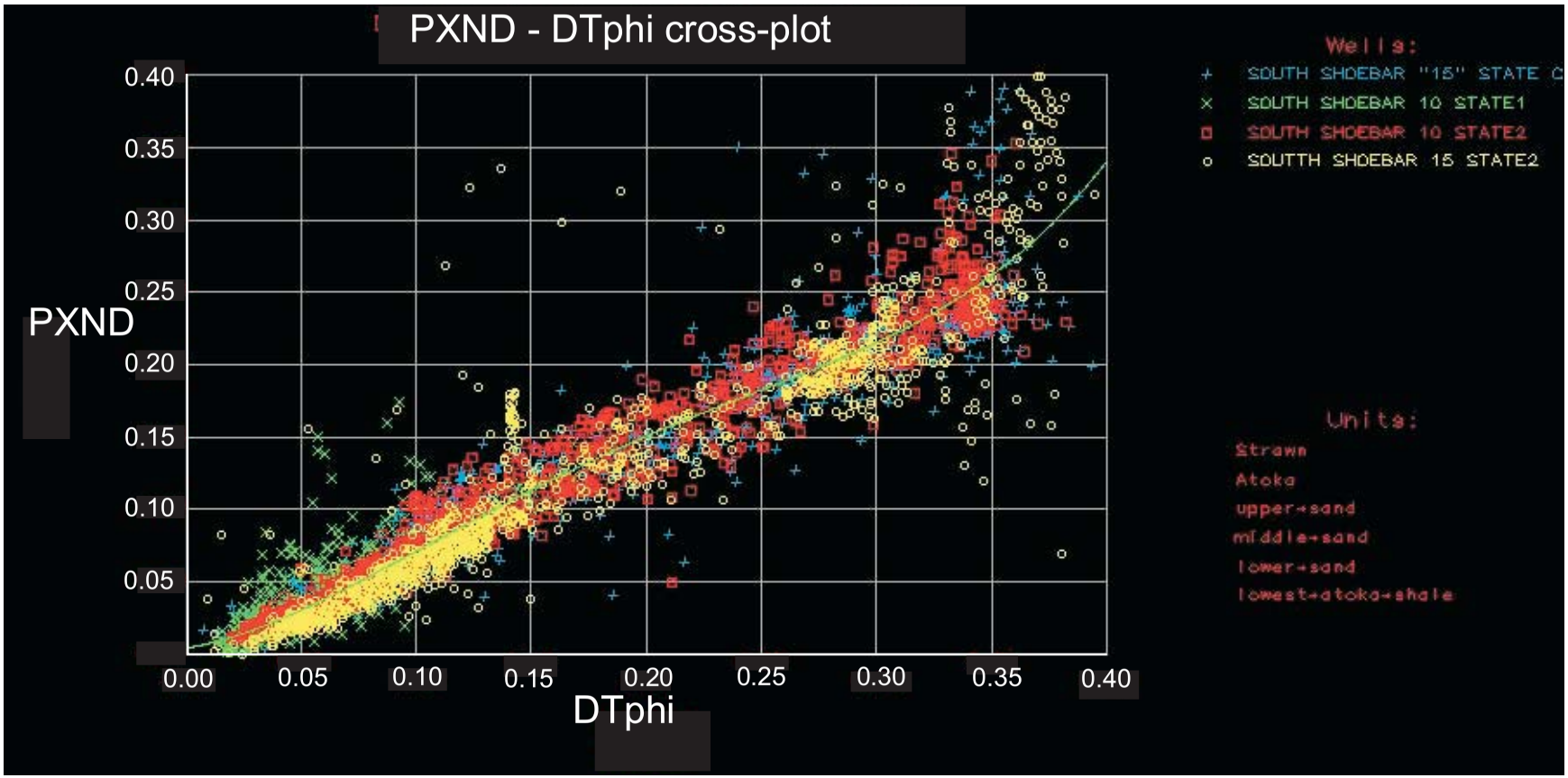

Figure 4.10: Sonic porosity (DTphi) vs. neutron-density-cross-plot porosity (PXND) cross plot.

Permeability of the Atoka Formation sandstone reservoirs is not necessary for interpreting seismic, but is an important reservoir characteristic that should be known when defining the average, or typical, sand. Permeability can be measured from core (measurements not available for this study), from engineering analysis of pressure and production (also not available) or from calculation from well log data. The latter is the method most likely to result in error. Only one well was examined (South Shoebar15 State2). Permeability calculations are valid only in intervals where the water saturation is irreducible, in other words, water cannot be produced by the well. The accumulated production for the South Shoebar 15 State 2 well is 1.8 Bcf of gas, 58,710 bbl of condensate, and 847 bbl of water. This is a relatively small amount of water and may result from producing fluids introduced to the hole during drilling and completion, thus the formation water saturation is assumed to be very near irreducible. Applying the permeability equation of Wylie-Rose (Asquith, 1999 and Landmark manual) for sandstones:

$$K = (C*phi^3/Swir)^2$$

Where C = 79 for dry gas, Swir = irreducible water saturation, and Phi = porosity,

the equation yields a permeability of 0.291 millidarcy. This value falls within the 0.1 to 0.9md range typical of similar Morrow Formation sandstone reservoirs (Gerstner and Malone, 1999).

Petrophysical data yields rock properties such as mineralogy, lithology, porosity, water saturation, relative permeability and so on. To determine mineral composition, the equation U Matrix / RHO Matrix cross-plot was performed where U Matrix is derived

from the Pef (photoelectric factor from density measurement) curve and RHO Matrix is derived from the bulk density curve. Four minerals on Figure 4.11 define end members. Lines between the four minerals denote the percentage of each mineral. Figure 4.11 demonstrates that the lower sand is composed mostly of quartz with some k-feldspar. This suggests derivation from a granitic source rock. For confirmation of mineralogy of each sand interval, a U Matrix (from Pef curve)/ RHO Matrix cross plot was calculated (Fig 4.11), which indicates that the main mineralogy of the lower sand is quartz and k-feldspar with minor calcite. Calcite is probably a cementing mineral that reduces porosity.

Water saturation determination was also performed. Low water saturation suggests high hydrocarbon saturation. Rocks with high gas saturation may behave very differently seismically from water-saturated rocks. However, the difference between the two is very small in low permeability, highly compacted and cemented "hard" rocks (Asquith, 1999). Water saturation was determined here strictly to identify sands with outstanding reservoir potential. Water saturation was calculated by the Archie equation, which is defined (Asquith, 1999) as

$$Sw = \sqrt[n]{(aRw / \Phi^m Rt)}$$

Where n = saturation exponent (2 from piket plot), a = tortuosity factor (1 from piket plot), Rw = temperature corrected formation water resistivity (0.078 from Picket plot), m = Cementation Exponent (3.277 from piket plot), Rt = Formation resistivity read from "deep" induction log. Figure 4.12 shows log response with water saturation curve for the entire Atoka Formation. In the intervals where the neutron and density porosity "cross-

over" in the lower sands, the water saturation is about 20%, indicating "pay" (high reservoir quality) and a value that is probably irreducible.

Based on petrophysical interpretation and a limited amount of core photos discussed above, the average Atoka Formation sandstone can be described. The lithology is sandstone with uniform or fining-upwards grain size, with grain size ranging from pebbly coarse sand to fine grained sand. The composition of the sand is subarkosic with probable calcite cement and clay matrix. Average porosity of the Atoka pay sand is about 8.5% with permeability on the order of 0.2 md. Net thickness of average-type pay sand ranges from 10 to 70 ft, with an average of 31ft. Chapter 6 includes a discussion of the potential to seismically resolve the average sandstone unit described here.

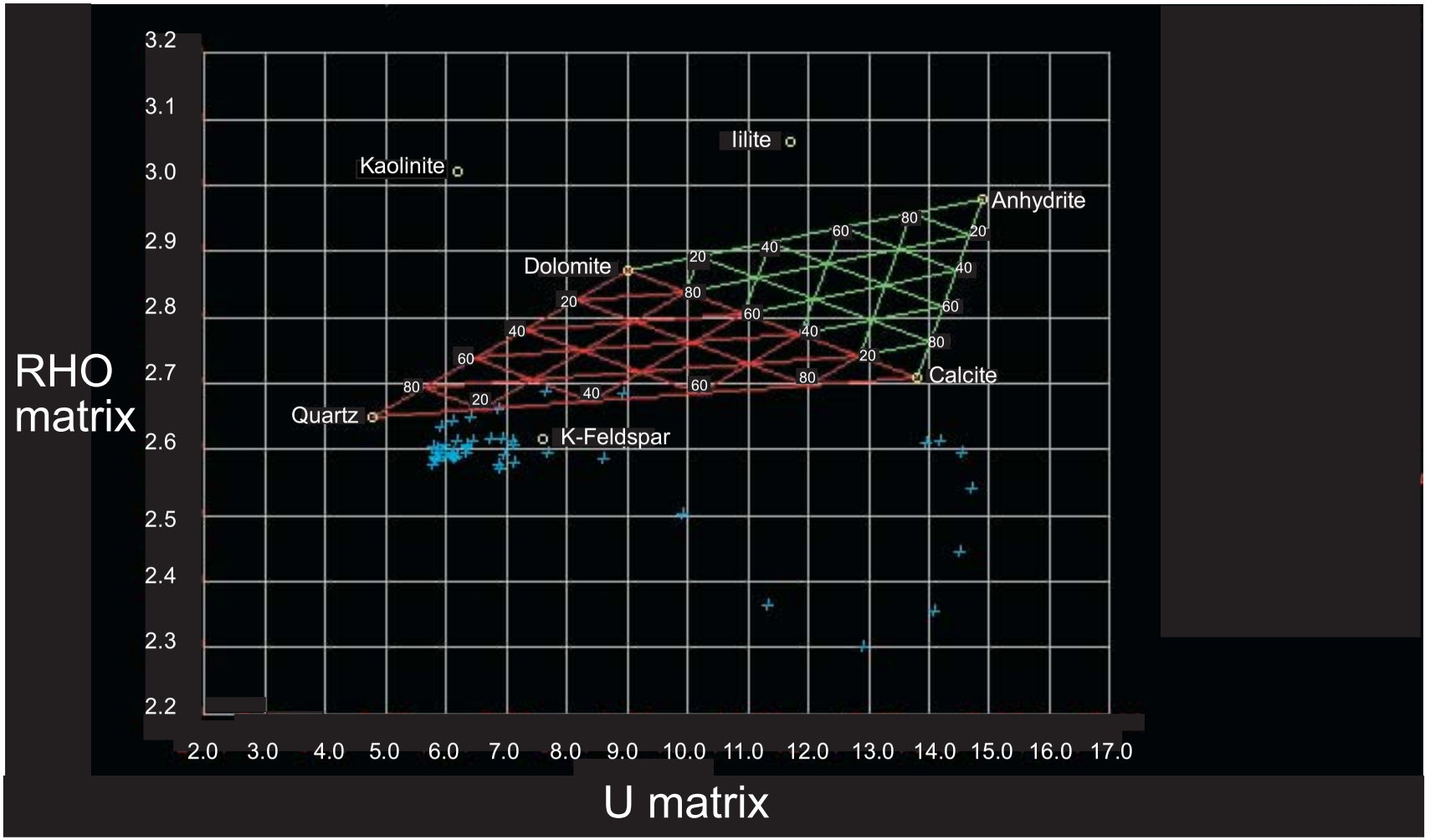

Figure 4.11: Umatrix/RHOmatrix cross-plot. Blue crosses indicate mineral composition and ratio of lower sand interval (South shoebar 15 state2).

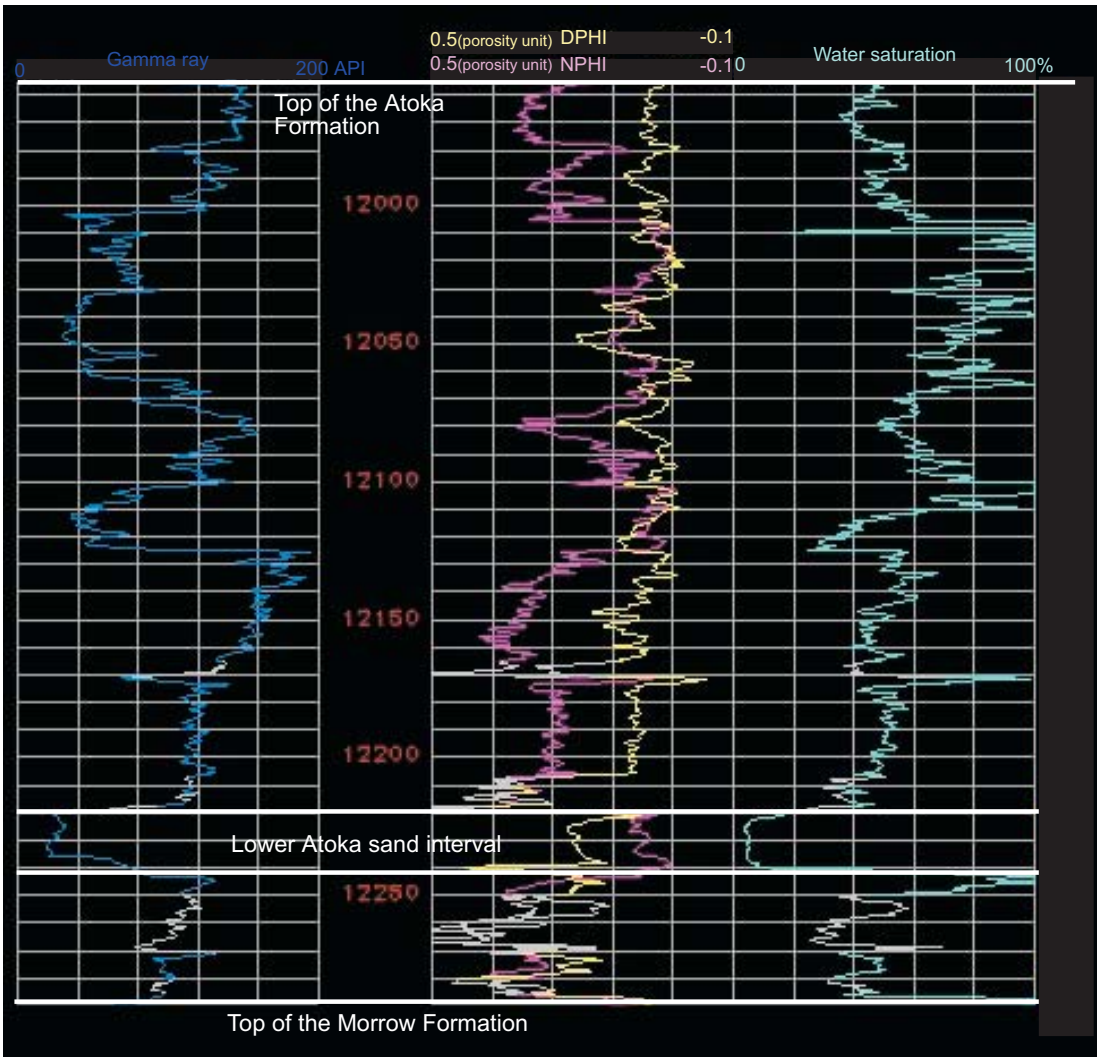

Figure 4.12: Log responses of (left to right) gamma ray, neutron porosity (pink), density porosity (yellow) and water saturation curves. Low water saturation is corresponding to the cross over of neutron/density porosity curves and low gamma ray responses.

4.4 Structure

The Pennsylvanian is well known for tectonic activity in southeastern New Mexico (Fig 2.3, e.g. Hill and Galley, 1988). Time structure mapping from the 3-D seismic depth structure mapping from the well data (Figs. 4.13 and 4.14) demonstrate that there is a boomerang-shaped structural high underlying Vacuum field structure (concavity oriented northeast). Comparing the two maps demonstrates the utility of using seismic maps to better visualize and quantify structure vs. using well data alone. This structure results from lower Pennsylvanian faulting, much of it is probably syndepositional to the Atoka Formation. Figure 4.15 and Figure 4.16 are seismic profiles (north-south and east-west respectively) that show interpreted faults. Figure 4.17 is a well-log cross-section that spans the study area from south to north and demonstrates stratigraphic omission of formations due to intra- and/or inter-formational unconformity related to the tectonic event. This supports the assertions of Mazzullo (1999) that the deposition and preservation of Morrow and Atoka formations were affected by local tectonics. Additional discussion of structural features as interpreted from seismic data is in Chapter 7.

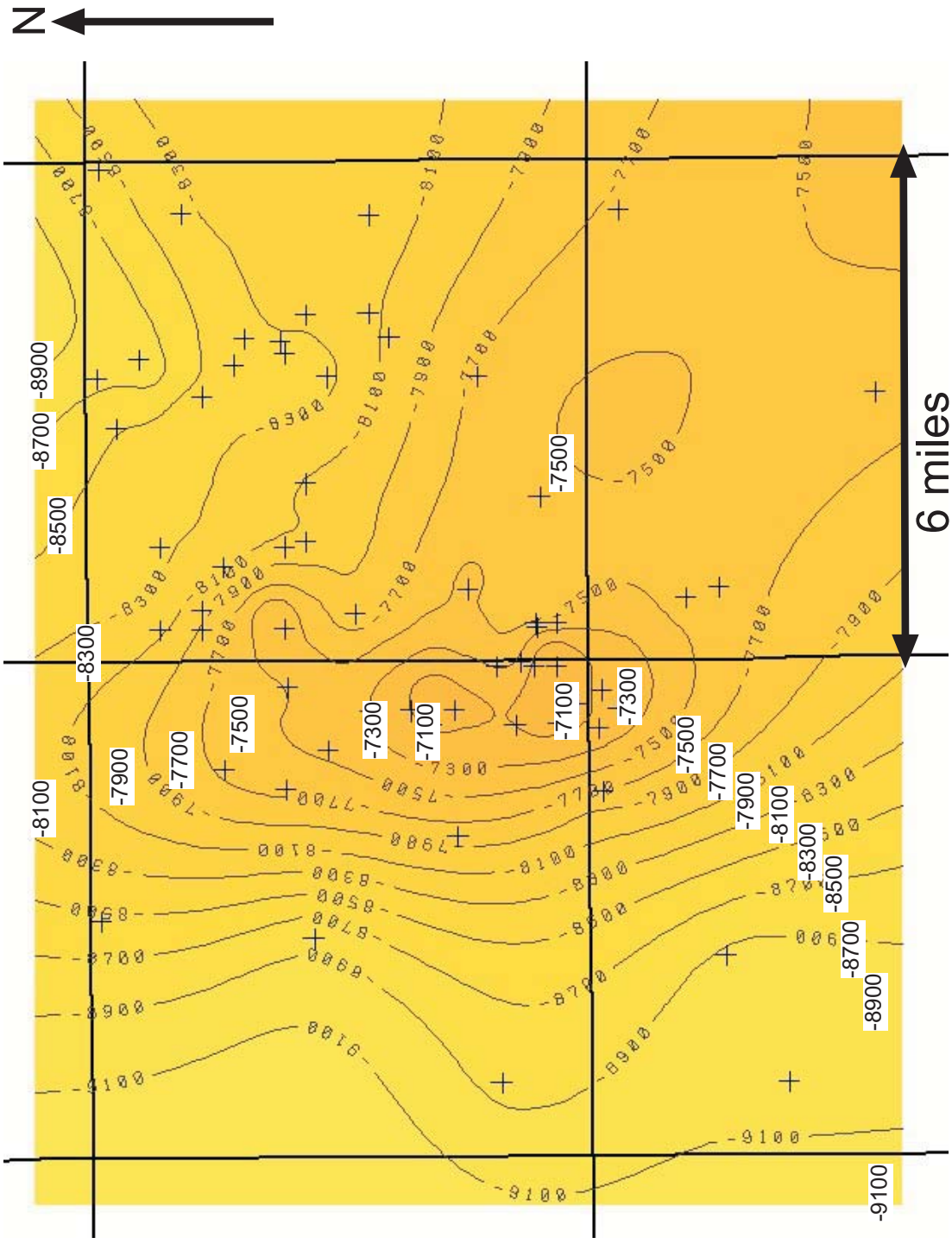

Figure 4.13: structural map (sub-sea) of the Morrow Formation by wells. Crosses are well control points.

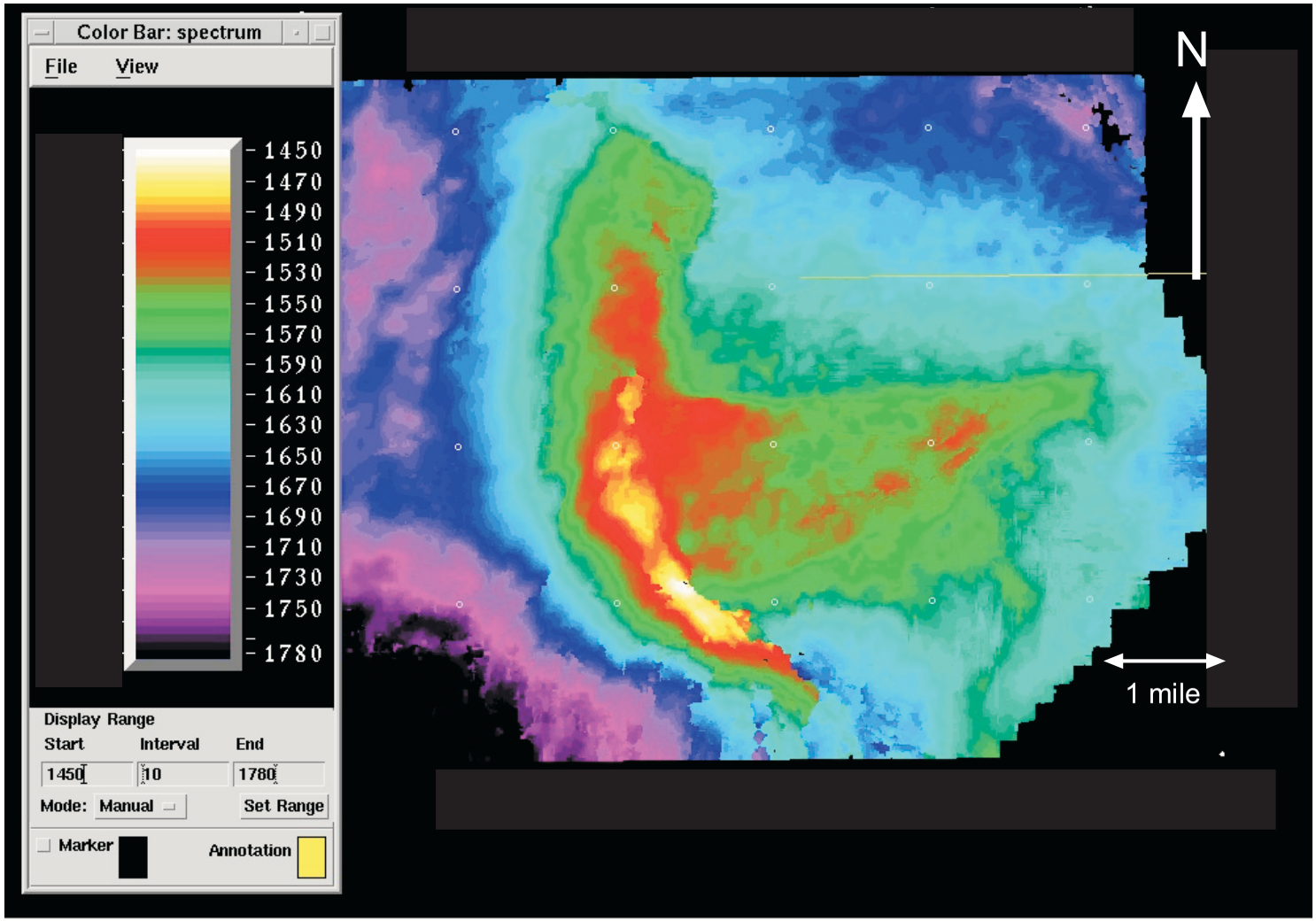

Figure 4.14: Time structure map of the Morrow Formation of the approximate area of fig 4.13. Units in the spectrum color bar legend are Two-way travel time (ms).

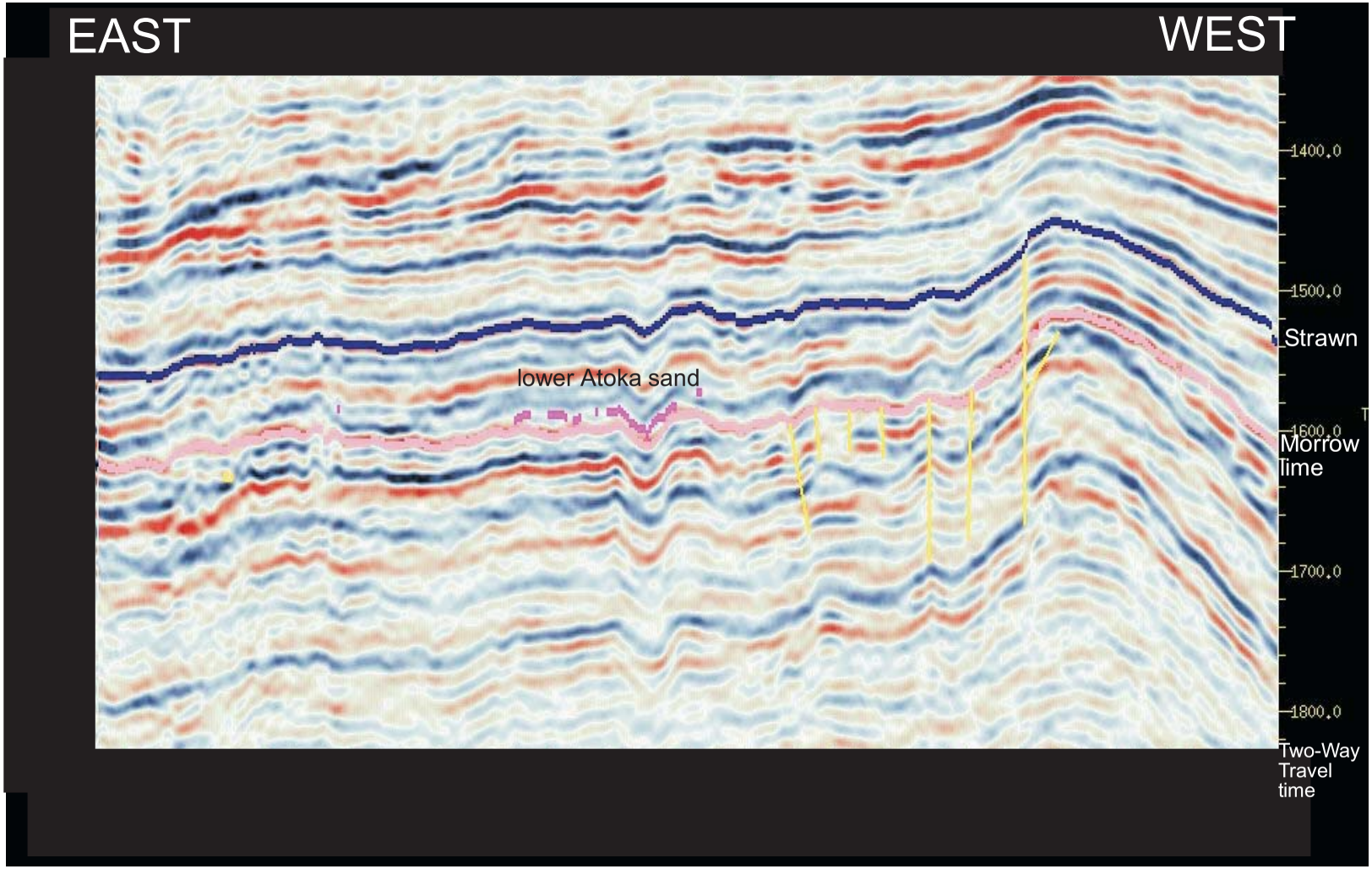

Figure 4.15: Typical vertical east-west seismic profile in NE quadrant focused study area of figure 4.14. Each color line represents top of formations/unit. Morrow Formation (pink), lower Atoka sand (purple) and Strawn Formation (blue) respectively from the bottom.

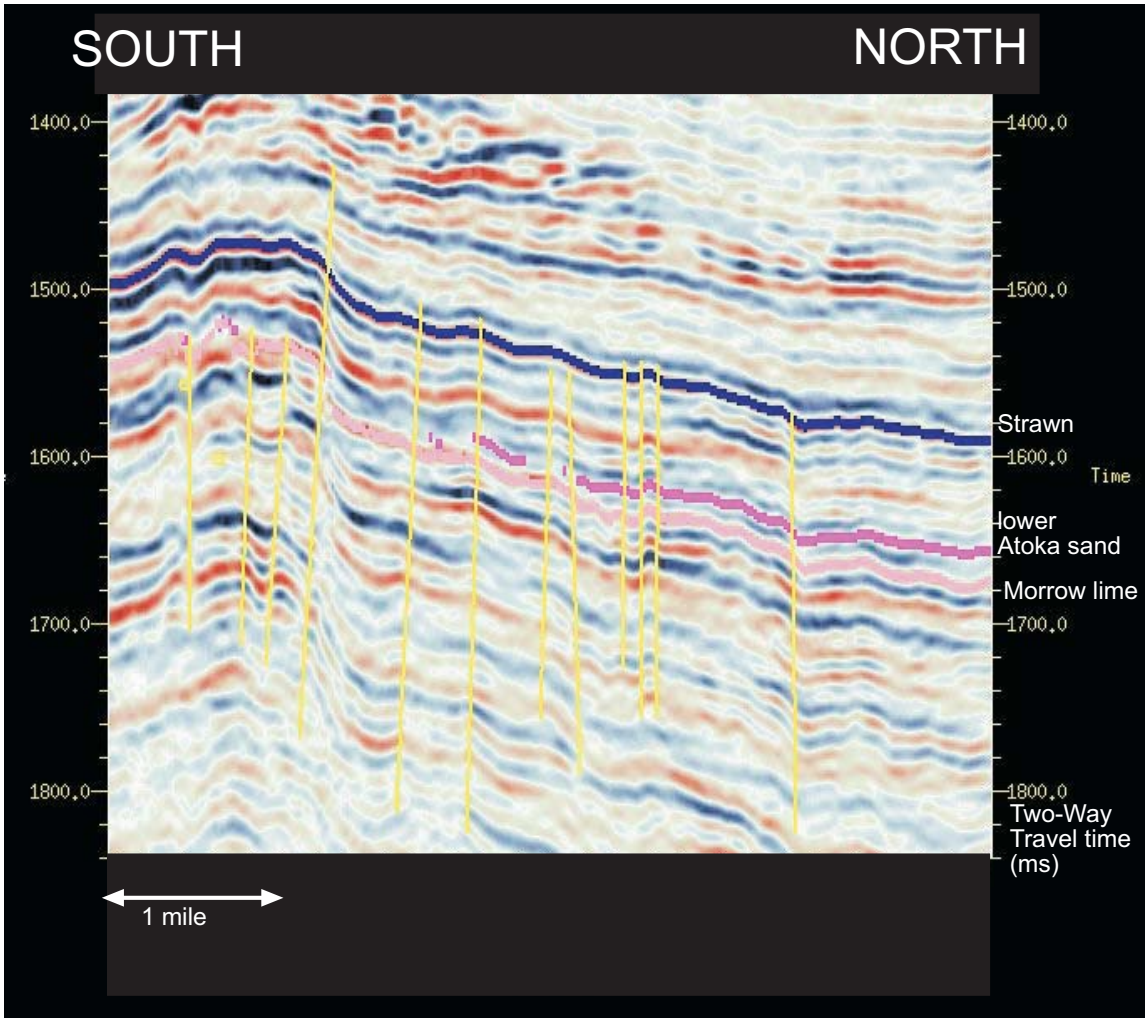

Figure 4.16: Typical vertical north-south seismic profile in NE quadrant focused study area of figure 4.14. Each color line represents top of formations/unit. Morrow Formation (pink), lower Atoka sand (purple) and Strawn Formation (blue) respectively from the bottom.

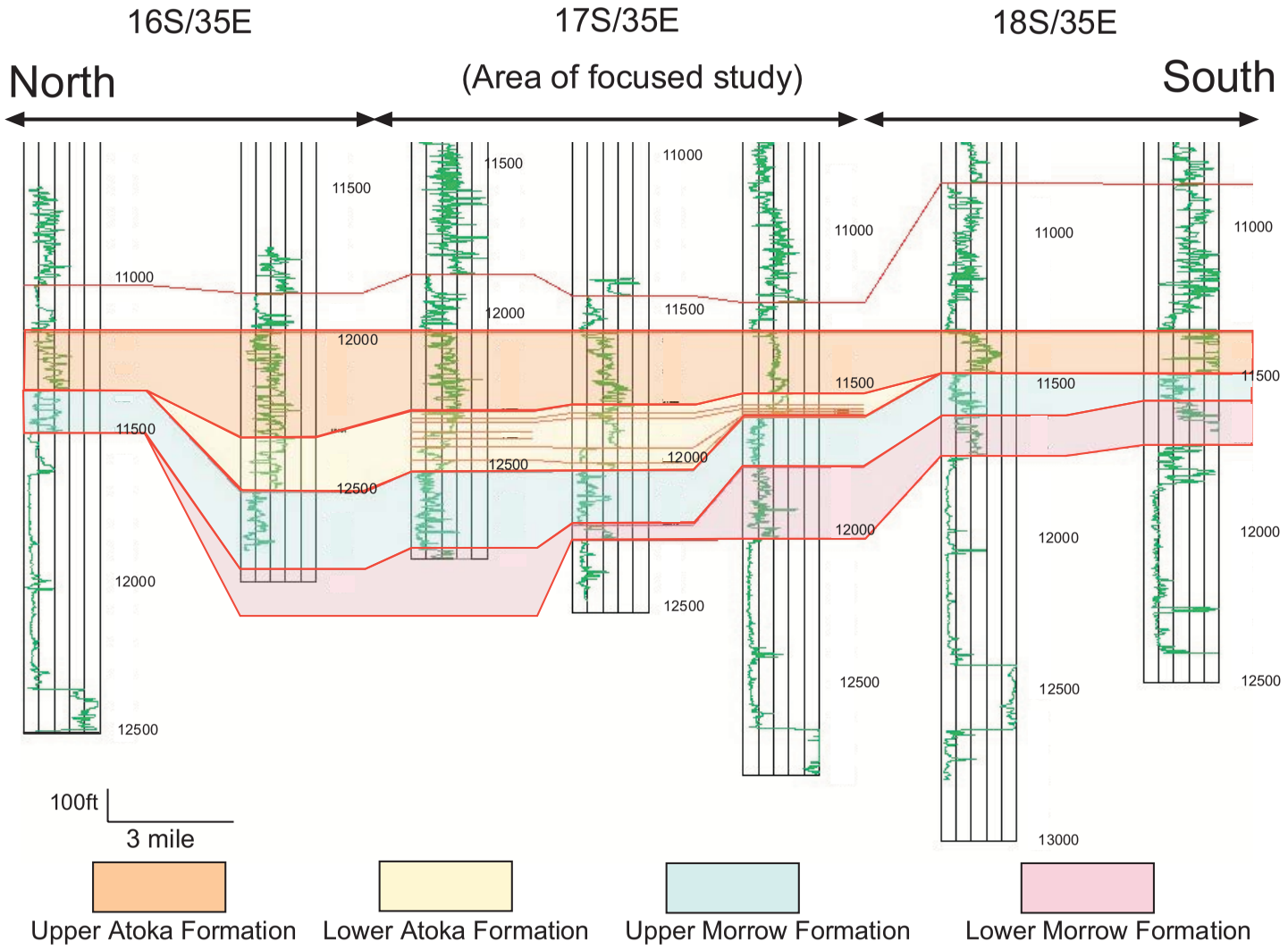

Figure 4.17: North-south simplified cross-section from 16S/35E to 18S/35E demonstrating preservation of lower Atoka Formation in focused study area.
Datum is top of the upper Atoka Formation (base of Strawn Formation).

5. APPLICATION OF SYNTHETIC SEISMOGRAMS FOR PROVIDING GEOLOGICAL CONSTRAINTS TO SEISMIC VOLUME

5.1 Method

Synthetic seismograms provide a bridge between geologic data and seismic data. They are produced from digital well logs to provide location-specific control for direct comparison to seismic data. Because of this, production of synthetic seismograms is one of the essential elements of this research, accomplished prior to seismic interpretation. Great care was taken to generate seismograms that best fit the seismic at a given point. This was not always easy to do because of the apparent phase shift (from zero phase) in the seismic data provided. Also, the lack of vertical velocity characterization at well locations, by vertical seismic profiles or check shot surveys, made it difficult to properly tune the response of the seismic wave modeled by the synthetic seismogram.

Usually, well logs are measured in depth, however, seismic data is in two-way travel time of the seismic wave. Due to the resolution of logs (inches to feet), small changes in lithology can be easily determined, down to the scale of a single bed or smaller. Industry-standard seismic data, on the other hand, tends to have resolution on the order of tens of feet at best. Seismic reflection series are controlled by the velocity, related to density, of a formation's average lithologic characteristics. The velocity character of various different, or even similar, lithologies can be drastically different. Changes in lithology can be masked by particularly fast or slow seismic characteristics of adjacent formations.

Seismic reflection strength of a horizon is referred to as its reflection coefficient, the product of velocity times density. Therefore, if a density log and sonic log are available, a seismic wavelet can be constructed synthetically by convolution (Sheriff and

Geldart, 1999) so that it can be compared directly to the field-acquired seismic data. Usually, the frequency used in acquiring a sonic log is much higher than that used on the wavelet generated by a vibroseis source in the field. This results in mismatching the two (Ewing, 1997; White and Hu, 1998). Checkshot surveys or VSP help to get more accurate correlation between log and seismic (Hardage and others, 1994; Leu and others, 1999). Because of a lack of such control, the synthetic seismograms generated in this study were corrected using software (Hampson-Russell Strata) that artificially plays the role of velocity control by field-based methods.

In the approximately one township area of focused study, there were fifteen wells with logs available of types appropriate for creating synthetic seismograms. Ten wells had sonic-bulk density pairs necessary for calculating the reflection coefficient. The remaining five wells lacked either density or sonic logs. In those wells, pseudo-sonic or pseudo-bulk density logs were generated by the methods described below.

If a density log was not available, but calculated density porosity was available, then a material balance equation was applied for generating bulk density,

$$\phi_{density} = \rho_{ma} - \rho_b / \rho_{ma} - \rho_f$$

where ρ_{ma} is matrix density, ρ_b is log measured density and ρ_f is fluid density.

If no density log (bulk density or calculated porosity) was available but a sonic log existed, or if no sonic log was available but bulk density existed, then the missing log was calculated using Gardner's rule (Sheriff and Geldart, 1999),

$$\text{Velocity} = 357.35 * \text{Density}^4$$

$$\text{Density} = 0.23 * V^{0.25}$$

5.2 Results

In all, fifteen synthetic seismograms were generated and compared to the seismic data. The conformance of the two was evaluated quantitatively by calculating coefficients. Where correlation coefficients were less than 50%, the synthetic seismogram was recalculated using Strata software by modifying the wavelet and/or formation pick. As a result of these procedures, synthetic seismograms with fair to good ties to the seismic data were generated. Table 5.1 shows parameters used in generating synthetic seismograms and the resulting correlation coefficients. Detailed synthetic seismograms are included in Appendix 2. Figure 5.1 is an example of one of the better correlating synthetic seismograms generated by this technique. It is important to note that significant effort was applied to get the results shown in Figure 5.2 and Figure 5.3, but the correlations are fair to good at best, presumably limited by the seismic data being somewhat out of phase. The synthetic seismograms were used primarily as a guide to correlation rather than being rigorously applied.

COMMON WELL NAME	CALCULATION TIME WINDOW	CORRELATION COEFFICIENT
STATE BG1	1190-1590	0.812
BETTY STATE 1	1210-1610	0.784
STATE 27 NO1	1140-1540	0.706
STATE17 COM2	1230-1630	0.76
STATE 17 COM3	1210-1610	0.677
STATE SEC22 COM1	1210-1610	0.724
SHOEBAR STATE COM NO1	1220-1620	0.827
NM "O" STATE NCT-4 NO1	1250-1650	0.602
STATE RIDGE B NO1	1130-1530	0.792
STATE SEC 7	1220-1620	0.516
STATE SEC 6	1250-1650	0.715
SOUTH SHOEBAR15 ST2	1250-1650	0.815
SOUTH SHOEBAR ST4	1280-1680	0.574
SOUTH SHOEBAR 10 ST2	1260-1660	0.803
SOUTH SHOEBAR 10 ST3	1240-1640	0.794

Table 5.1: Parameters used in generating synthetic seismograms and the resulting correlation coefficients of synthetic seismogram generations.

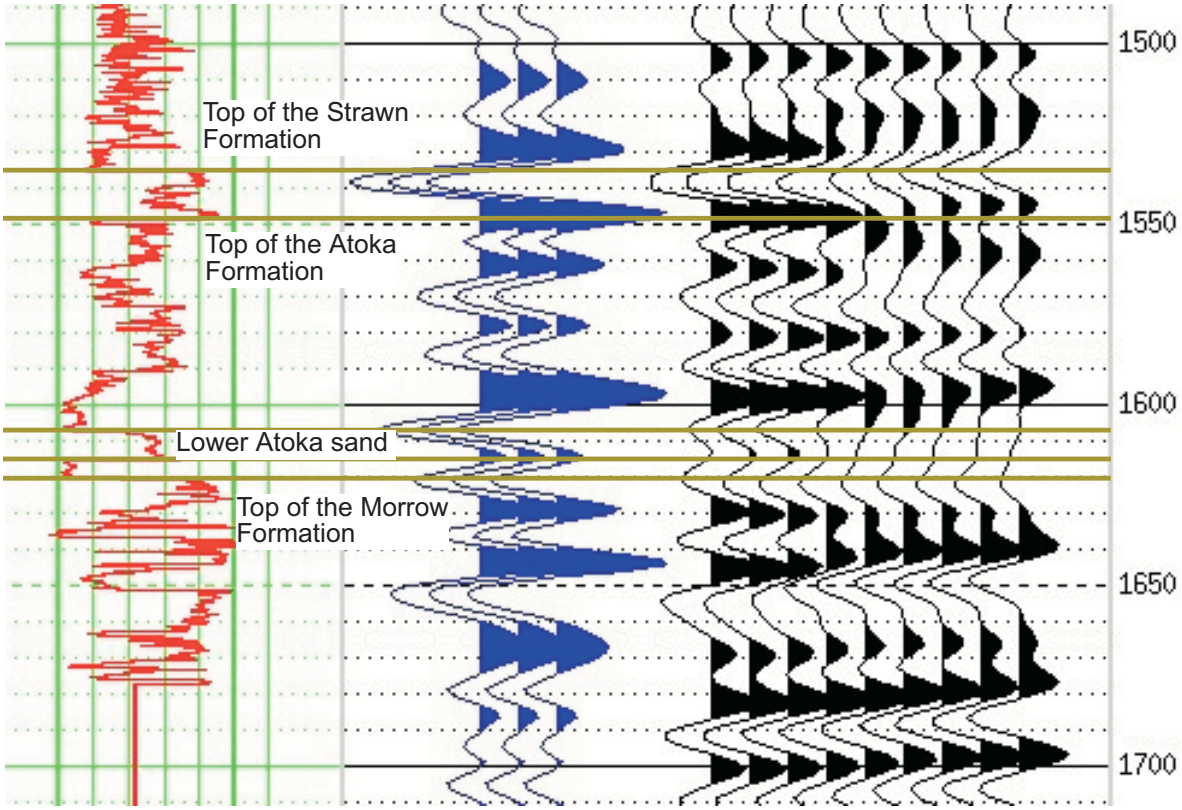

Figure 5.1: An example of synthetic seismogram generation. First curve (red) indicates sonic log, second curves (blue) indicate synthetic and third curves (black) indicate actual seismic data.

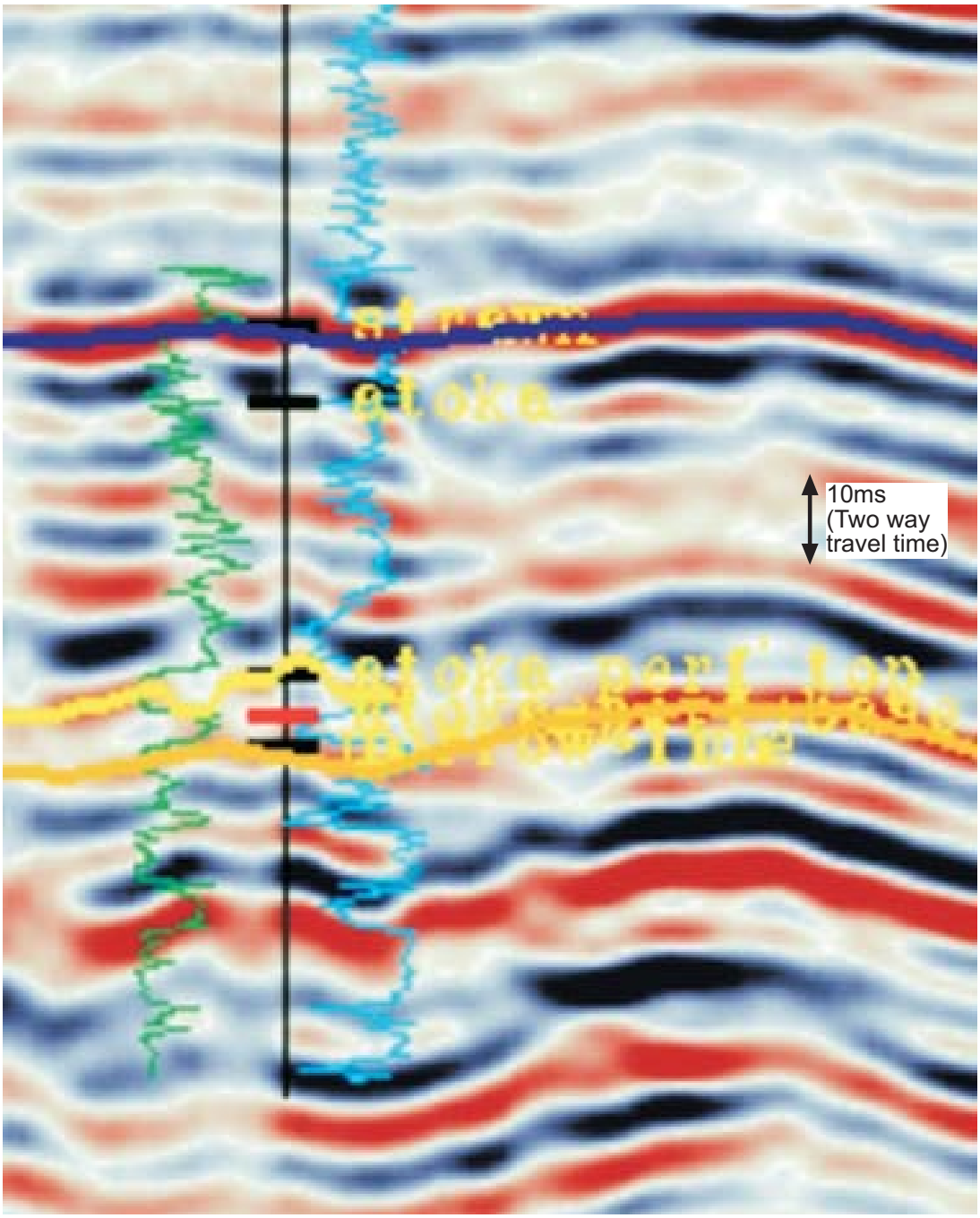

Figure 5.2: The result of determination of formation tops based on synthetic seismogram comparison to seismic data. Strawn Formation (blue line), Atoka, lower sand top (yellow line) and Morrow (orange line) indicated. Green curve shows gamma ray log and light blue curve shows sonic log.

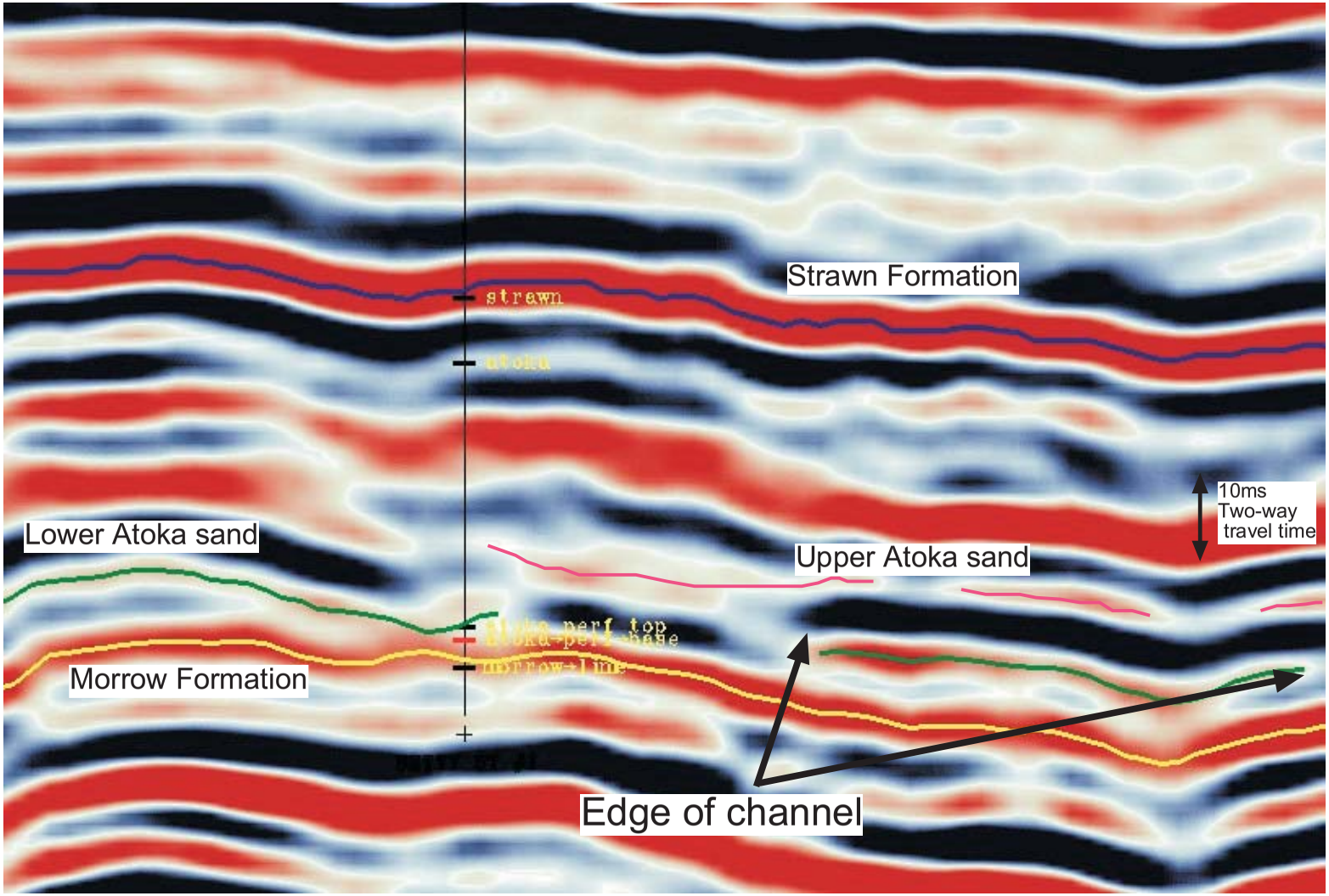

Figure 5.3: Picking interesting formations and intervals on a 2-D vertical seismic profile based on synthetic seismogram. Discontinuous characteristics of sand intervals indicate channel edges.

6. SEISMIC MODEL OF RESERVOIR SANDSTONE BODIES

6.1 Discussion: vertical resolution theory

The synthetic seismogram bridges depth and time. The resulting depth-time conversion is then used to constrain the seismic data. However, vertical resolution of 3-D seismic data is poorer than that of log-derived depth data. It is important to carefully calibrate the synthetic seismogram model considering bed thickness, particularly in fluvial sand bodies (Hardage and others, 1994; Pendleton and Hardage, 1999). Vertical resolution of seismic data depends upon acoustic impedance contrast, bed thickness, and data quality (including signal-to-noise ratio and frequency content; Sheriff and Galdart, 1999; and Brown, 1999). Therefore if these parameters are available, vertical resolution can be derived. Table 6.1 describes interval velocity, travel time, and depth for a sand-body interval in the lower Atoka Formation, derived from the synthetic seismogram model for the State 17 com2 well.

Average velocity, calculated by RMS velocity formula (see below) is used to estimate vertical resolution. RMS velocity can be defined as (Sheriff and Geldart, 1999):

$$V^2 \text{rms} = \sum_i Vi^2 \Delta t_i / t$$

Applying this equation to Table 6.1, the result is 11673.55 ft/sec. This value, divided by frequency yields a wavelength value ($\lambda = v/f$). The frequency extracted from wavelet data, from 1230 ms to from 1630 ms, ranged from 20 Hz to 90 Hz with mode of 65 Hz (Fig 6.1). Based on 65 Hz and an assumption of either 1/4 λ, vertical seismic resolution can be estimated to be 45ft (15 m). Below this limit, resolution of thinner beds requires modeling to account for thin-bed tuning effects.

TVD	Vi	TWT	Time interval
11956	11062.8	1601.169	
11962	11753.2	1602.169	1
11698	12038.2	1603.206	1.037
11974	12145.3	1604.199	0.993
11980	11846.7	1605.202	1.003
11986	11677.8	1606.218	1.016
11992	11907	1607.237	1.019
11998	12226.9	1608.238	1.001
12004	12145.3	1609.231	0.993
12010	9051.9	1610.265	1.034

Table 6.1: interval velocity and time and depth within production interval derived from synthetic seismogram model of State 17 com2. TVD is Total Vertical Depth. Vi is interval velocity. TWT is Two Way Travel time.

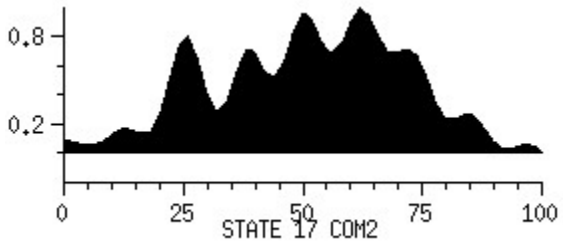

Figure 6.1: Frequency range extracted by seismic trace on State 17 com2. X axis indicates frequency. Y axis indicates intensity of frequency.

6.2 Two-Dimensional vertical bed thickness modeling

Two-dimensional (2-D) synthetic seismic modeling is an essential step to match seismic wavelets and their lateral changes to geologic bodies and their physical properties (Galloway et al, 1977). In order to observe lateral change in amplitude associated with changes in lateral thickness of sand bodies, 2-D synthetic seismic modeling is required (Moore and Shipley, 1993; Tobin et al, 1994). For this study, GXII software was used to model the Atoka sandstone channel-fill bodies. In the case of the study area, lower Atoka sand-filled channels cut down to just above the Morrow lime, but there is an intervening shale in all wells drilled to date. Figure 6.2 shows a double wedge multi-layer model, where sand is enclosed by shale and thickness of the sand ranges from 0 to 150 ft (0 m to 45 m). Formation parameters (e.g. velocity, density) were determined by the average values measured from log data (Fig 6.2). To model this geological scenario, 50 traces were calculated at zero offset.

Figure 6.3 describes the result of the 2-D synthetic seismic model. Beginning at about 20 ft, the sandstone becomes resolvable as an extra trough. Thinner beds cause interference in the wavelet and do not have predictable seismic character. Figure 6.4 is a simple model generated from synthetic seismograms that demonstrates the same characteristics. In both models, thicker sands are easily detected by their strong amplitude. Conceptually, vertical resolution is calculated as 45ft based on the 1-D modeling (1/4 λ). However, vertical resolution on the 2-D modeling demonstrates about 20ft. It results from the relationship between bed thickness and acoustic impedance contrast, and thus causes higher vertical resolution than the conceptual result (Fig 6.5). These beds may cause a weaker amplitude of the Morrow beneath them due to

interference of the wavelets. On the other hand, if there is no sand, or thin sand, above the Morrow lime, then Morrow amplitude is much stronger because of no wavelet interference. This exercise has demonstrated that if the lower Atoka Formation sandstone bodies are 20 or more feet thick, they may be resolved on seismic data and can be mapped on the basis of picking the resulting extra trough or by mapping changes in Morrow lime amplitude.

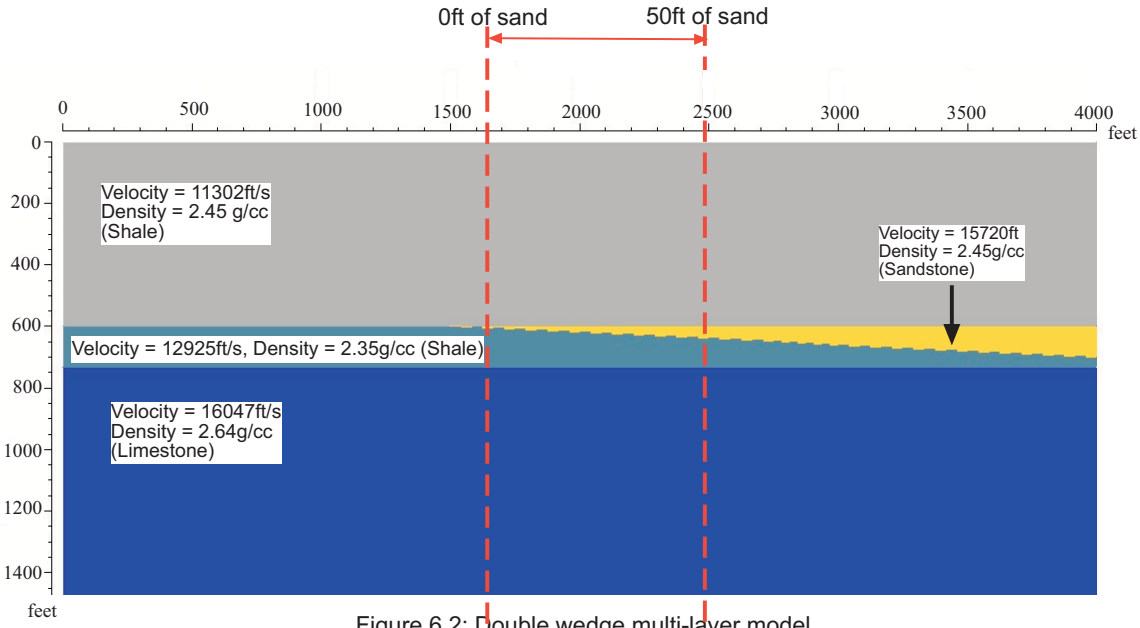

Figure 6.2: Double wedge multi-layer model

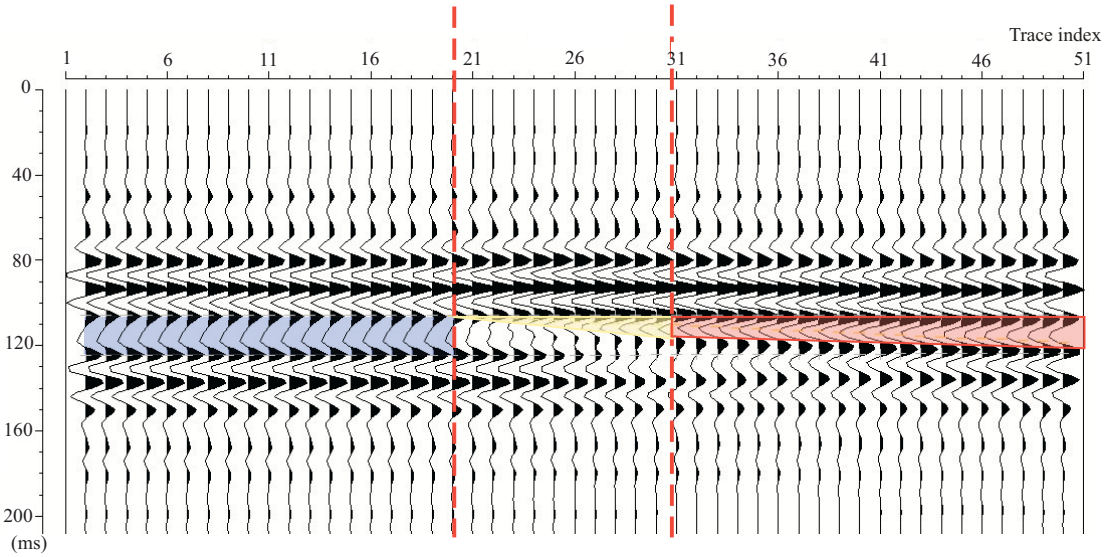

Figure 6.3: Synthetic seismic model based on the double wedge multi-layer model

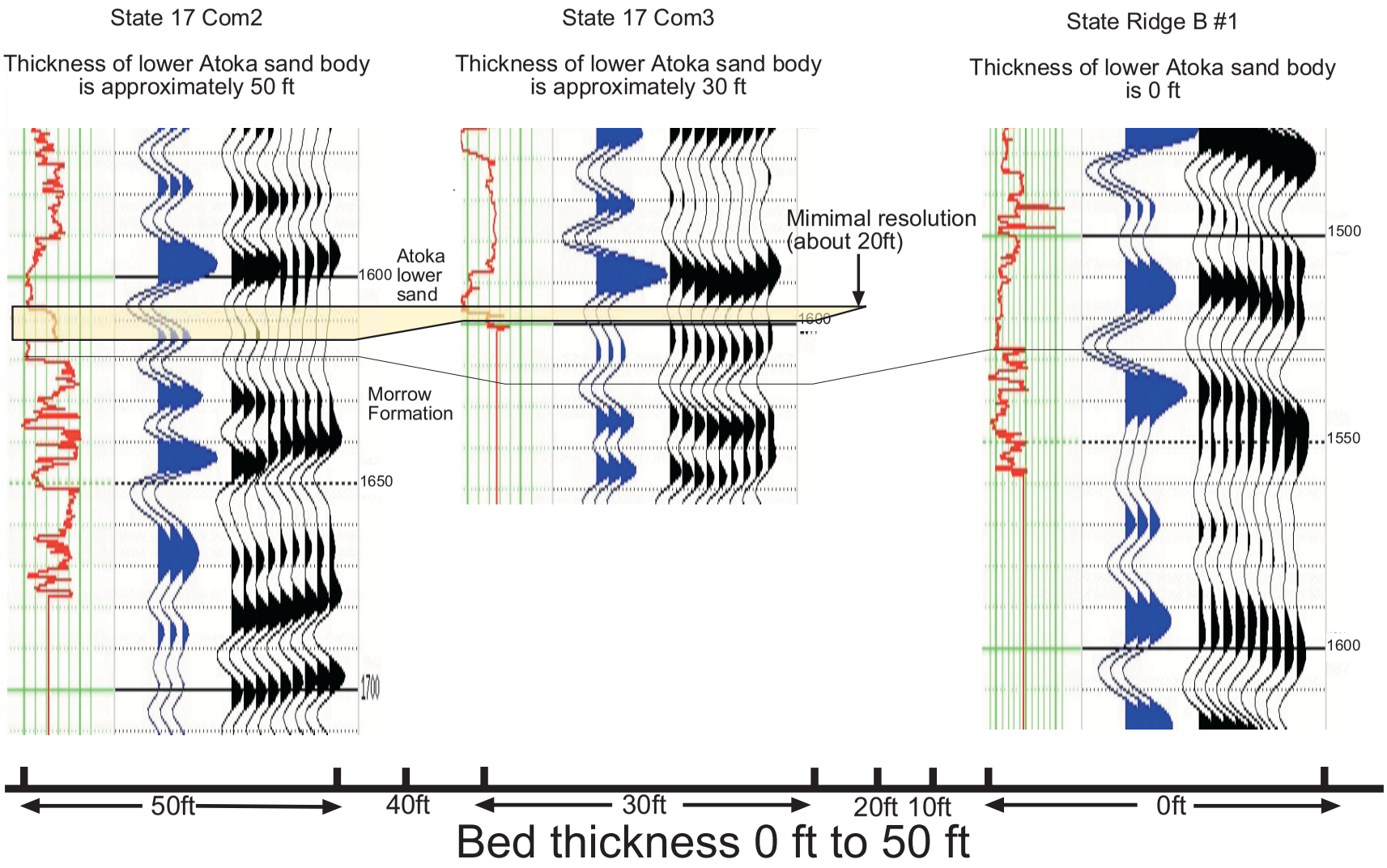

Figure 6.4: Synthetic seismogram modeling based on the log data. Extra trough can be recognized when thickness of sand body exceeds 20 ft.

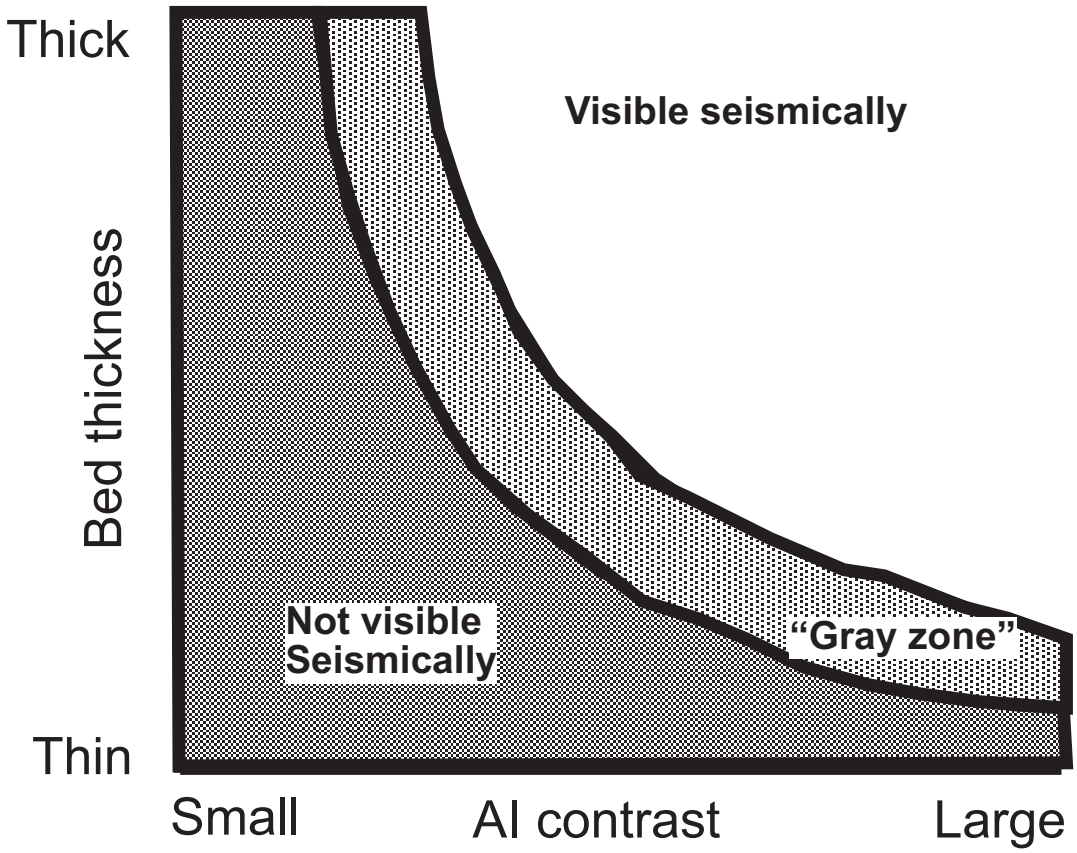

Figure 6.5: Conceptual diagram indicating how thickness and acoustic impedance (AI) contrast interact to determine whether a bed will be resolved seismically. Adapted from Meckel and Nath (1997).

7. BASIC SEISMIC INTERPRETATION

7.1 Method of mapping seismic horizons

A seismic horizon represents arrivals of energy that vary systematically from trace to trace and are believed to represent reflected energy (Sheriff and Geldart, 1999). Any continuous reflection in the seismic volume can be mapped as a horizon, however, only some of these might have real value in solving the specific problems addressed in this thesis. Seismic horizons do not necessarily correspond to major lithology changes, nor do they resolve thin beds (as discussed in Chapter 6). However, sometimes fairly subtle changes in petrology, porosity or fluid content can cause reflections that might be mapped as horizons. In some cases, sequence boundaries or other surfaces may cause a reflection and be mapped as a horizon (Miail, 1997). Often, seismic horizons may exist due to interference/tuning effects and not represent anything geological (e.g. multiples); this is a common pitfall in seismic interpretation (Hart, 1998). In this study, geology was integrated into the interpretation of the seismic volume in order to best understand and recognize the important seismic horizons for mapping Atoka Formation sandstones.

Based on stratigraphic and lithologic analysis, the most important seismic horizons that bracket the Atoka Formation are reflections corresponding to the top of the Strawn Formation limestone (in the lower Strawn) and the top of the Morrow Formation limestone (top of the Morrow). Other significant horizons mapped were the top of lower Atoka (nonmarine-marine change) and the tops of lower Atoka sand units that were seismically resolvable. In some areas there is a seismically mappable upper sand and/or lower sand where these sands are thick enough to be seismically resolvable.

Seismic horizon mapping is accomplished by "picking" the peak or trough or other part of the wavelet in a reflection (horizon) that corresponds to the surface being mapped. Figure 7.1a is an example of how this process develops. For this project every 10^{th} line profile and every 10^{th} crossline profile was picked manually using synthetic seismograms as a guide. The computer was then allowed to "autopick" between the manually-picked lines using an interpolation algorithm (Fig. 7.1b). If the results are not acceptable within geologic constraints, additional lines are picked in the questionable areas. Results are expressed as presence/absence maps, time structure maps which approximate depth-structure maps, or between-time-horizon interval (isochron) maps which approximate isopach maps.

7.2 Horizon mapping results

Due to the strong acoustic impedance contrast at the top of the Strawn limestone and Morrow limestone (shale above limestone), these two formations yield very strong amplitude reflections that are readily mappable seismic horizons. Each top of formation consists of carbonate. On the other hand, the top of the Atoka formation is not represented by a mappable reflection. The top of lower Atoka (nonmarine-marine contact) is roughly mappable as a seismic horizon. Only the thicker sand bodies in the lower Atoka are mappable.

Morrow limestone horizon: The time structure map of the Morrow (Fig 7.2) is continuous across the study area. Due to strong acoustic impedance and lateral continuous extent, the Morrow limestone horizon can be mapped over the entire survey area. It is complexly faulted in the center of the survey area, where it is structurally high

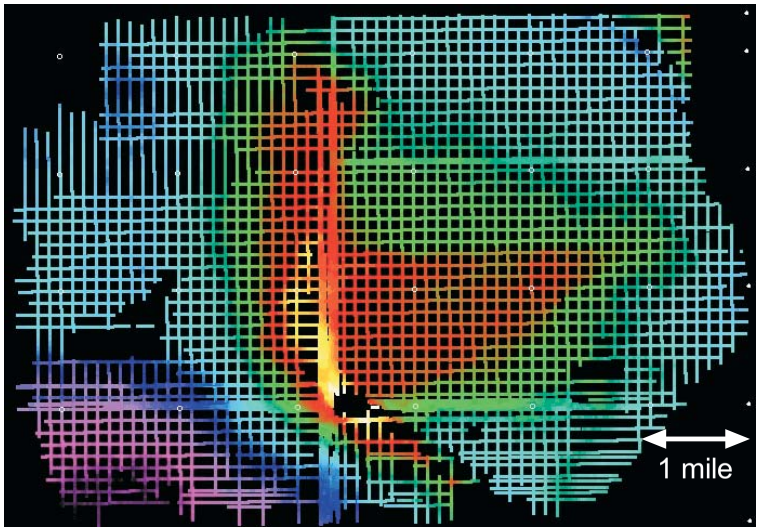

Figure 7.1a: Horizon time structure map after picking seed lines.

N

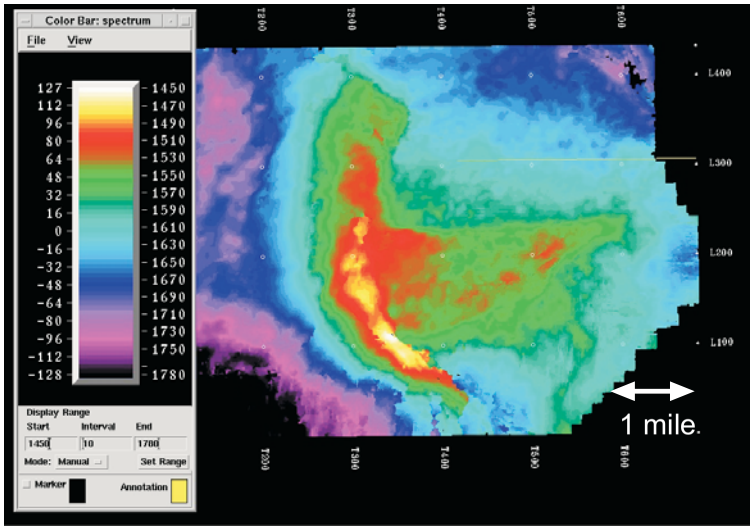

Figure 7.1b: Horizon time structural map after applying an interpolation algorithm. Hot color indicates shallow time “depth”, cold color indicates deep time “depth”.

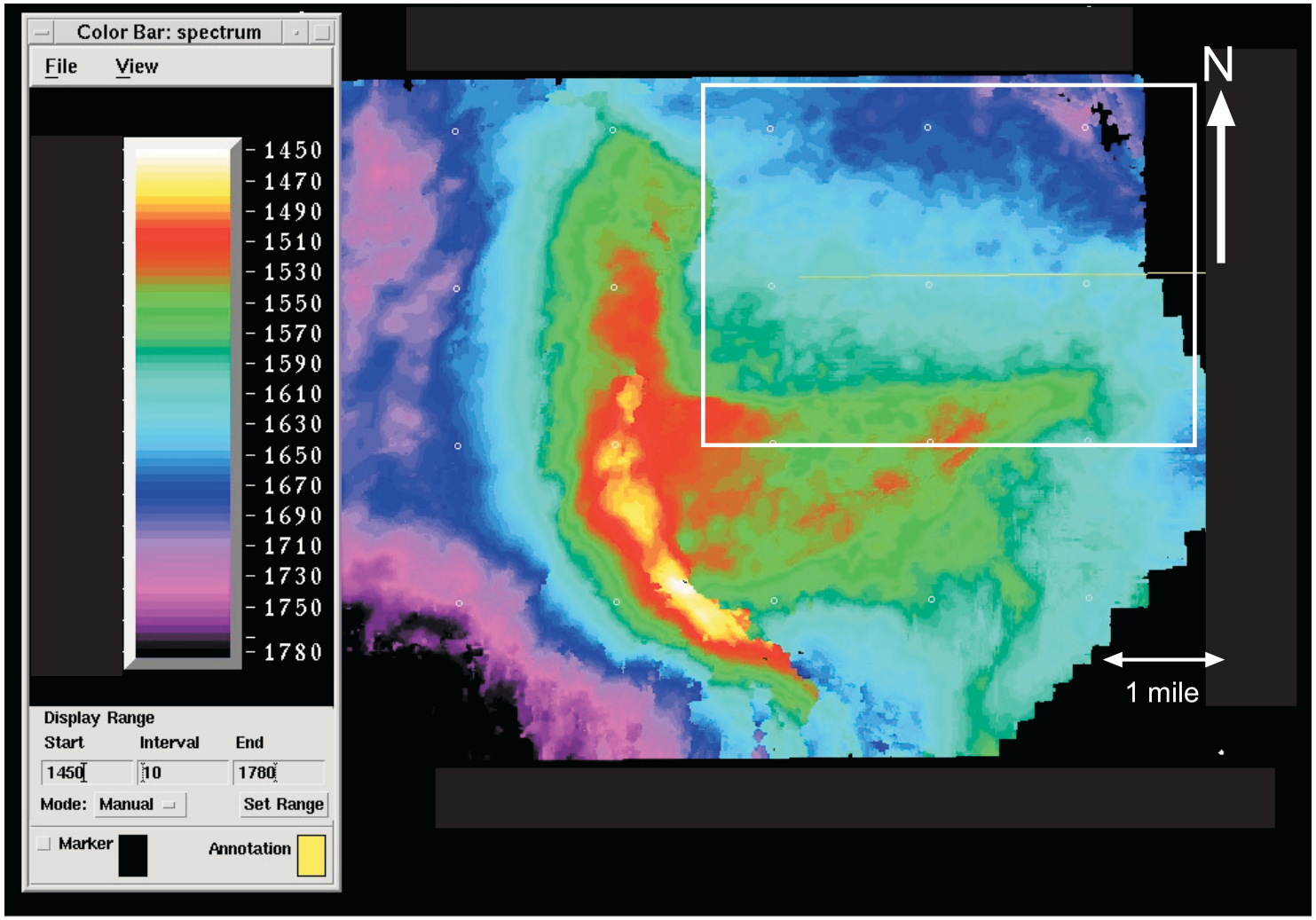

Figure 7.2: Time structure map of the Morrow Formation, larger area of study. White rectangle indicates approximate focused study area. Units in spectrum color bar are in Two-way travel time (ms).

with a boomerang shape. Faults trend mainly north-south and east-west. The Morrow tends to be more steeply dipping on the west side of the seismic volume than on the east side and south side.

Lower Atoka, lower sand horizon: Figure 7.3 shows the time structure of the lower Atoka, lower sand. The map was generated by tracking every inline and crossline in the northeast quadrant because apparent absence or thinness of the sand in many areas resulted in no pickable horizon or acoustic impedance contrast. Hence, there is a possibility that the channel sands exist, even though seismically it is not resolvable. In general, the horizon dips toward to northeast. Two major, wide, incised, channel belts are identified on Figure 7.3. One is northeast-trending in the east half of the map. The other is north-northwest-trending on the west side of the map. There is a large area of sand between that appears to be stratigraphically higher than the channels, which may represent migration of the channel systems out of the confining channels as the system aggraded above the level of channel incision (Figs. 7.4 and 7.5).

Lower Atoka, upper sand horizon: The lower Atoka, upper sand was also mapped by picking every line and cross-line in the study area (Fig 7.6). The upper sand tends to have strong channel system characteristics on the time structural map. The thickness of the upper sand is generally less than that of the lower Atoka sand. Therefore, it has weak acoustic impedance contrast, probably due to wavelength interference. The general trend of the channels is northeast. The channels of the upper sand are much more distinguishable than that of the lower sand because they are narrower and separated by areas of less or no sand. The area between the channels is assumed to be flood plain deposits (overbank deposits) or thin sands below the thickness required for

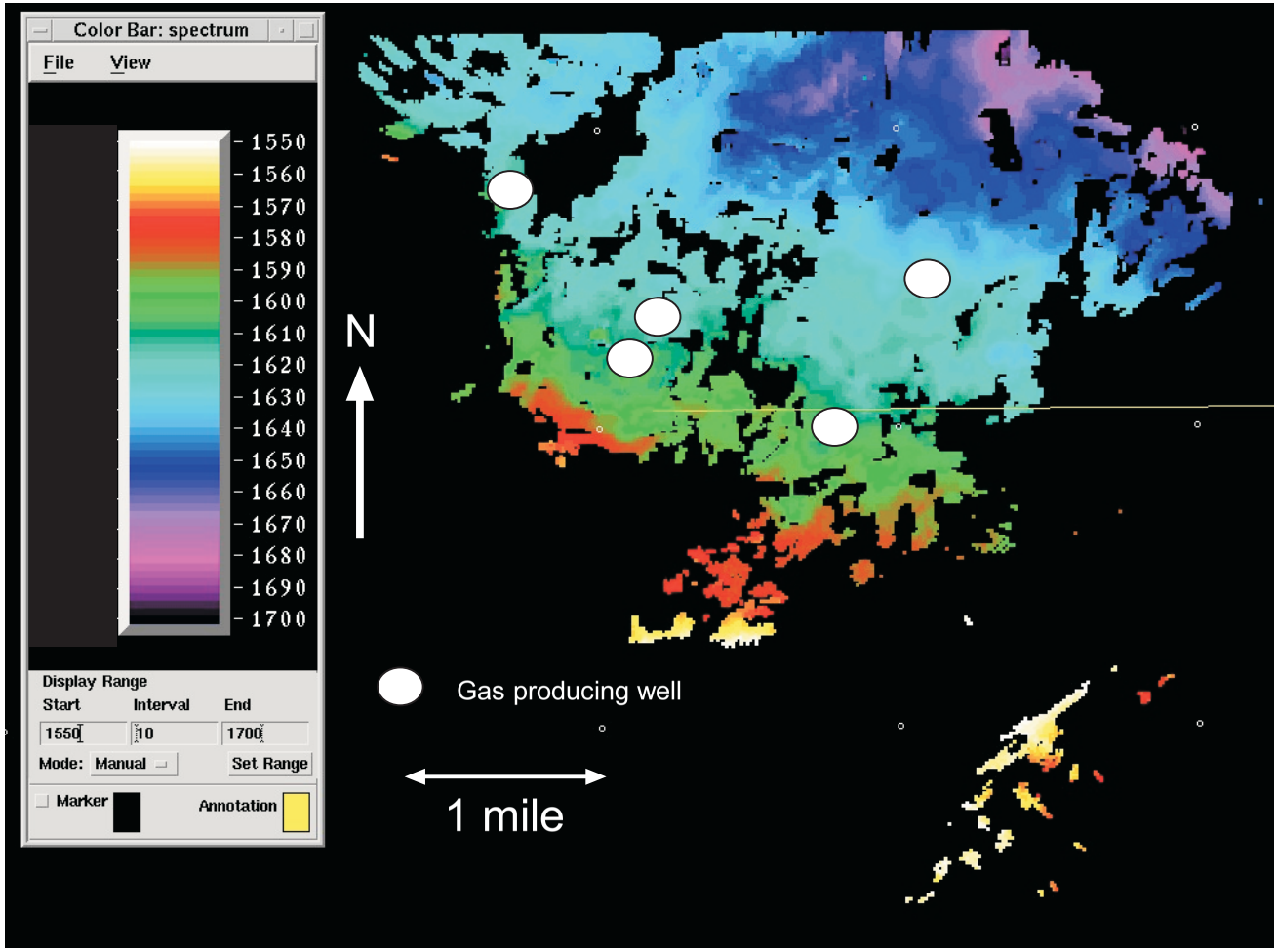

Figure 7.3: Time structural map of the lower Atoka sand focused study area. Note, apparent absence of sand where thin (seismically invisible) or non-existent. Ellipse shows major gas producing well locations. Units in spectrum color bar are in Two-way travel time (ms)

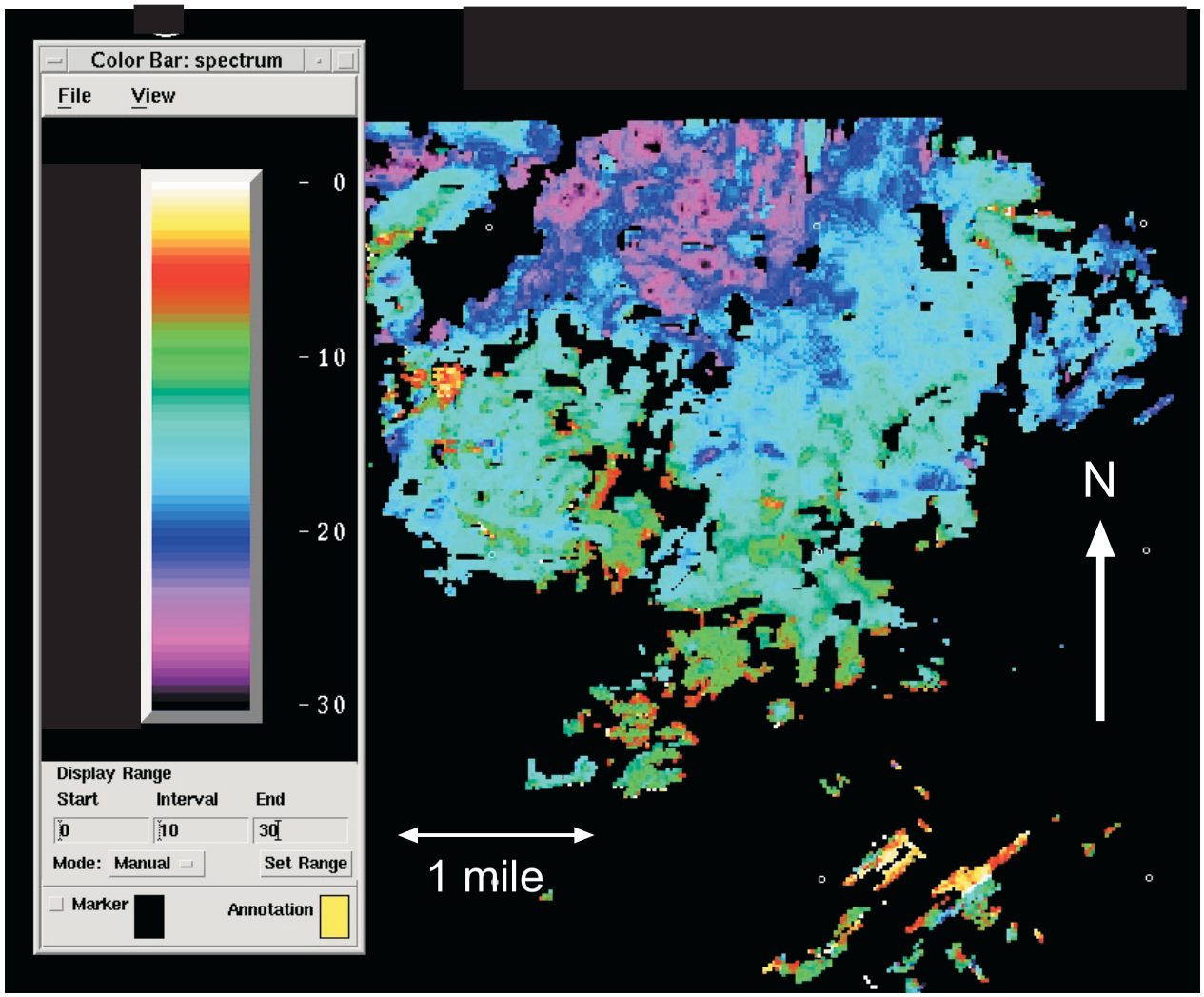

Figure 7.4: Isochron map between lower Atoka sand and top of the Morrow Formation focused study area. Units in spectrum color bar are in Two-way travel time (ms).

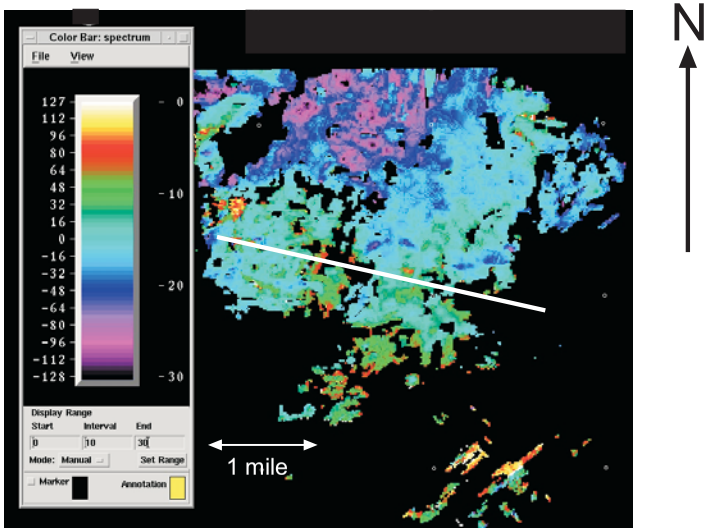

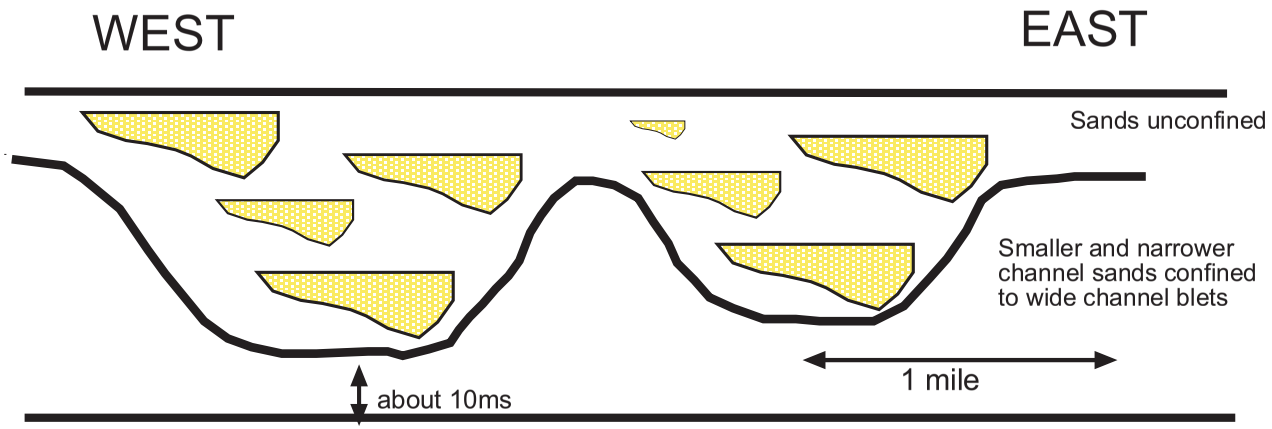

Figure7.5: Schematic diagram of isochron map of figure7.4. Shallow thickness on the isochron map indicates channel belt incising into Atoka marine shale.(white line shows cross section for this diagram)

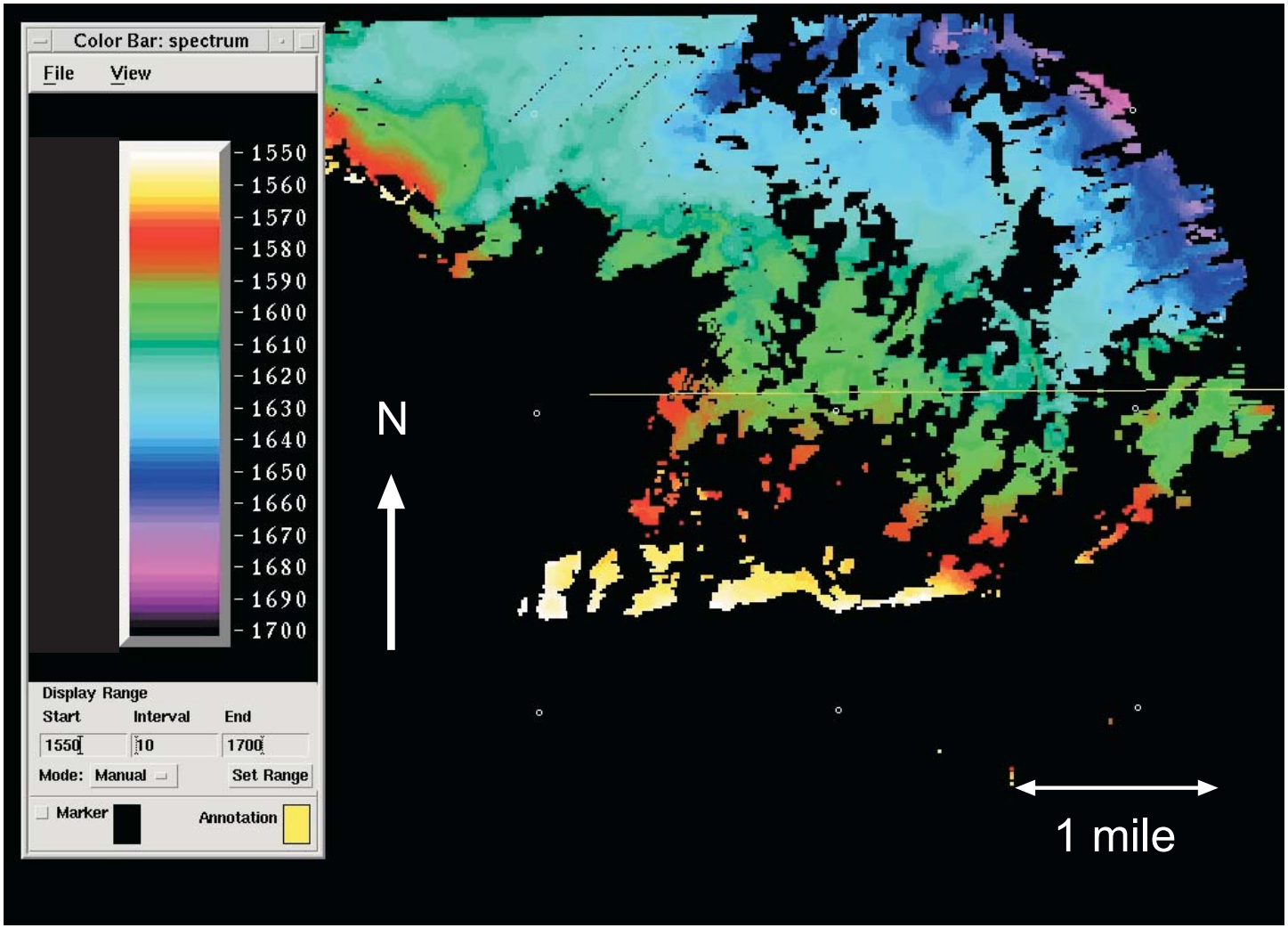

Figure 7.6: Time structure map of the upper Atoka sand focused study area.
Note, apparent absence of sand where thin (seismically invisible) or nonexistent.
Units in spectrum color bar are in Two-way travel time (ms).

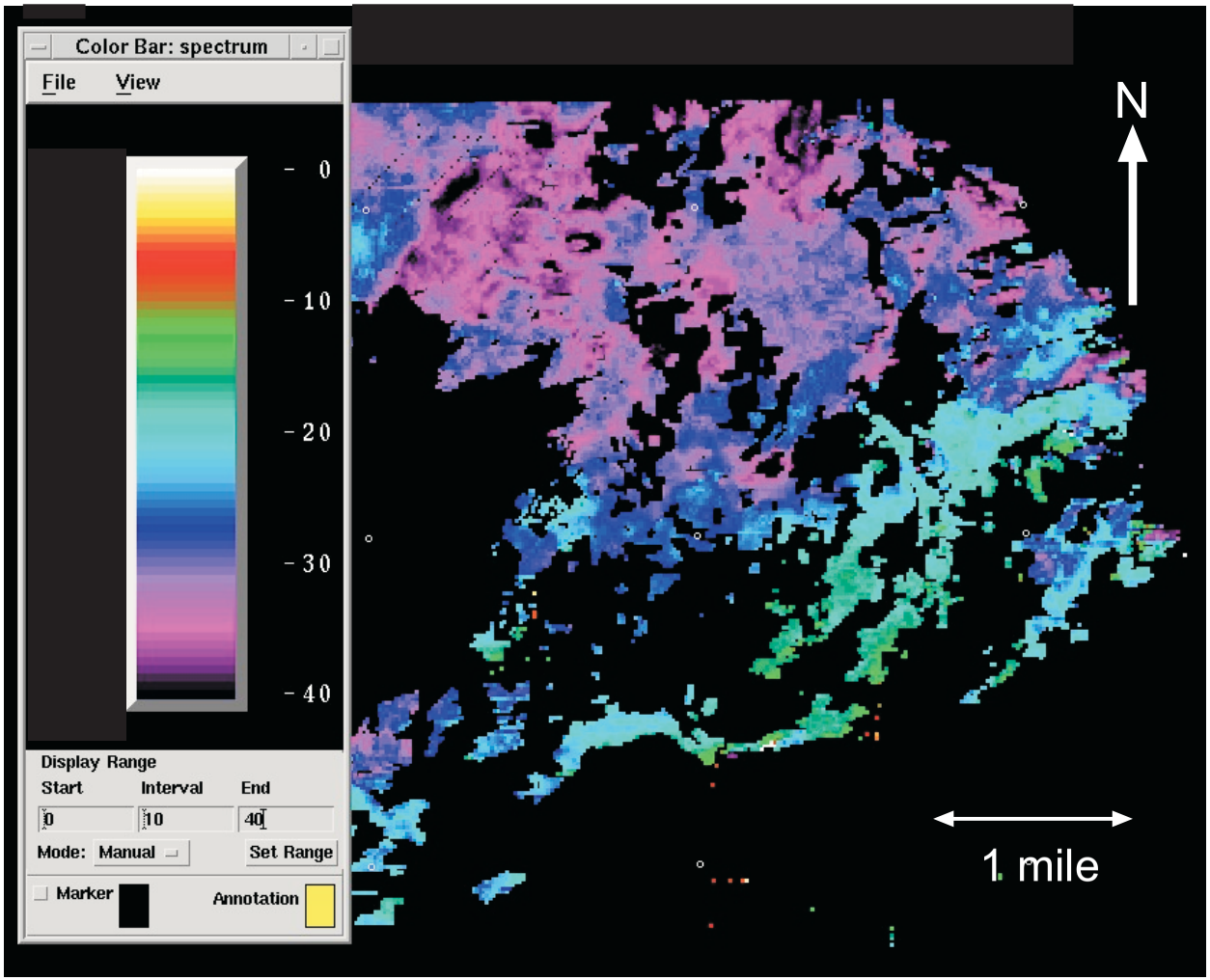

Figure 7.7: Isochron map between upper Atoka sand and top of the Morrow Formation focused study area. Units in spectrum color bar are in Two-way travel time (ms).

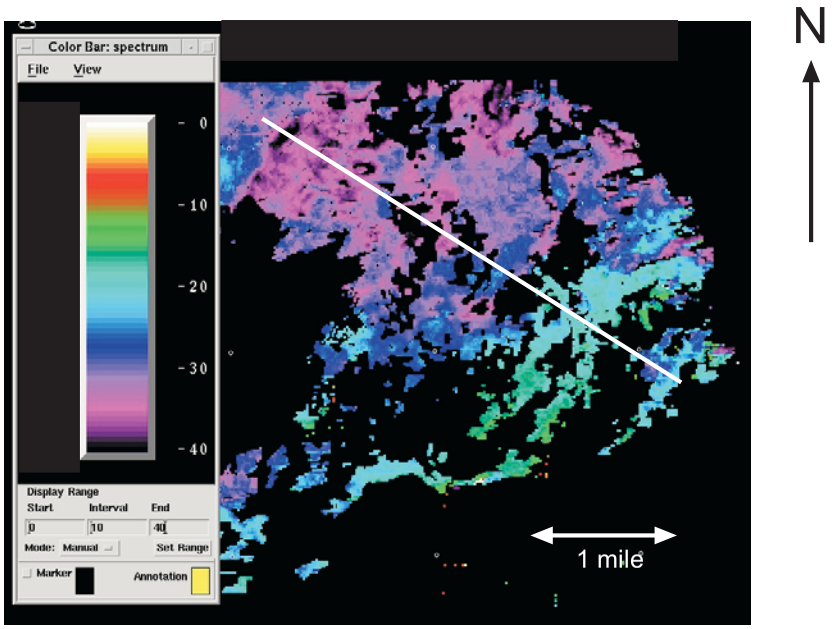

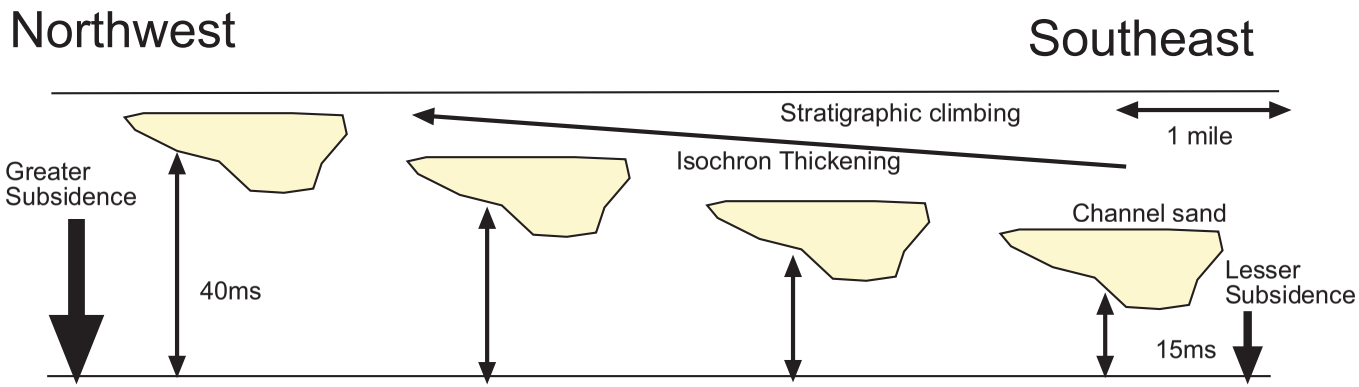

Figure 7.8: Simple schematic diagram of lateral migration of channels. They migrate to northwest (young channel) from southeast (old) (white line shows cross-section for this diagram).

resolution. Four curving channels are illustrated in Figure 7.6. It is assumed that lateral channel migration is responsible for these parallel channels, supported by the observation that the upper sand horizon climbs stratigraphically northwestward, possibly suggesting syndepositional northwest tilting. (Figs.7.7 and 7.8).

Strawn limestone horizon: Figure 7.9 shows the time structure map of the Strawn Formation limestone. Similar to the Morrow horizon, the Strawn horizon is mappable over the entire survey area due to strong acoustic impedance and laterally continuous extent. It is less complexly faulted than the Morrow Formation, indicating that faults were active during the Atokan. The major fault trend is the same as the time structural map of the Morrow Formation, north-south and east-west. Like the Morrow horizon, the Strawn horizon appears to dip more steeply on the west side of the seismic volume than on the east and south sides.

7.3 Fault-pattern mapping methods

Faults and other structures can be, but are not always, readily identified on time structure maps. Ability to resolve faults is limited to the time (depth) of the strata being faulted and the resolution of the seismic volume determined by quality of the data. There are several methods to detect faults on the seismic data volume (Brown, 1999). A horizon time structure map sometimes reveals general structural trends if vertical displacement on the faults is large enough to detect on the horizon time structural map. For example, the time structure map of the Morrow Formation (Fig 7.2) depicts a highly faulted high structure in the center of map. An amplitude vertical profile or amplitude horizon extracted map also reveals faults by amplitude variation with linear character (Enachescu, 1993). Conventional amplitude time slices are generally helpful to detect

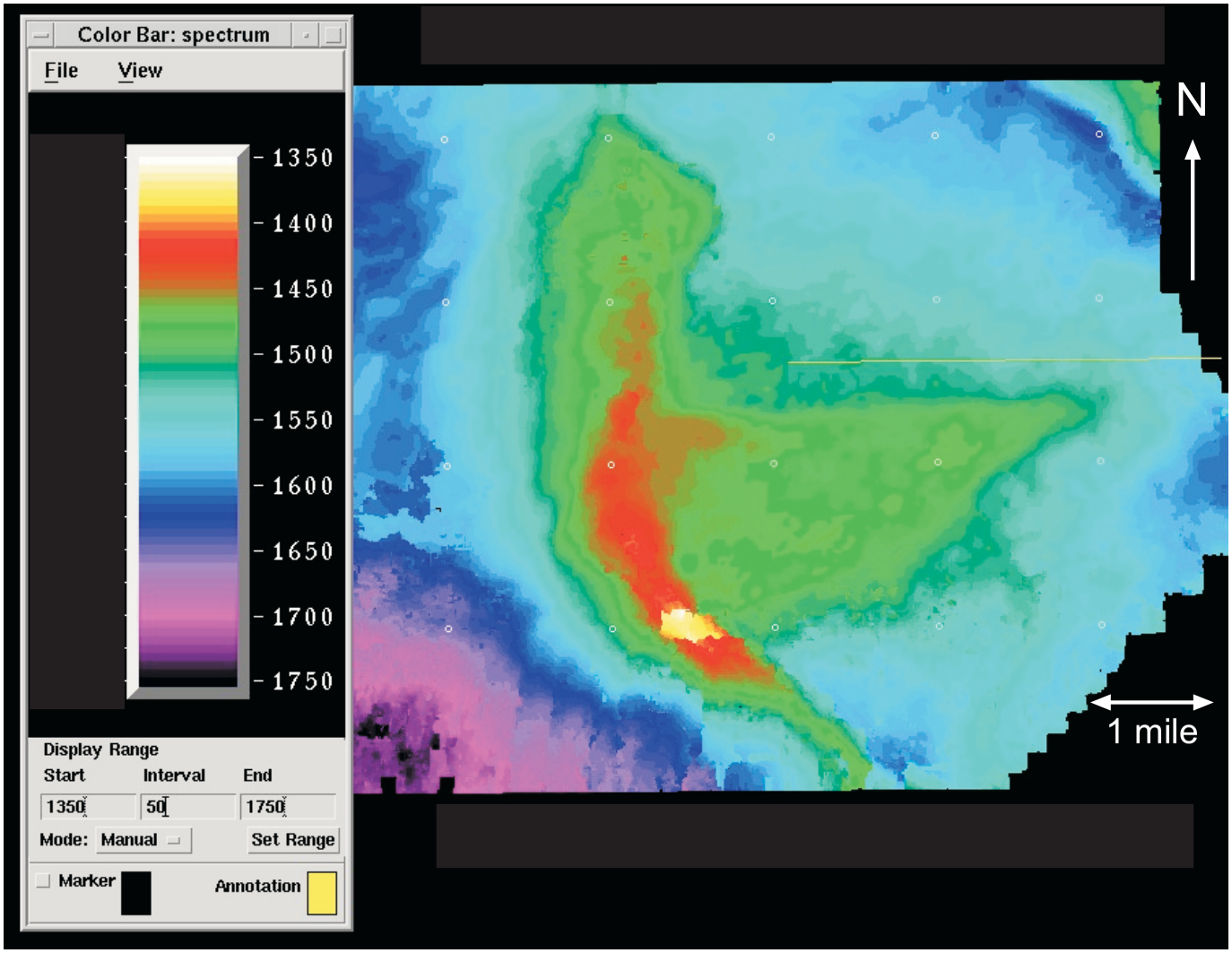

Figure 7.9: Time structural map of the Strawn Formation, larger area of study. Units in spectrum color bar are in Two-way travel time (ms).

faults though, in the case of faults parallel to strike detection is difficult because fault lineaments tend to be superimposed on bedding lineaments (Bahorich and Farmer, 1995). The coherency algorithm reduces laterally consistent characteristics, in effect removing the bedding. Figure 7.10 is a lower Atoka Formation time slice map where coherency analysis was applied.

7.4 Fault pattern mapping results

Figure 7.10 illustrates faults recognized on the coherency map. Fault trends are primarily north-oriented in the center of the map. On the east side of the map, there is a relatively major fault (see time-structure maps above) that is east-trending. These fault systems bound the boomerang-shaped high illustrated on time-structure maps.

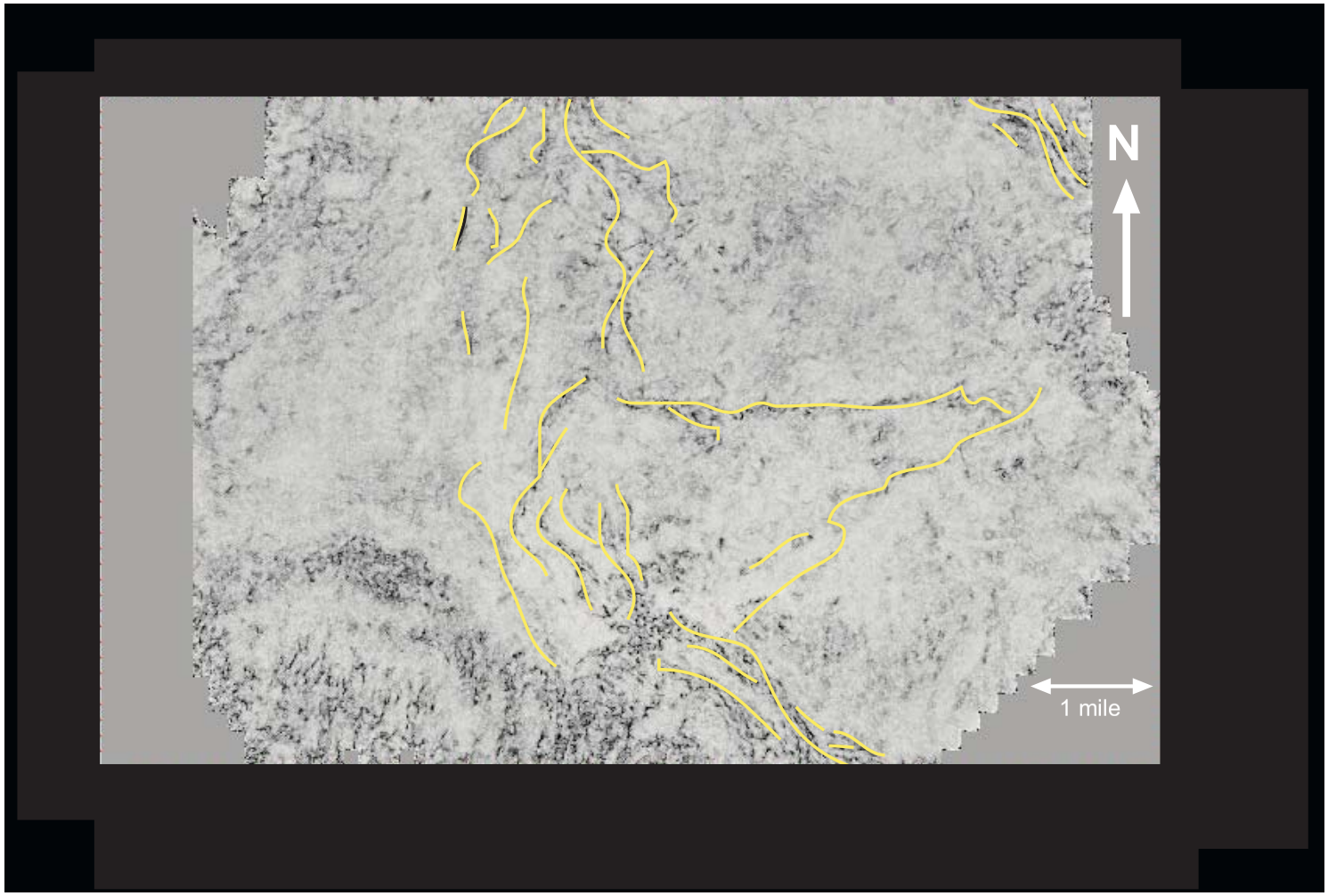

Figure 7.10: Fault recognition on the coherency analysis map, larger area of study. Yellow lines indicate major faults.

8. ADVANCED SEISMIC INTERPRETATION OF RESERVOIR

Advanced seismic interpretation goes beyond automated basic interpretation in that advanced methods are used to find and map subtle geological features and the interpreter must use more geological insight into the problem to be solved. The two methods to be discussed here are coherency analysis and attribute analysis. Coherency analysis measures the lateral continuity/discontinuity of seismic reflections. It is useful for both stratigraphic analysis (e.g. edge of channels) and structural analysis (e.g. fault offsets of beds/reflection horizons). Attribute analysis investigates physical properties of seismic waves, such as amplitude, phase and frequency. Trial-and-error was used to determine that, for the subject data set, amplitude attribute analysis was most useful, whereas most other attributes did not contribute unique results. Both coherency and amplitude attribute mapping were extremely useful in mapping the channels and channel belts in the lower Atoka.

8.1 Coherency analysis for identifying channelized reservoirs

8.1A Method

Coherency analysis is one of the best analytical methods for detecting channelized sandstone reservoirs (Bahorich and Farmer, 1995; Wescott and Boucher, 2000). Coherency is the lateral continuity of a correlated reflection, on a trace-by-trace analysis. For detailed discussion of coherency analysis concepts, see Appendix 3. For analyzing coherency in the 3-D seismic data, PostStack ESP (Event Similarity Prediction) FScan 3D, which is one component of the Landmark Graphics software package, was used. The software measures the levels of dissimilarity of windowed traces.

In order to reduce processing time, coherency was analyzed in only the focused study area. Because the Atoka sand is relatively thin, a narrow time and lateral trace window was chosen to find subtle continuity changes in the sand-equivalent reflection. Maximum dip search on adjacent traces was used to trace vertical changes in continuity. In addition, for removing structural effects on the coherency output, the Morrow formation was flattened at 1700 ms and numerous relative time slices were generated (Appendix 3) based on this datum. After these processes were performed, horizontal slice images were enhanced by removing noise, which smoothes the data and emphasizes dissimilarity. A total of 23 time slices were generated by this procedure spaced every 2 ms from 1700 ms (top of flattened Morrow) to 1656 ms. See Appendix 3 (only 20 time slices) for the complete set.

8.1B Results

Coherency analysis delineates not only larger-scale channel features that were evident from horizon structure and isochron mapping, but also the complex internal features within these channels. As an example, Figure 8.1 is a coherency time slice at 10 ms above the flattened Morrow horizon reference datum which corresponds to the base of the lower Atoka, lower sand horizon. An obvious interpretation of this map is that within the boundaries of a channel belt, are "wormy", meandering smaller channels. The ability to image this degree of complexity is quite remarkable and is repeated in subsequent time slices (see Appendix 3).

Figures 8.2 and 8.3 are two time slices through the lower Atoka, upper sand horizon. Figure 8.2 shows an older channel on the east side of the map, whereas Figure 8.3 shows a younger channel to the west. Therefore the fluvial system axis migrated

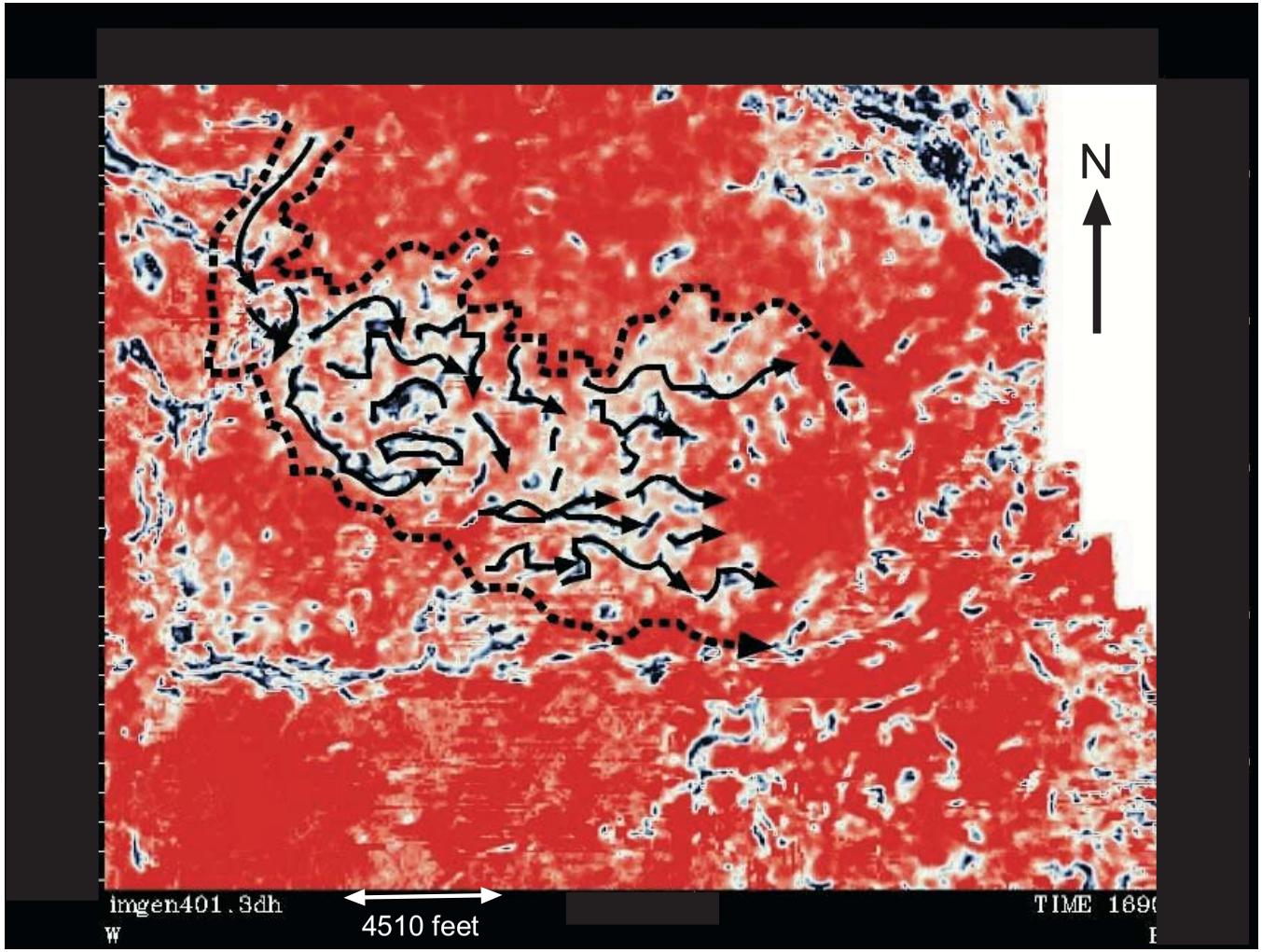

Figure 8.1: Coherency analysis at 10 ms (1690ms) from the flattened-Morrow seismic datum in area of focused study. Interpreted to depict meandering channels (solid lines) within laterally limited channel belt (dashed lines).

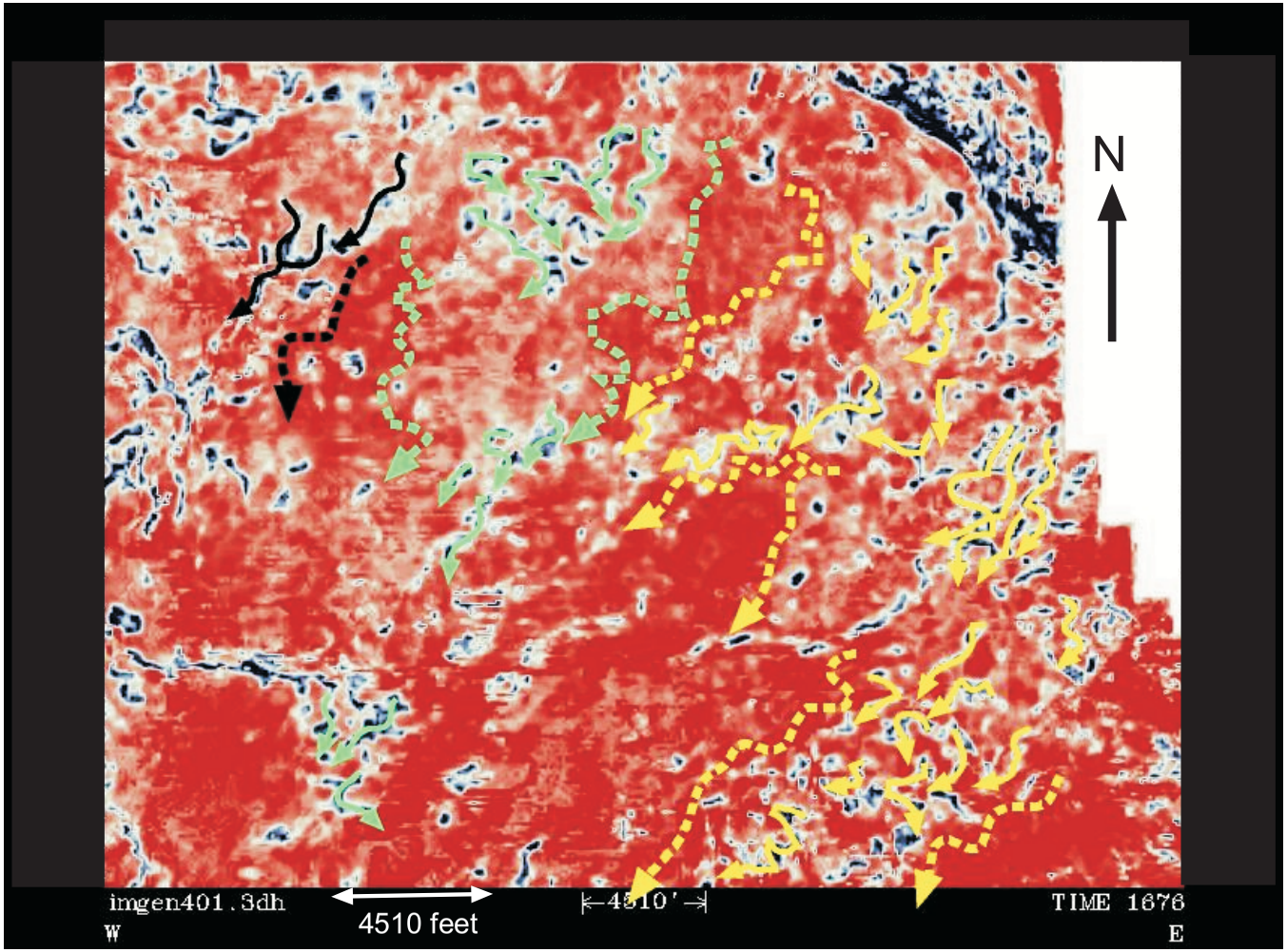

Figure 8.2: Early time slice of upper Atoka sand focused area of study. Each color indicates channels (solid lines) and channel belts (dashed lines) generated in different times - First channel system (black), second channel system (yellow) and third channel system (green).

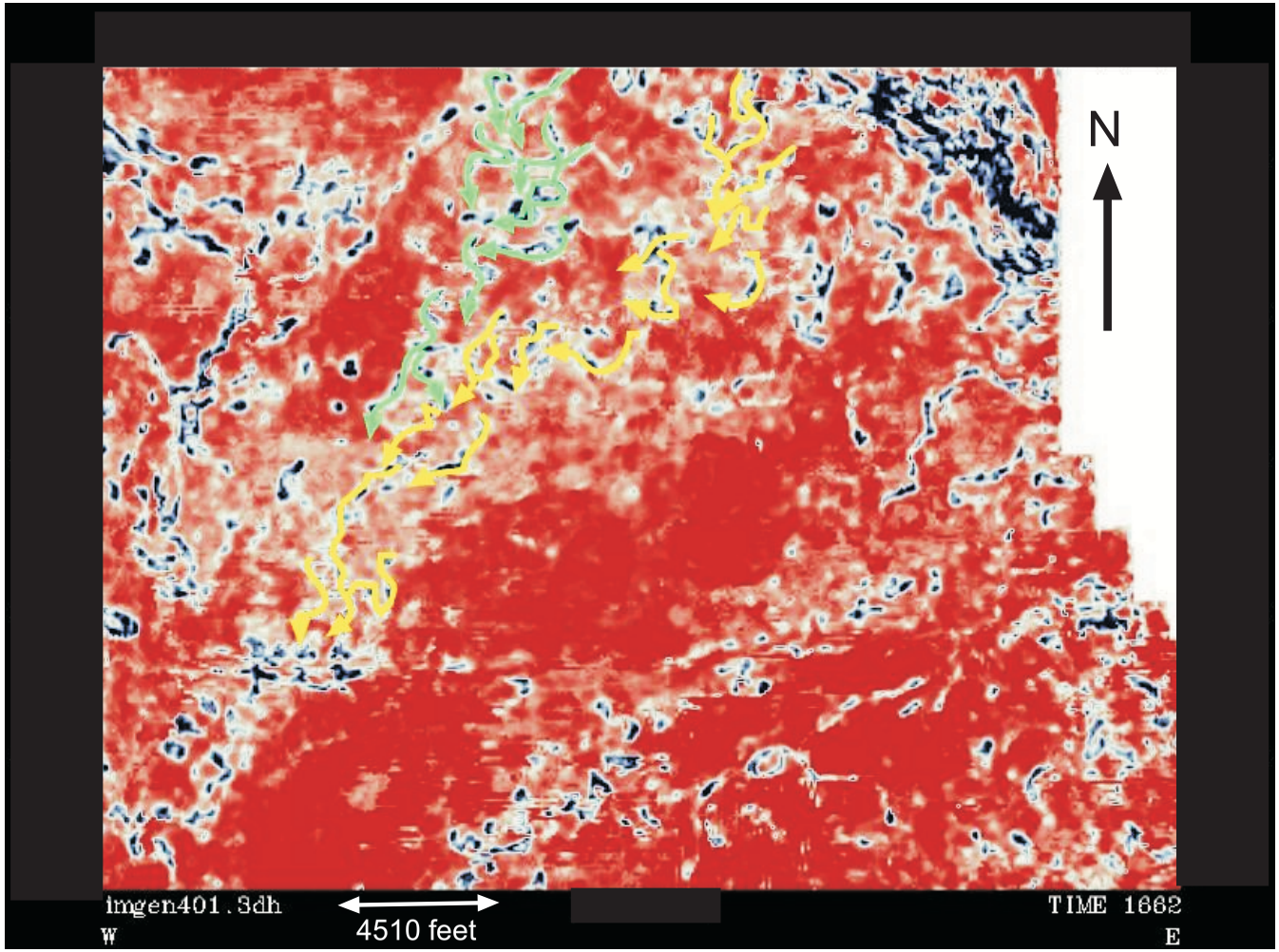

Figure 8.3: End time slice of the upper Atoka sand focused area of study. Each color indicates channels (solid lines) generated in different times - second channel system (yellow) and third channel system (green).

perpendicular to flow. Both figures show narrower channels than that shown in Figure 8.1, yet both clearly have similar internal structures, interpreted to be smaller meandering channels within the larger channel belt. The migration of the channel system axis apparent in these two figures supports the observations made from the isochron interval map in Figures 7.7 and 7.8.

It appears that coherency mapping of channels may be the most useful method applied in this study. It enables prediction of locations of channels in a map sense and matches closely with well locations where lower Atoka, upper or lower sands are demonstrated to exist and are prolific producers. It also suggests areas with lesser potential for single or stacked channels where exploration for sands might be avoided.

8.2 Attribute analysis for identifying channelized reservoirs

8.2A Method

The purpose of attribute analysis is to investigate physical properties that are part of the seismic data and attempt to correlate them with reservoir properties (Brown, 1999). Generally, seismic attributes are classified into four categories - time, amplitude, frequency, and attenuation, and many sub-divisions of these attributes (Brown, 1999). Attribute analysis is performed using software due to tedious calculations. Attribute extractions were performed by PAL (Post Stack Attributes Library), which is one of the Landmark software components. According to Brown (1999), amplitude, phase, and frequency information is useful in characterizing the following physical features: gas and fluid accumulation, gross lithology, channel and deltaic sands, certain types of reefs, unconformities, and stratigraphic sequences. Unfortunately, tuning effects or poor data

quality may cause attribute shifts independent of these features. Single and multiple attribute analysis was performed. Most methods yielded very poor results. See Appendix 4 for discussion of failed attribute tests.

8.2B Results

Attribute extractions of phase and frequency for the lower Atoka sand horizons yielded unsatisfactory results in that no distinct trends or features were identified beyond indicating simple presence or absence of the sand channels that are obvious from other maps such as time structure and coherency. An attribute extraction of the Morrow horizon was attempted under the assumption that deeply cut channels or thick lower sand channels might interfere with Morrow amplitude. Again, no obvious new information was extracted to contribute to the analysis of channel sand distribution. The results of these and other failed attributes are presented further in Appendix 3.

Figure 8.4 shows the maximum trough amplitude extraction of the lower Atoka Formation, lower sand. The maximum trough amplitude was extracted from a 4 ms time window above and below the maximum point. Strong amplitude trends are depicted on Figure 8.4 that appear to correspond to the distribution of lower Atoka Formation, lower sand. Trough amplitude intensity shows the strength of the amplitude by color scheme and appears to be highest where the channel sands might be interpreted to be thickest.

Figure 8.5 shows the maximum trough amplitude extraction for the lower Atoka Formation, upper sand. The maximum trough amplitude was extracted from a 3 ms time window above and below the maximum amplitude of the trough. Like the lower sand,

amplitude anomalies correspond roughly with channels determined by other methods, but these channels have fewer strong amplitude anomalies associated with thick sandstone.

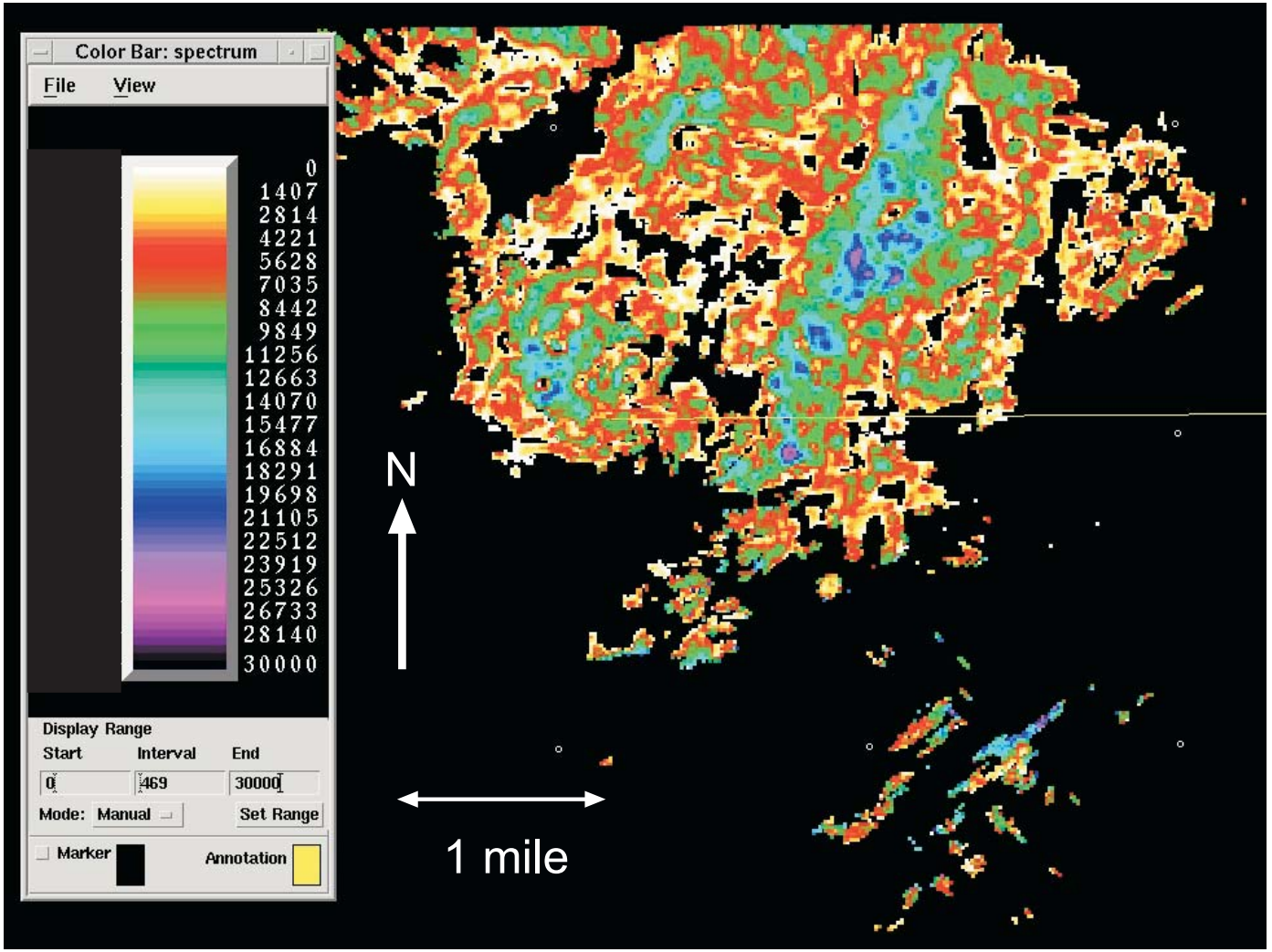

Figure 8.4: Maximum trough amplitude extracted map of the lower Atoka sand focused area of study. Numbers indicate amplitude intensity with blue/purple color suggesting relatively thick sand.

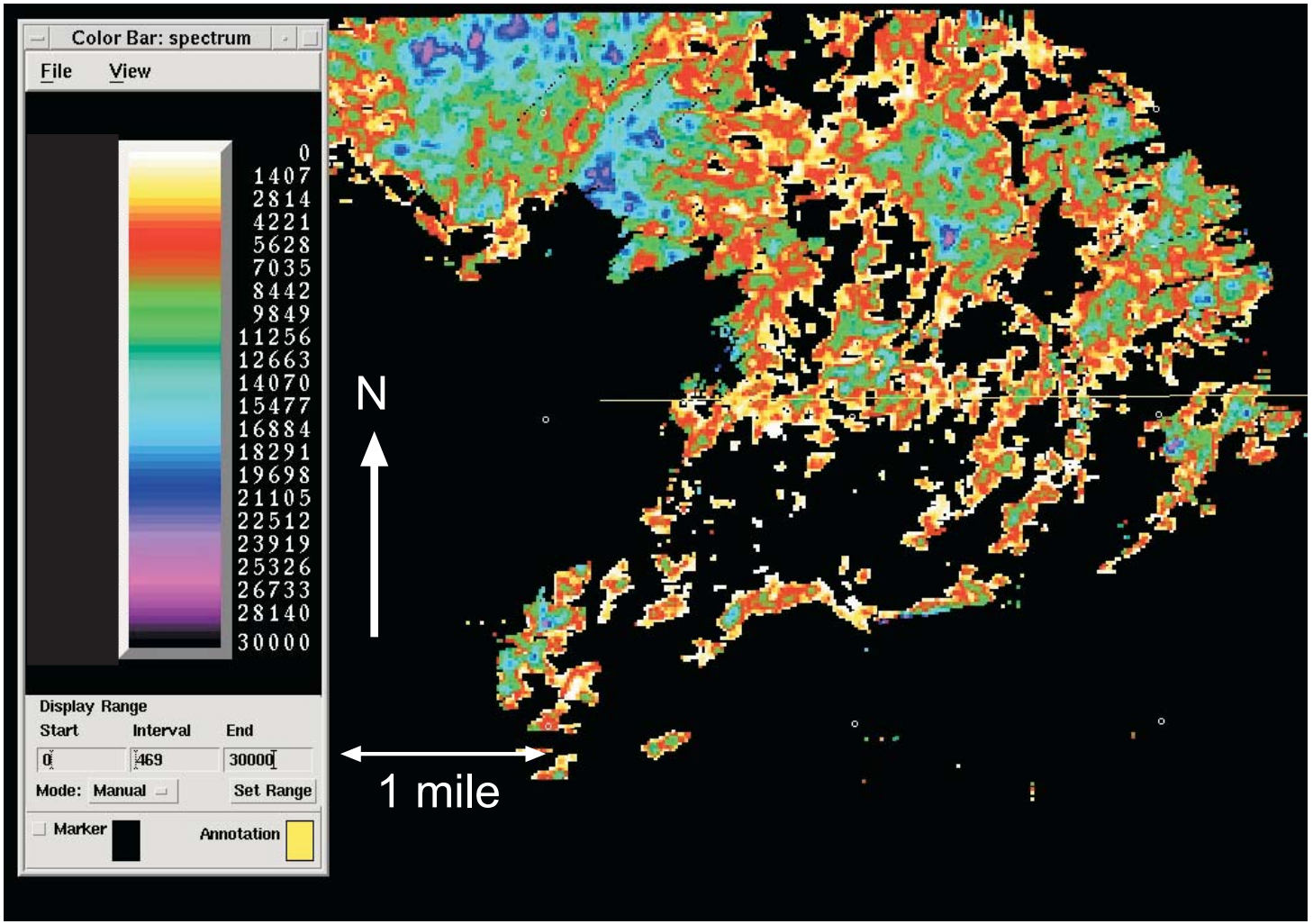

Figure 8.5: Maximum trough amplitude extracted map of the upper Atoka sand focused area of study. Numbers indicate amplitude intensity with blue/purple/green color suggesting relatively thick sand.

9. DISCUSSION: INTEGRATED ANALYSIS

Through the application of geological control to 3-D seismic data interpretation, a clearer picture of the depositional environment can be attained for the Atoka Formation sandstone reservoirs in the Vacuum Field area. Seismic data interpretation is complementary to the geological data in that it allows the visualization of structure and reservoir bodies in a much greater degree of detail. In all, the fluvial depositional environment suggested by features visible in the seismic data are entirely consistent with the fining upwards, fluvial nature interpreted from well logs and core photographs.

Based on coherency mapping, small-scale meander loops appear to be confined to narrow fairways. In the lower Atoka lower sand fairways, the channels are broad and probably cut into the underlying marine shale. As aggradation proceeded, these broad channels were eventually filled. In the upper part of the lower sand channels appear to be relatively unconfined and lie outside of the broad channels.

The lower Atoka Formation, upper sand bodies appear to have migrated freely from southeast to northwest, perhaps due to northwest tilting. The upper sand bodies are not strictly confined to broad channels as in the lower sand and appear to be much thinner based on amplitude attribute analysis and well log observations.

It is apparent from a larger-scale examination of well logs that the study area is rare in its preservation of the lower Atoka section. The tectonic implication here is that the study area encompasses a block that was down dropped relative to the region such that the lower Atoka was preserved from intraformational, pre-upper Atoka Formation unconformity. Therefore, it may be assumed that the lower Atoka was deposited everywhere regionally, but only locally preserved due to Atokan tectonic activity.

One question posed by Marathon Oil was, “Did the channels flow northward, or southward” (suggested on Fig. 2.4). The proximity to the Central Basin Platform might suggest northward flow. However, the basinward direction was southward from the location of the study area. The sand grain size suggested by the core photos coupled with the overall dominance of fine-grained shale in the lower Atoka section suggests that the source of the clastic material was derived from a significant distance, favoring the Pedernal-Matador uplift over the nearer Central Basin Platform. In addition, the orientation of channels in the upper sand is essentially parallel to the Central Basin Platform, rather than being perpendicular to it as might be expected if streams were draining from the platform. The southeast-northwest orientation of the western channel, lower sand, may be more related to proximity to faults, i.e. near-fault subsidence, than to orientation related to provenance.

10. CONCLUSIONS

An integrated geological, petrophysical and 3-D seismic analysis successfully and effectively provides a solution to the problem posed in this thesis: that of delineating Atoka Formation sandstone reservoirs and defining methods to predict their distribution beyond existing well control. It is recommended that for this area and similar settings in the region, an integrated and stepwise approach be followed in order to achieve similar results. Because of the relatively thin sand bodies comprising the Atoka reservoir, basic seismic thickness modeling is a necessary aspect to test the applicability of seismic for delineating such bodies. Careful construction of synthetic seismograms and equally careful tuning to derive a satisfactory match with seismic is critical in order to identify the exact reflection of interest for key seismic horizons. Basic horizon structure and isochron maps were useful in the particular case at Vacuum field. Coherency and amplitude analyses were also very complementary to other mapping procedures. Coherency analysis has been demonstrated to be the most effective for detecting subtle structural and depositional features.

Based on the integrated observations and interpretations from this study, the Atoka Formation sandstone reservoirs are believed to be a possibly rare preserved section of the lower Atoka Formation that was eroded from much of the region by an intraformational unconformity. The lower Atoka Formation sands were deposited in meandering streams in a fluvial depositional environment. The meandering streams appear to be confined to larger channel features in the lower part of the lower Atoka, whereas in the upper part of the lower Atoka, they were unconfined and migrated freely across the area. Lateral channel migration may have been the result of local tectonic

activity that tilted the depositional plain to the northwest. The combination of a complex fluvial depositional system with syndepositional tectonic activity makes the Atoka an interesting and challenging natural gas play with substantial potential for further exploration and development.

REFERENCES

Adams, J.E., 1965, Stratigraphic-tectonic development of Delaware Basin: AAPG Bulletin v. 49, no. 11, p. 2140-2148.

Asquish, G and Gibson, C., 1982, Basic well log analysis for Geologists: AAPG Methods in Exploration Series Number 3, p. 216.

Bahorich, M and Farmer, S., 1995, 3-D seismic discontinuity for faults and stratigraphic features: The Coherence Cube: The Leading Edge, October 1995, p. 1053-1058.

Boucher, P.J., and Wescott, W. A., 2000, Imaging submarine channels in the western Nile Delta and interpreting their paleohydraulic characteristics from 3-D seismic: The Leading Edge, June 2000, p. 580-591.

Bridge, J.S., and Tye, R. S., 2000, Interpreting the dimension of ancient fluvial channel bars, channels, and channel belts from wireline-logs and cores: AAPG Bulletin v. 84, no .8, p. 1205-1228.

Brown, A. R., 1999, Interpretation of three-dimensional seismic data 5th edition: AAPG Memoir 42/SEG Investigations in Geophysics, no 9, p. 514.

Burnham, D. E., 1990, Determining the depositional environment of a braided channel sand using formation MicroScanner images, North Vacuum Field, Lea County, New Mexico: AAPG Bulletin v. 74, no. 5, p. 622 (Abstract).

Cant, D., 1982, Fluvial facies models and their application, *in* Scholle, P., and Spearing, D eds., Sandstone depositional environments: AAPG Memoir 31, p. 115-137.

Casavant, R., 1999. Speculations on basement tectonics: Insight from the White City Penn Field, Eddy county, NM: A Symposium of Oil and Gas Field of Southeastern New Mexico 1999, p25-53.

Cys, J., and Gibson, W., 1988, Pennsylvanian and Permian geology of the Permian Basin region, The Permian Basin region, *in* L. L. Sloss ed., Sedimentary Cover- North American Craton: U.S. Geological Society of America, v D-2, p. 277-289.

Ewing, T. E., 1997, Real answers for synthetic issues: The AAPG EXPLORER, July and August 1997.

Enachescu, M., 1993, Amplitude interpretation of 3-D reflection data: The Leading Edge, June 1993, p. 678-685.

Galloway, W., Yancey, M., and Whipple, A., 1977, Seismic stratigraphic model of depositional platform margin, Eastern Anadarko Basin, Oklahoma: AAPG Bulletin v. 61, P. 1437–1447.

Gerstner, M., and Malone, M., 1999, Successful fracture simulation in tight gas sands of Southeast New Mexico with Binary Foam: A Symposium of Oil and Gas Fields of Southeastern New Mexico 1999, p. 97-111.

Ham, W. E., and J. L. Wilson, 1967, Paleozoic epeirogeny and orogency in the central United States: American Journal of Science, v. 265, p. 332-407.

Hardage, B. A., Levey, R.A., Pendleton, V., Simmons, J and Edson, R., 1994, A 3-D seismic case history evaluating fluvially deposited thin-bed reservoirs in a gas-producing property: Geophysics v. 59, no. 11, p. 1650-1665.

Hart, B., 1998, Three-dimensional seismic interpretations: A primer for geologists: Geological Society of America, Continuing Education Manual, p. 114.

Hills, J.M., 1984, Sedimentation, tectonism, and hydrocarbon generation in Delaware Basin, West Texas and Southeastern New Mexico: AAPG Bulletin v. 68, no. 3, p. 250-267.

Hills, J., and Galley, E., 1988, General introduction, The Permian Basin region, *in* Sloss, L. L, ed., Sedimentary Cover-North American Craton: U.S. Geological Society of America, v D-2, p. 261-267.

James, A. D., 1985, Producing characteristics and depositional environment of Lower Pennsylvanian reservoirs, Parkway-Empire South Area, Eddy County, New Mexico: AAPG Bulletin v. 69, no. 7, p. 1043-1063.

Kluth, C.F, 1986, Plate tectonics of the Ancestral Rocky Mountains, in J. A. Peterson, Ed., Paleotectonics and sedimentation in the Rocky Mountain region, United States: AAPG Memoir 41, p. 353-369.

Landmark Graphics Corporation, 1999, World Wide Tech Forum ESP (Event Similarity Prediction: World wide tech forum, p. 56.

Landmark Graphics Corporation, 1996, PostStack/ PostStack Attribute Library manual, Landmark Graphics corporation, p. 420.

Leiphart, D, 2000, Comparison of linear regression and a probabilistic neural network to predict porosity from 3-D seismic attributes in Lower Brushy Canyon Channeled Sandstones, Southeast New Mexico: M.S. Thesis of New Mexico Institute of Mining and Technology.

Mazzullo, L.J., and Mazzullo, S.J., 1989, Southern Shelf of Belize: An analog to Morrow and Atoka Formations, Permian: AAPG Bulletin v. 73, p. 256 (Abstract).

Mazzullo, L. J., 1999, Geologic history and reservoir development in the Shoebar Field Area, Lea County, New Mexico: AAPG Bulletin v. 83, p. 385.

Mazzullo, L. J., 1999, Significance of intraformational unconformities in the Morrow Formation of the Permian Basin; in D.T. Grace and G.D. Hinterlong eds., The Permian Basin: Providing Energy for America; West Texas Geological Society Publ. 99-106, p.55-61.

Mazzullo, L. J., 1999, Pitfalls of 3-D seismic interpretation in the Permian Basin; in S. T. Reid, ed., Geo-2000: Into the Future; Transactions, Southwest Section-AAPG, Midland, Texas Publ. 2000-107, p. 8-20.

Mazzullo, S,J., 1981, Facies and burial diagenesis of a carbonate reservoir: Chapman Deep (Atoka) Field, Delaware Basin, Texas: AAPG Bulletin v. 65, p. 390 (Abstract).

Meckel, L.D. Jr., and Nath, A.K., 1997, Geologic considerations for stratigraphic modeling and interpretation, Seismic Stratigraphy – Applications to hydrocarbon exploration: AAPG Memoir 26, p. 53- 62.

Meyer, R, F., 1966, Geology of Pennsylvanian and Wolfcampian rocks in southeast New Mexico: Socorro, New Mexico Bureau of Mines and Mineral Resources Memoir 17, p. 123

Miall, A. D., 1996, The geology of fluvial deposits – Sedimentary facies, basin analysis, and Petroleum Geology, Springer, p. 582.

Miall, A. D., 1997, The geology of stratigraphic sequences, Springer, p. 433.

Moore, G., and Shipley, T., 1993, Character of the decollement in the Leg 131 area, Nankai Trough, Proceedings of the Ocean Drilling Program, Scientific Results, v. 131, p. 73-82.

Pearson, R. A., 1999, Sequence stratigraphy and seismic-guided estimation of log properties of the Second Sand Member of the Bone Spring formation, Delaware Basin, New Mexico: M.S. Thesis of New Mexico Institute of Mining and Technology.

Pendleton, V.M., and Hardage, B.A., 1999, 3-D seismic imaging of a thin, vertically isolated fluvial depositional system reservoir in Seeligson Field: The Leading Edge, April, p. 464-477.

Schlumberger, 1989, Log interpretation Principles/Applications.

Sheriff, R and Geldart, L, 1999, Exploration seismology 2nd edition, Cambridge University Press, p. 592.

Speer, S., 1993, PP-3 Atoka, Permian Basin Pre-Permian [PP] plays, in Robertson, J and Broadhead, R., Atlas of Major Rocky Mountain Gas Reservoirs, p. 153-164.

Tobin, H., Moore, C., and Moore, G., 1994, Fluid pressure in the frontal thrust of the Oregon accretionary prism: Experimental constraints, Geology, v. 22, p. 979-982.

White, R. E., and Hu.T., 1998, How accurate can a well tie be ?: The Leading Edge, August 1998, p. 1065-1071.

Wangoner, J.C. V., 1990, Siliciclastic Sequence Stratigraphy in Well Logs, Core, and Outcrops, AAPG Methods in Exploration Series, no7, p. 55.

Worthington, R. E., 1999, Discovery, development, and extension of Pennsylvanian (Atoka, Morrow) gas reservoirs in the Shugart and North Shugart field areas, Northeastern Eddy County, New Mexico: A Symposium of Oil and Gas Field of Southeastern New Mexico, p 125-137.

APPENDIX 1: PETROLOGIC DESCRIPTION AND INTERPRETATION OF UPPER ATOKA FORMATION

Typically, the upper Atoka Formation in the Delaware Basin and Northwestern Shelf consists of sediments ranging from deltaic marine sandstone and shale to carbonate (Mazzulo, 1981; Mazzulo, 1989; Cys and Gibson, 1988). Atoka cores from two wells in the collection at the New Mexico Bureau of Geology and Mineral Resources were studied. Both wells are in Chaves County. They are the Reid B #1 (Section 10-10S-31E) and the White-Federal #1 (Section 13-9S-30E). The cores were examined, described, and correlated to well logs. Petrographic descriptions were prepared from six thin sections to demonstrate the range of lithologies present. Figure A1-1 describes log correlation between the two wells.

Core description

Figures A1-2 and A1-3 are core description logs. To construct the logs, the cores were examined with and without magnification. In general, sandstone beds in both cores are fine to medium grained (upward-coarsening), have angular to moderately rounded (mostly subangular) grain shape, are moderately sorted, and have cross, parallel or wavy lamination.

Limestone and calcareous shale beds are the main lithology in both of the cores. Fossils include brachiopods, crinoids, algae and corals. Moderate to strong bioturbation is common in these beds. Three types of shale are present; they are non-marine (?), calcareous marine and black marine shale. Variegated color, non-marine (?) shale contains root casts and makes up a minor percentage. Black shale is apparently organic-

rich , noncalcareous and is also a minor constituent in the cores. Dark gray calcareous shale is the primary type of shale and is difficult to distinguish from dark gray limestone with which it is interbedded, the difference between the two being primarily presence or absence of clay.

Petrographic analysis of upper Atoka Formation sandstone

Figures A1-4 to A1-9 are photomicrographs from six thin sections prepared from the cored sandstone beds. Based on examination of these thin sections, the sandstone units in the two cores range from quartz arenite to sublitharenite. Angularity range is from angular to moderately rounded, however most grains are subangular. Relative cementation and compaction of the sandstones varies, but in most cases the sandstones are cemented with calcite and silica (primarily as quartz-grain overgrowths). Additionally, many original pore spaces now contain authigenic clay (primarily kaolinite). The sum of these diagenetic effects is to reduce porosity to less than 5%. In some cases, pores are recognized that appear to be secondary and are interpreted to be due to dissolution of calcite cement or feldspar grains.

Interpretation of upper Atoka Formation

The Atoka formation was deposited mainly in a marine environment. Calcareous and black shale, as well as carbonate are the dominant lithologies and contain marine fossils. As a minor lithology, non-marine shale with coal fragments was identified. Coarsening upwards sandstone beds suggest deltaic deposition. The upper Atoka, therefore, appears to record fluctuating relative sea level where shelfal marine deposits represent higher

relative sea level, whereas the interbedded deltaic deposits (sandstone, variegated shale) represent lower relative sea level or seaward progradation of the deltas.

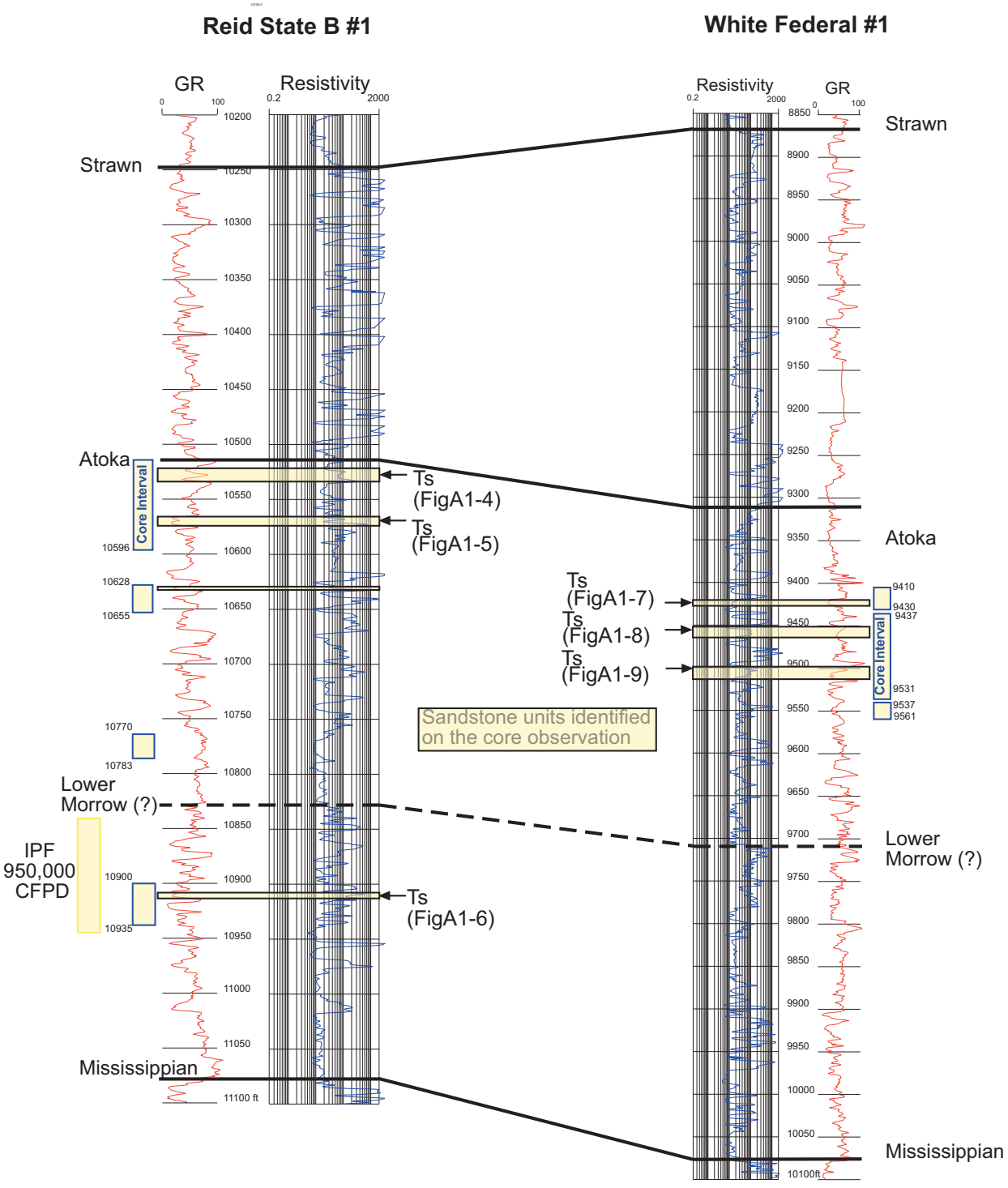

Figure A 1-1: Log correlation between 2 wells for which two cores were available. Depth measures from KB.

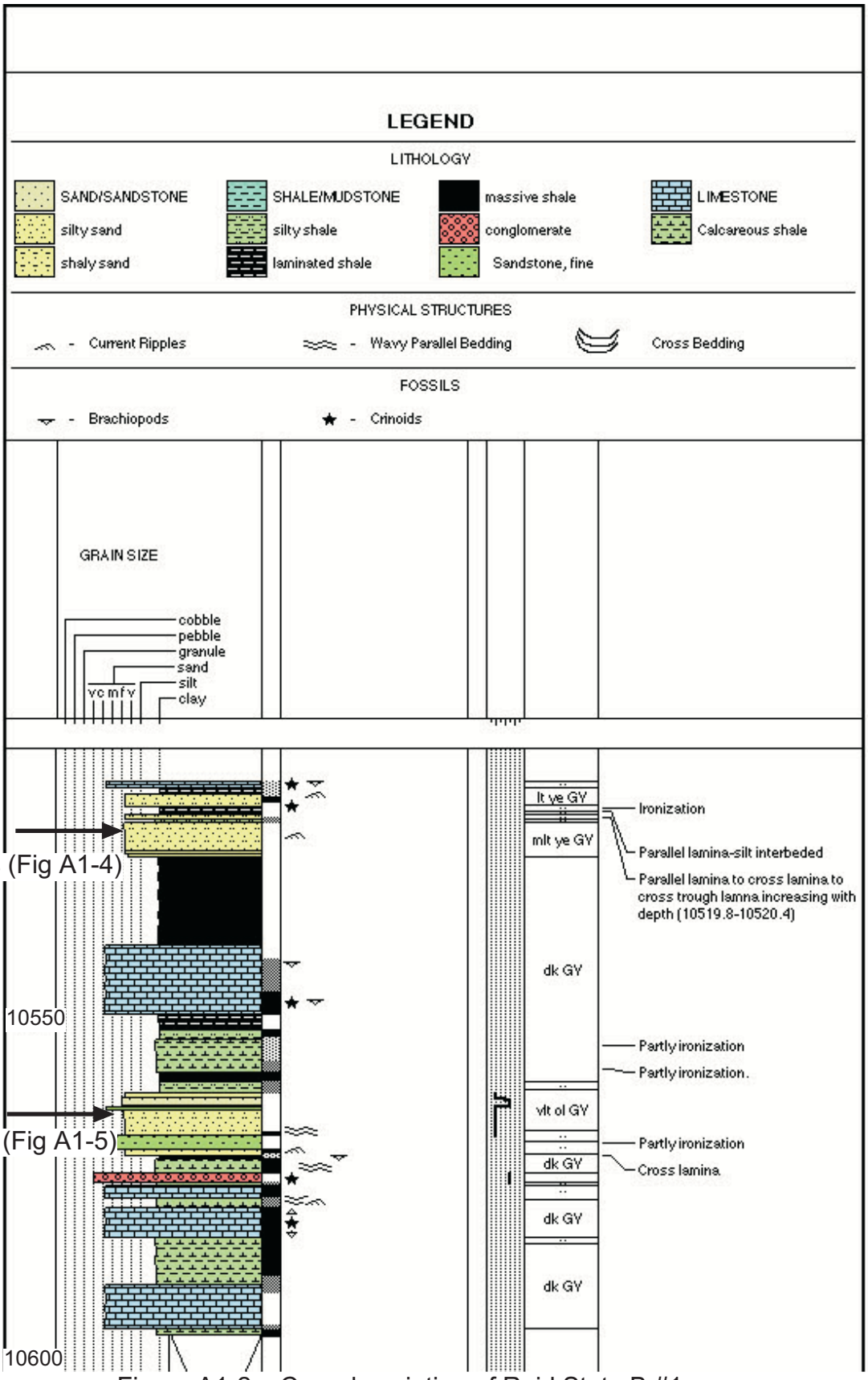

Figure A1-2a: Core description of Reid State B #1

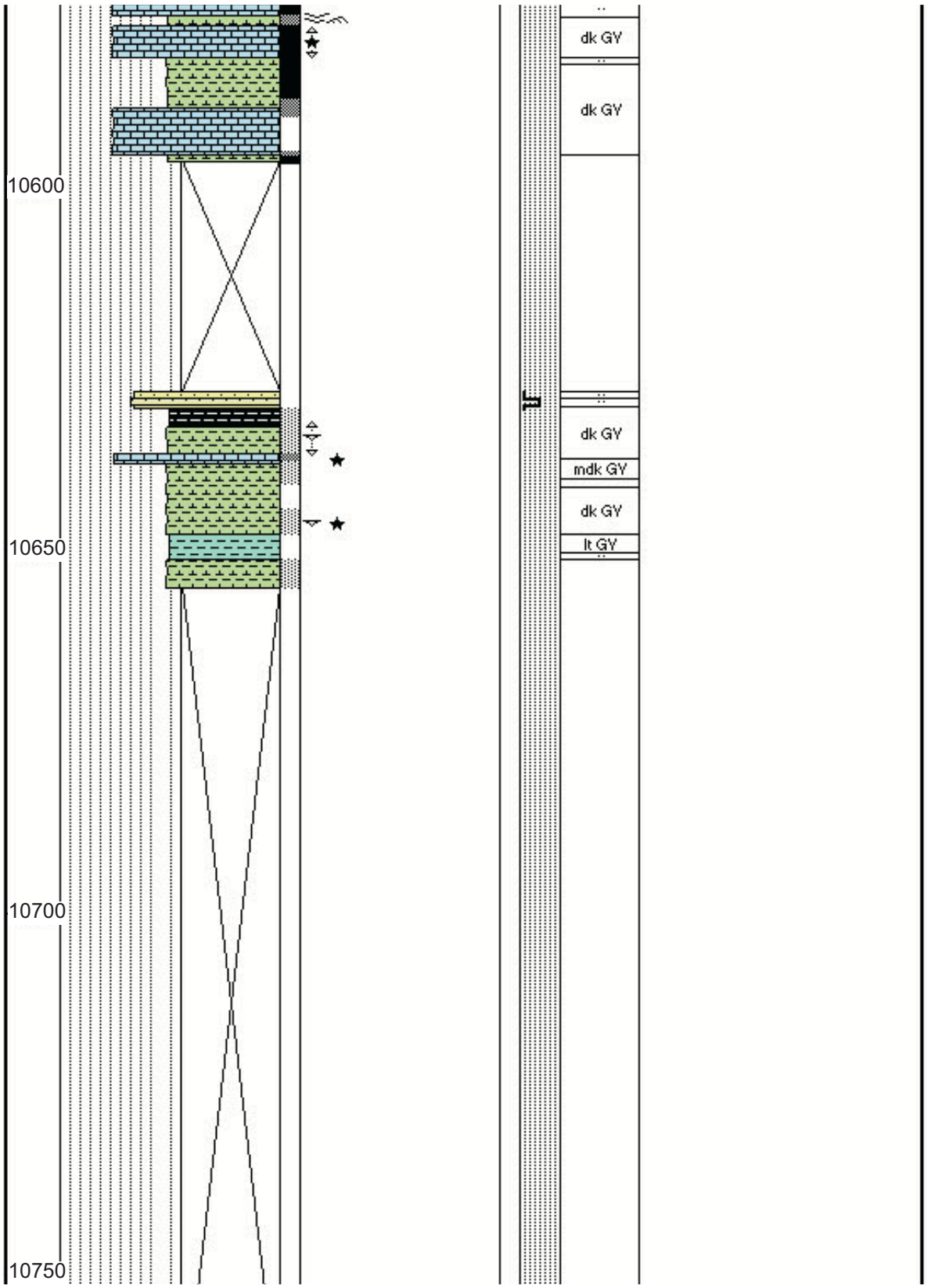

Figure A1-2b: Core description of the Reid State B #1

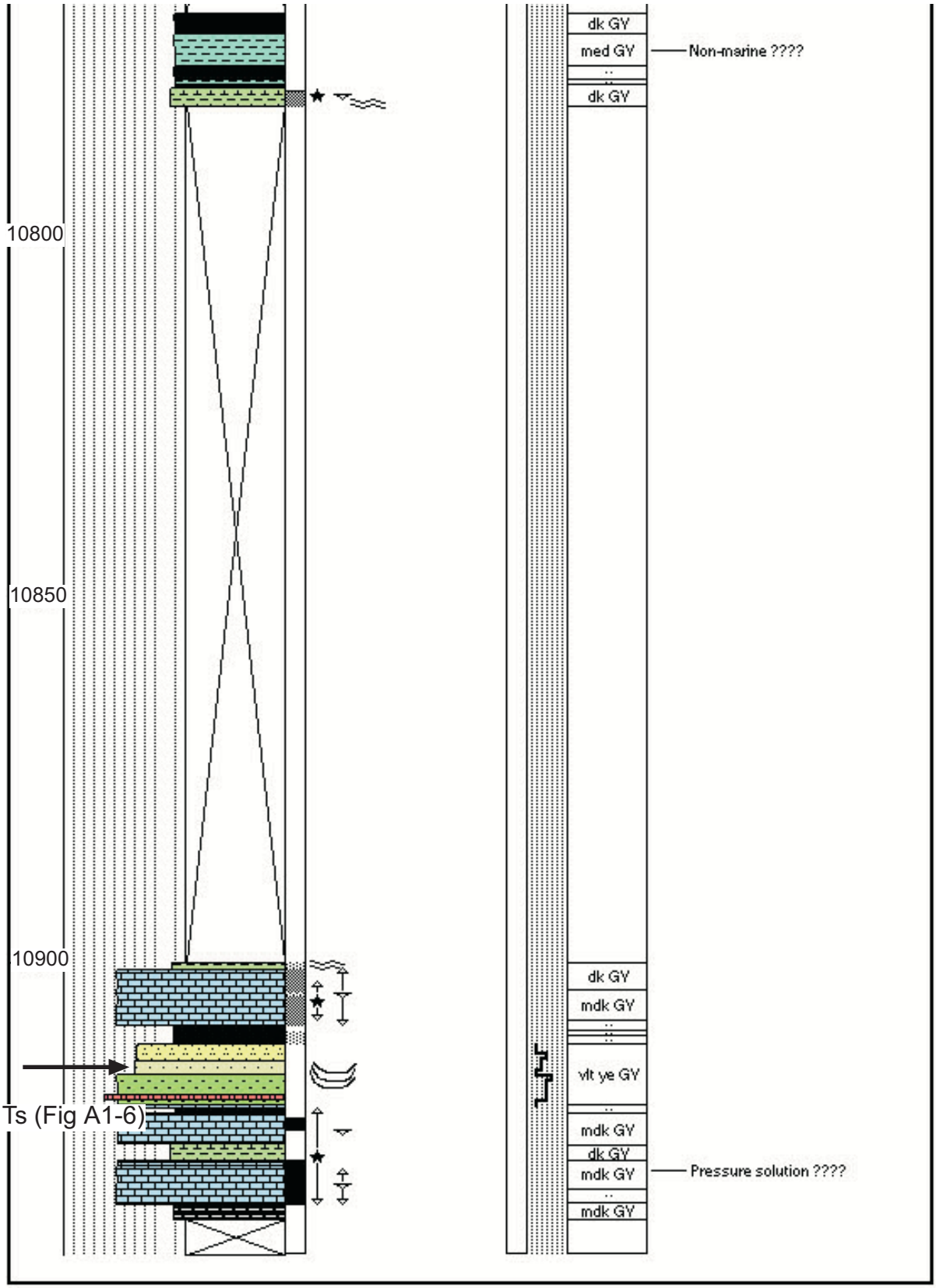

Figure A1-2C: Core description of the Reid State B #1

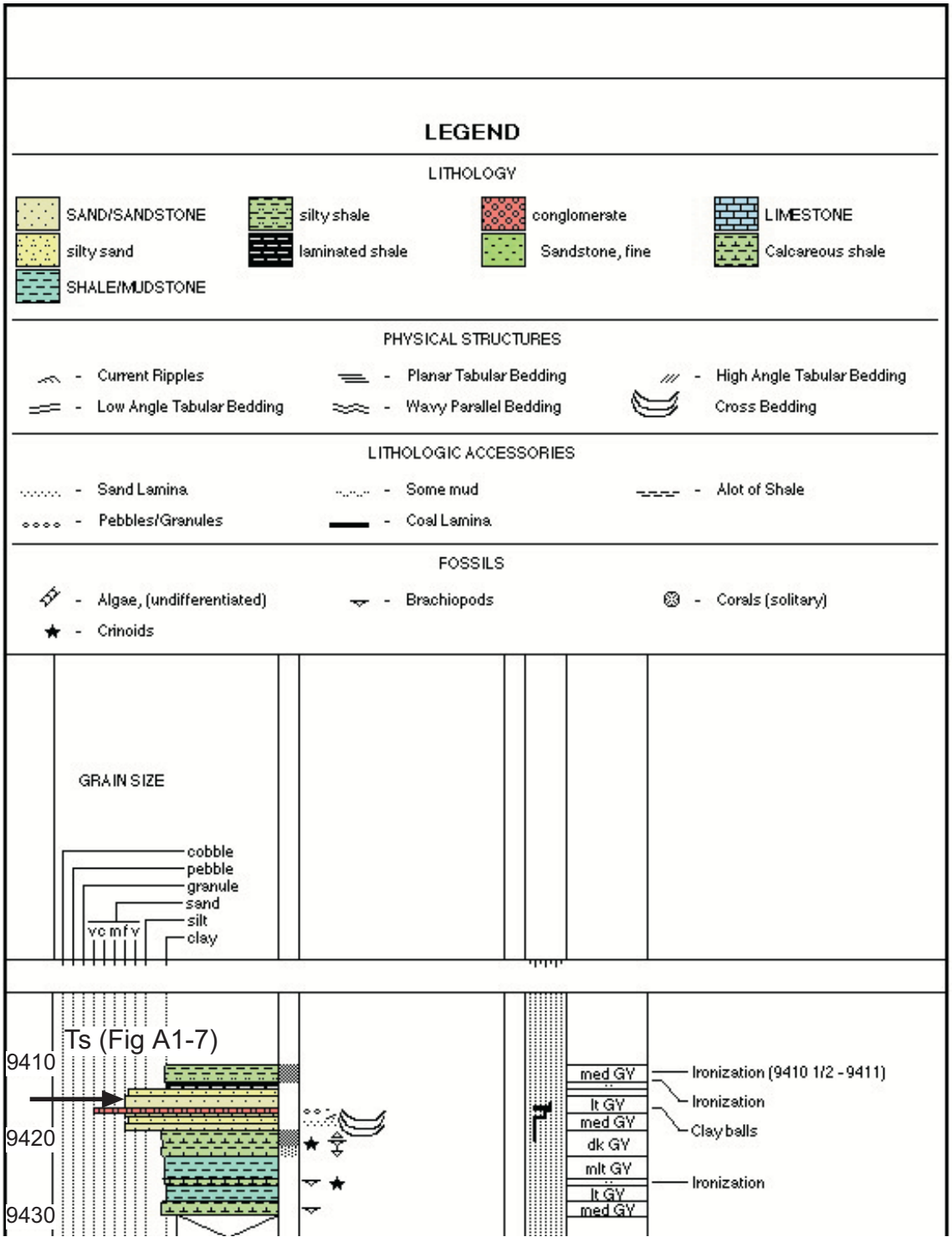

Figure A1-3a: Core description of White Federal #1.

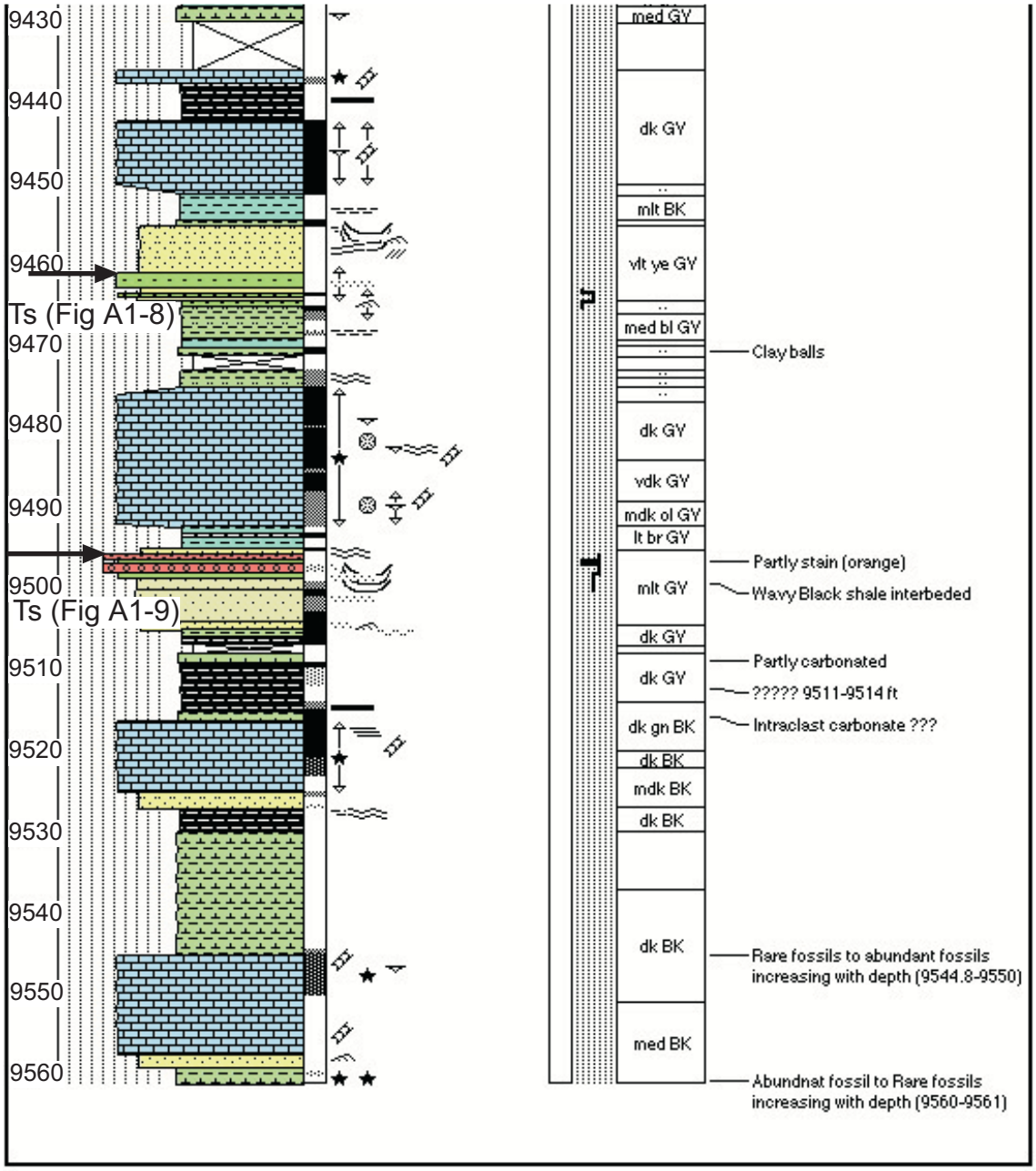

Figure A1-3b: Core description of White Federal #1

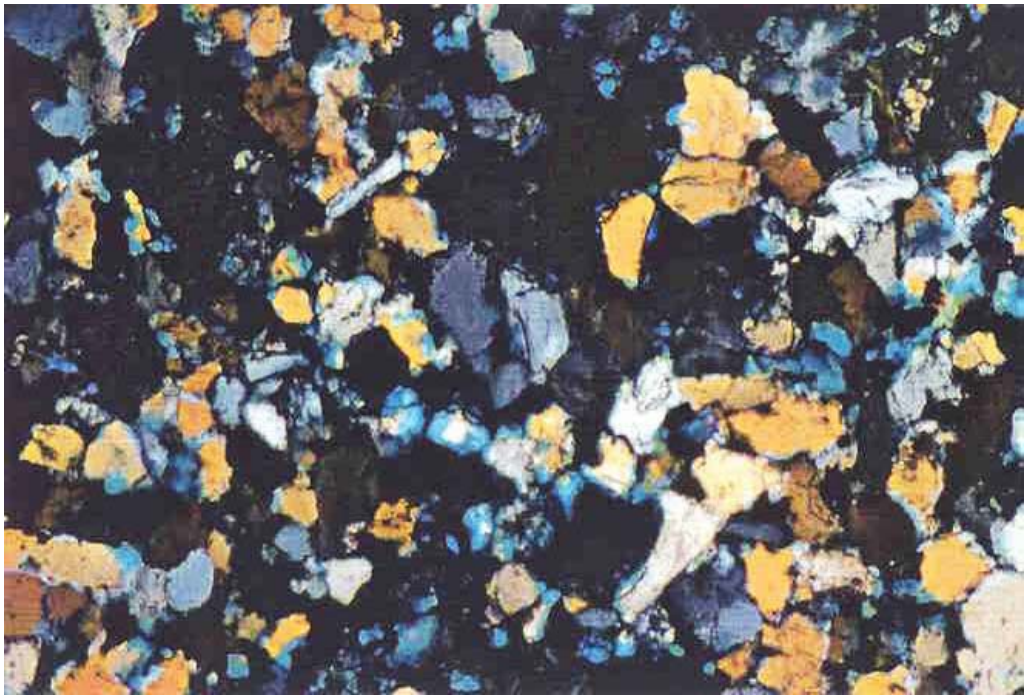

Figure A 1-4 Quartzarenite, Authigenic clays (Kaolinite and ?) reduce pore spaces. Secondary porosity was produced by partial dissolution of Feldspar. Reid State B No1. 10519.5 ft-10520.2 ft. LA (Long Axis) = 2.18mm

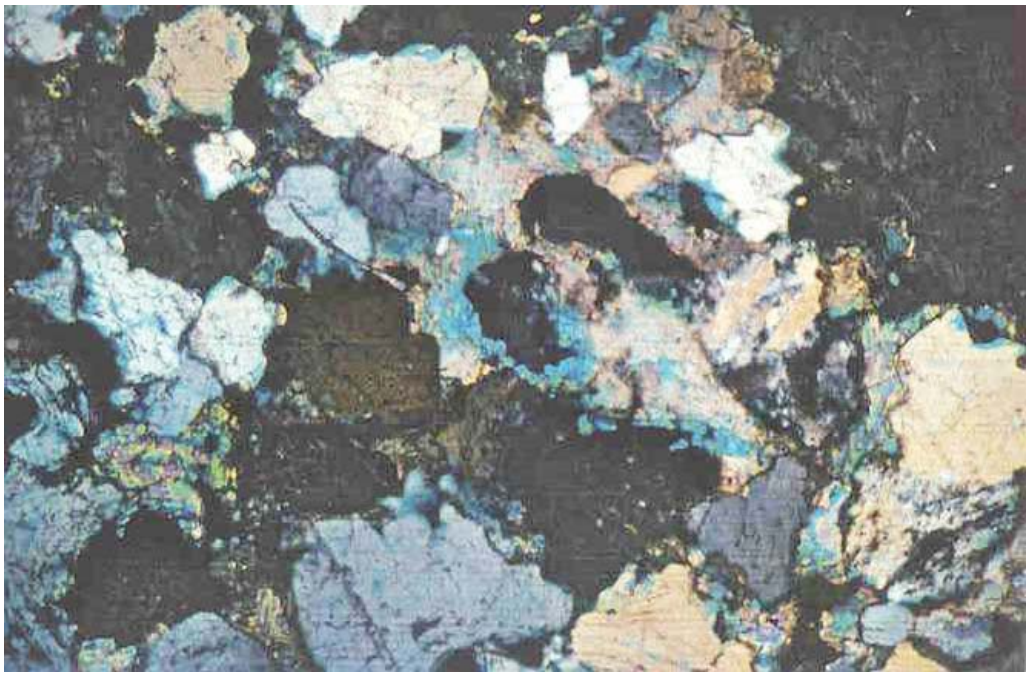

Figure A 1-5: Sublitharenite. Authigenic calcite fills primary porosity. Partial dissolution of calcite created secondary porosity. Overgrowth of quartz results in reduction of secondary porosity. Reid State B No1. 10561.4 ft– 10562.5 ft. LA (Long Axis) = 2.28mm

Figure A 1-6: Quartzarenite. Partial/total dissolution of feldspar produced pore spaces. These pore spaces were filled by calcite. Reid State B No1. 10914.7 ft-10915.6 ft. LA (Long Axis) =3.77mm

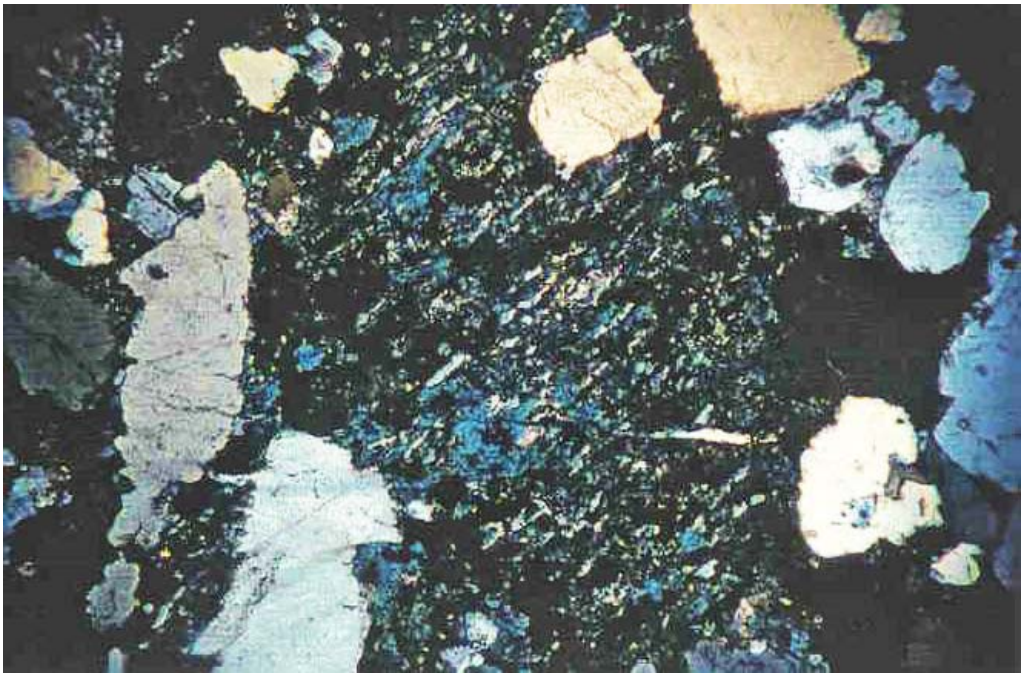

Figure A1-7: Sublitharenite. Partial/total dissolution of feldspar caused secondary porosity. White Federal No1. 9416 ft. LA (Long Axis) = 2.75mm.

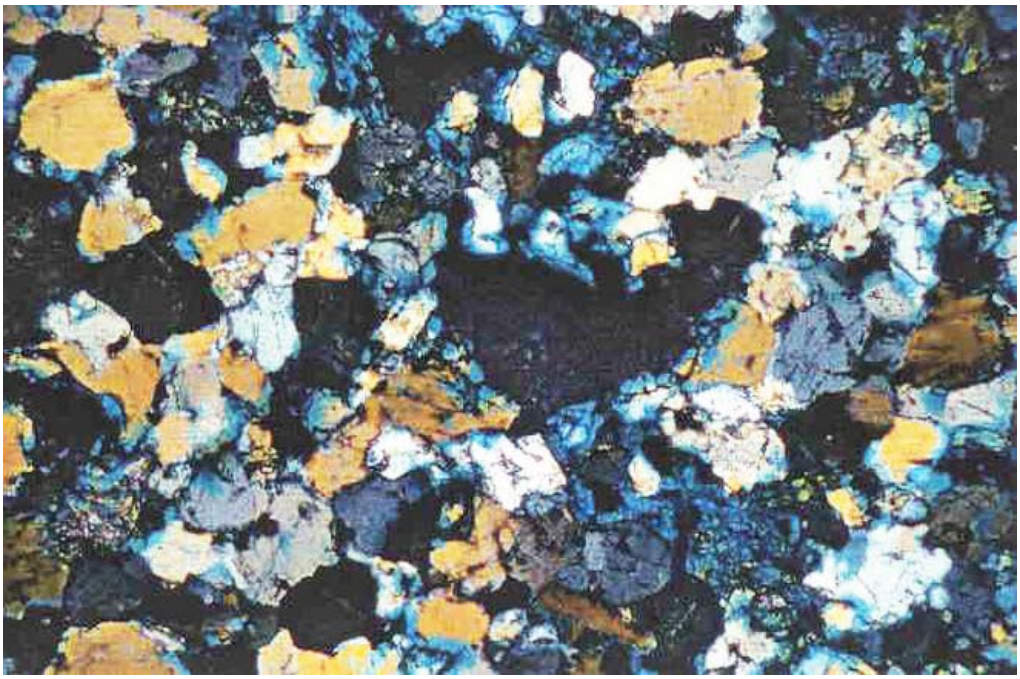

Figure A 1-8: Quartzarenite. Calcite and kaolinite fill pore spaces. Calcite and feldspar dissolution produced secondary porosity. White Federal No1. 9461ft to 6462ft. LA (Long Axis) = 2.28 mm.

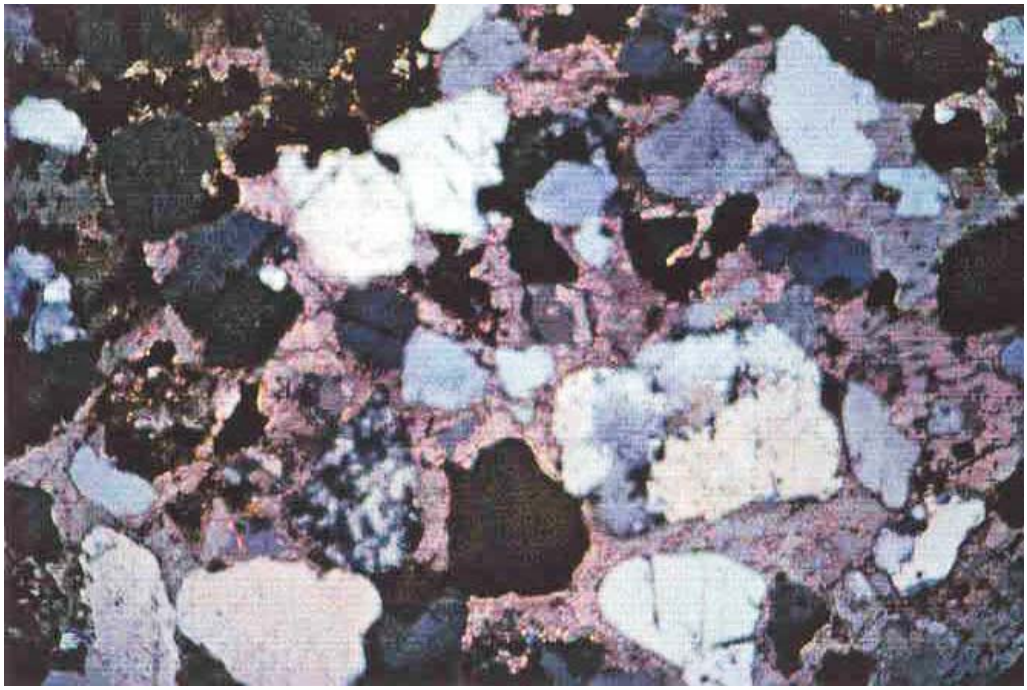

Figure A 1-9: Sublitharenite. As in Figure A1-6, calcite in pore spaces caused reduction of primary porosity. White Federal No1. 9497 ft – 9498ft. LA (Long Axis) = 2.28mm.

APPENDIX 2: SYNTHETIC SEISMOGRAM

Construction of synthetic seismograms is an essential step for seismic interpretation. Logs usually measure depth in feet. Seismic records measure depth in time (two-way travel time). Synthetic seismograms convert between these two measurements. Vertical resolution of logs is small compared to seismic data; therefore, a key function of the synthetic seismogram is to provide a method of comparison between the two data sets. Synthetic seismograms presented in this Appendix were generated using STRATA software by Hampson Russell Software Services, Ltd. from digital well logs either donated by Marathon Oil Company or digitized from paper logs using the Neuralog log digitizing system at the New Mexico Petroleum Recovery Research Center.

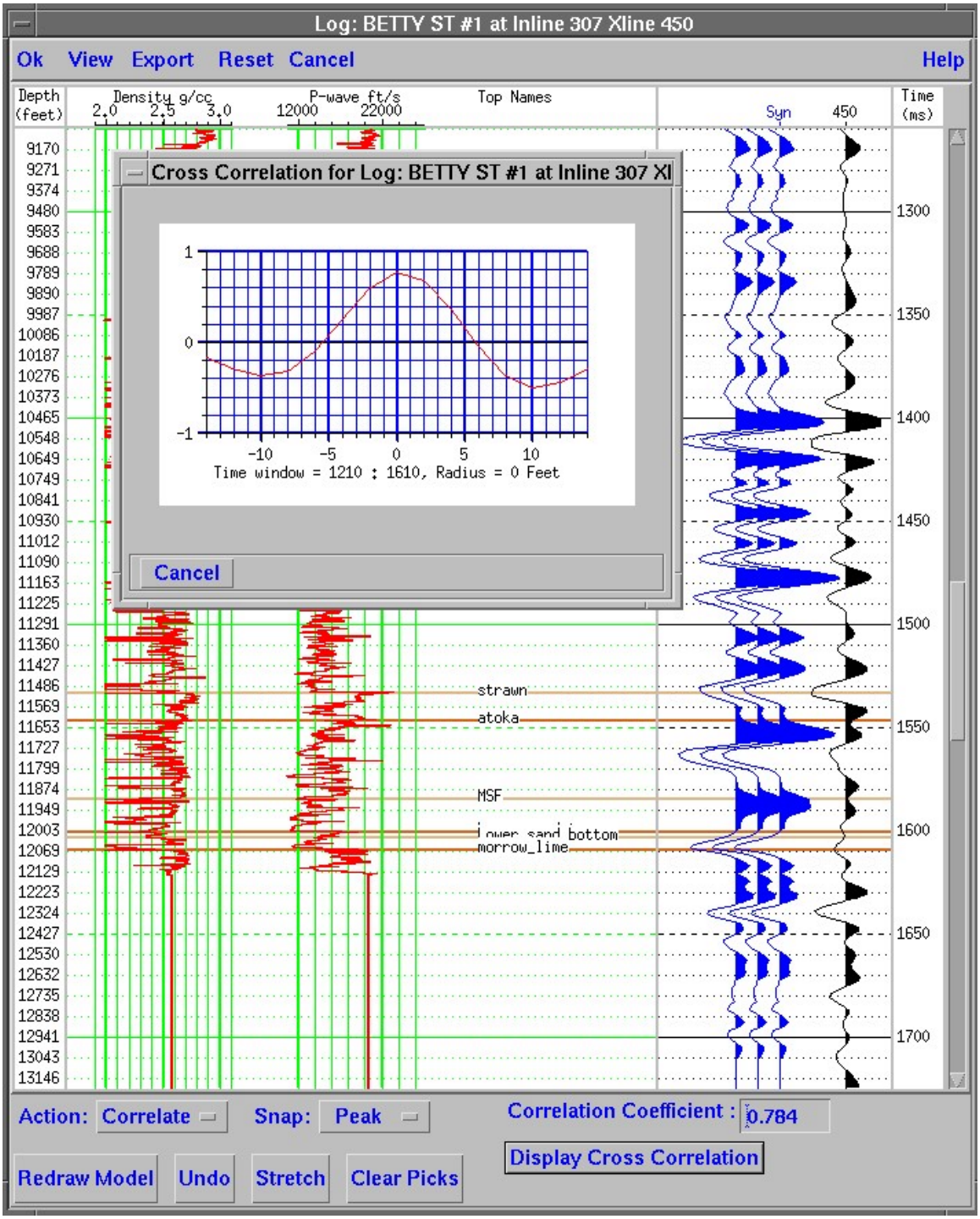

Figure A 2-1: Synthetic seismogram for BETTY ST 1

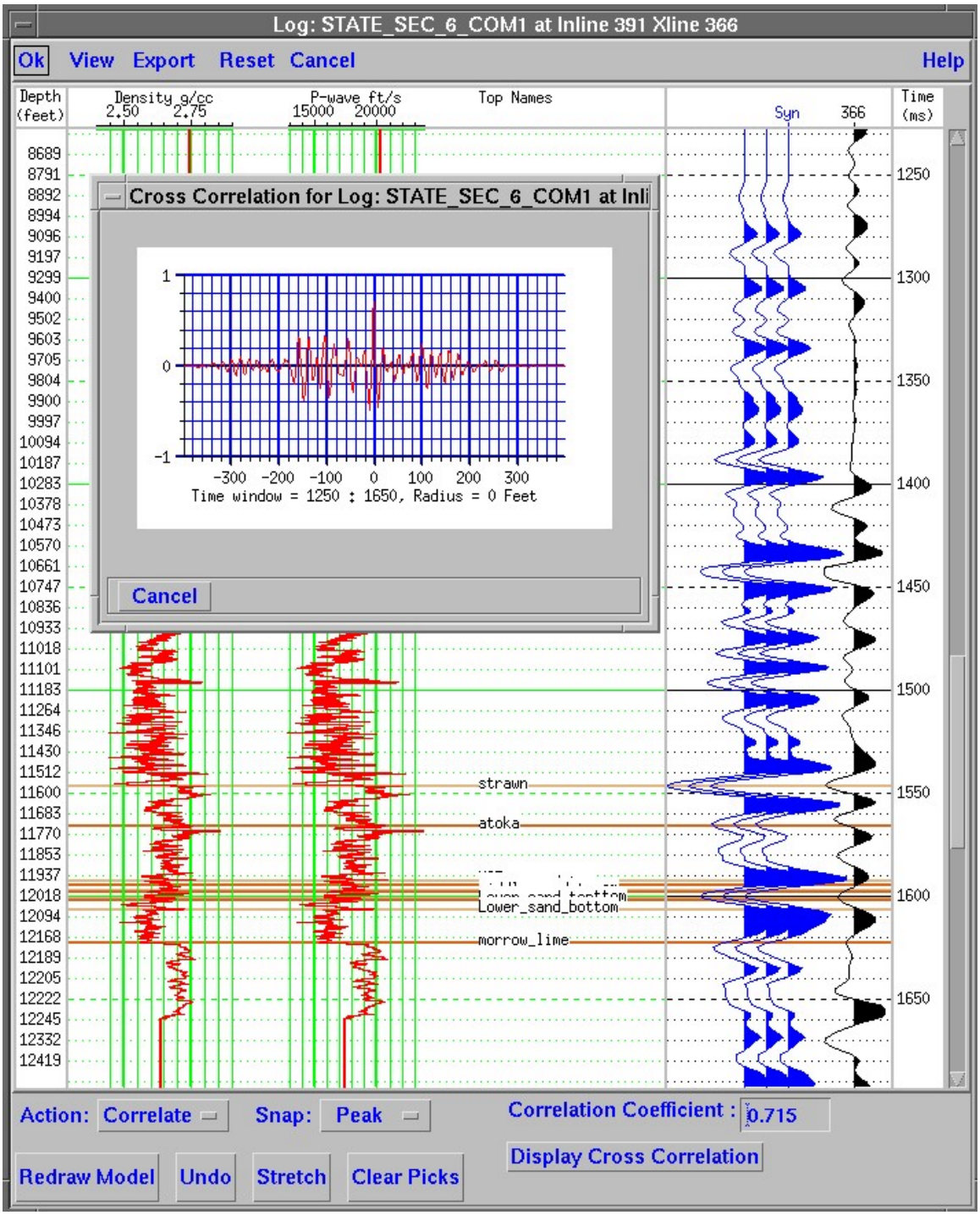

Figure A 2-2: Synthetic seismogram for STATE SEC6 COM1

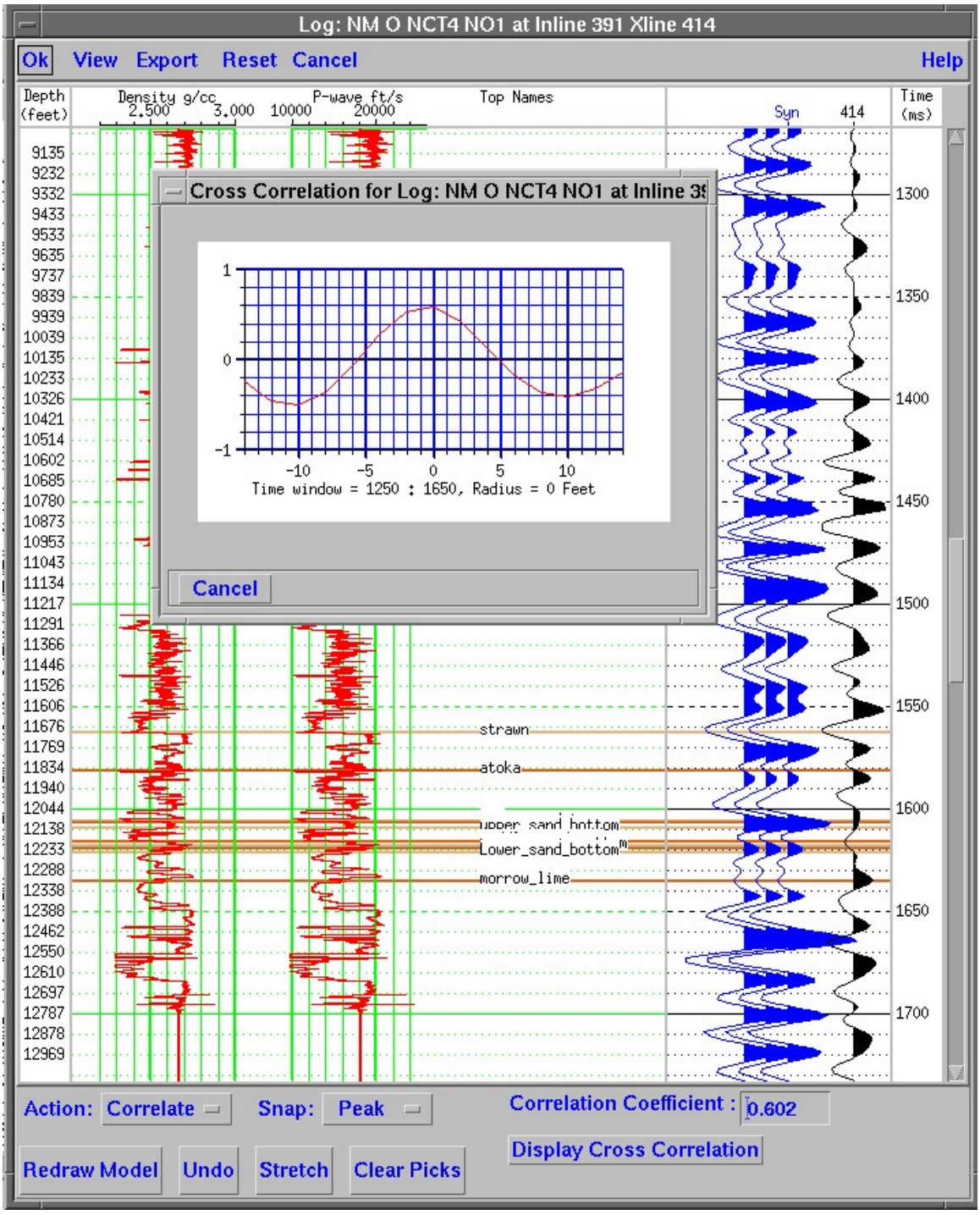

Figure A 2-3: Synthetic seismogram for NM O NCT4 NO1

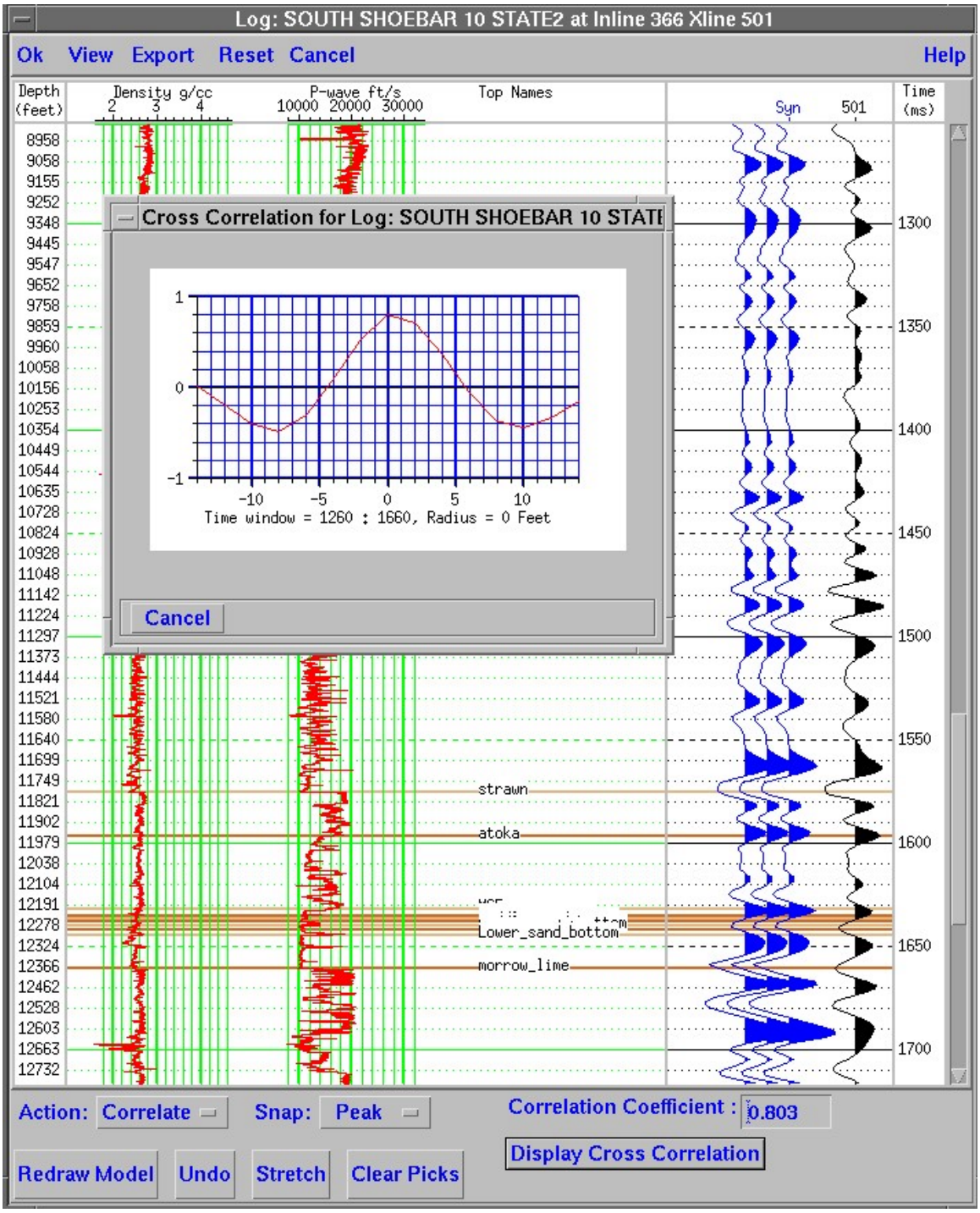

Figure A 2-4: Synthetic seismogram for SOUTH SHOEBAR 10 STATE2

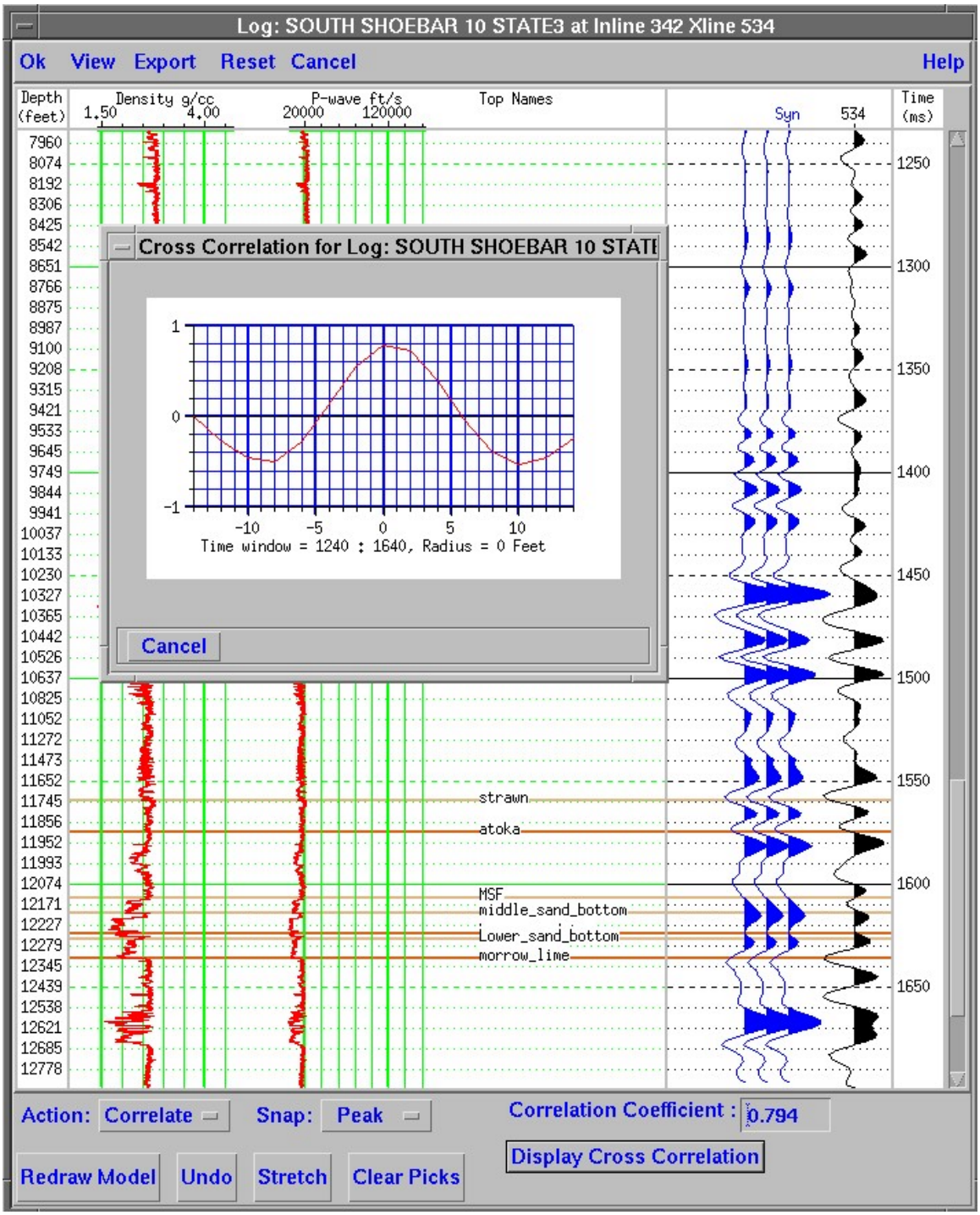

Figure A 2-5: Synthetic seismogram for SOUTH SHOEBAR 10 STATE 3

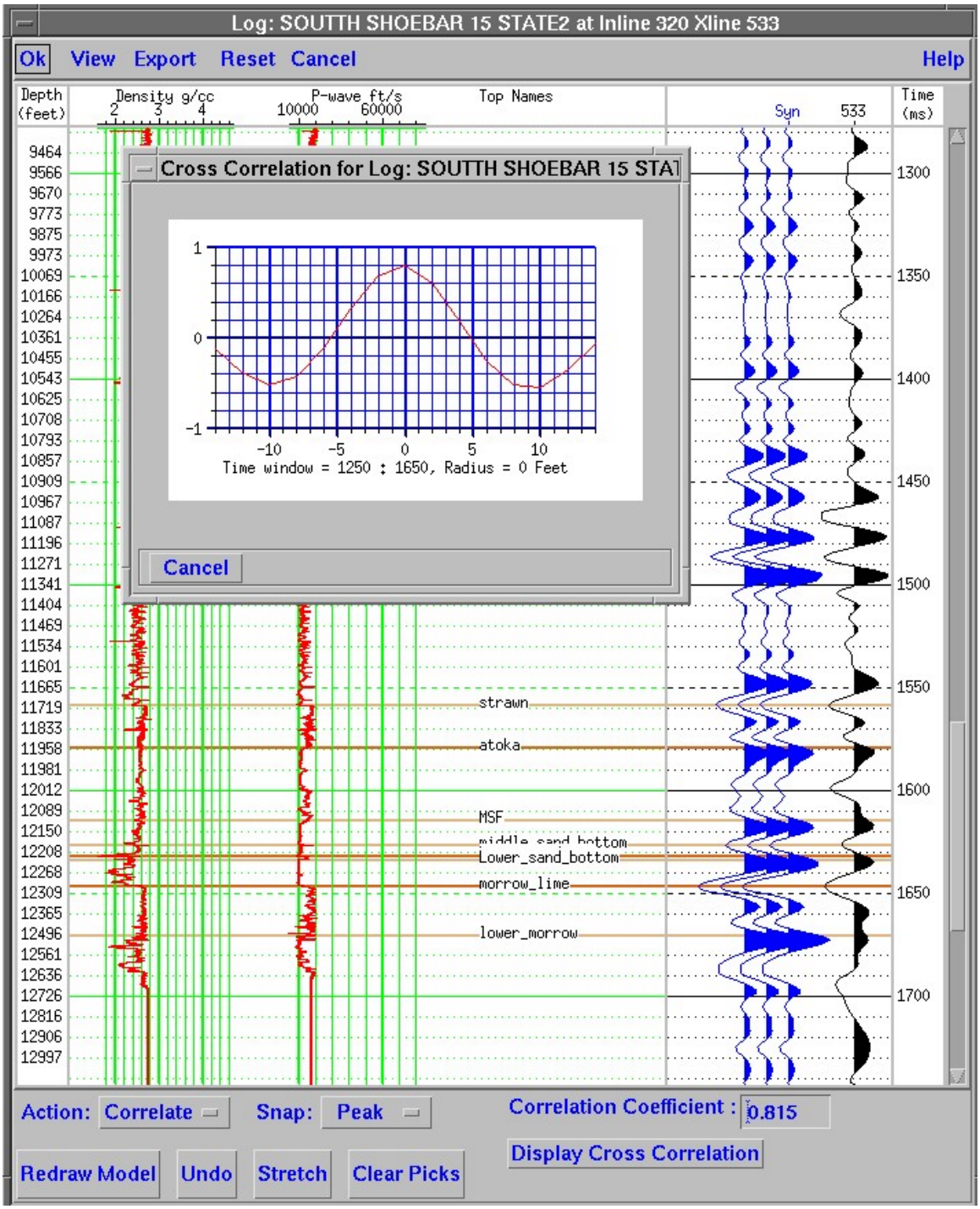

Figure A 2-6: Synthetic seismogram for SOUTH SHOEBAR 15 STATE2

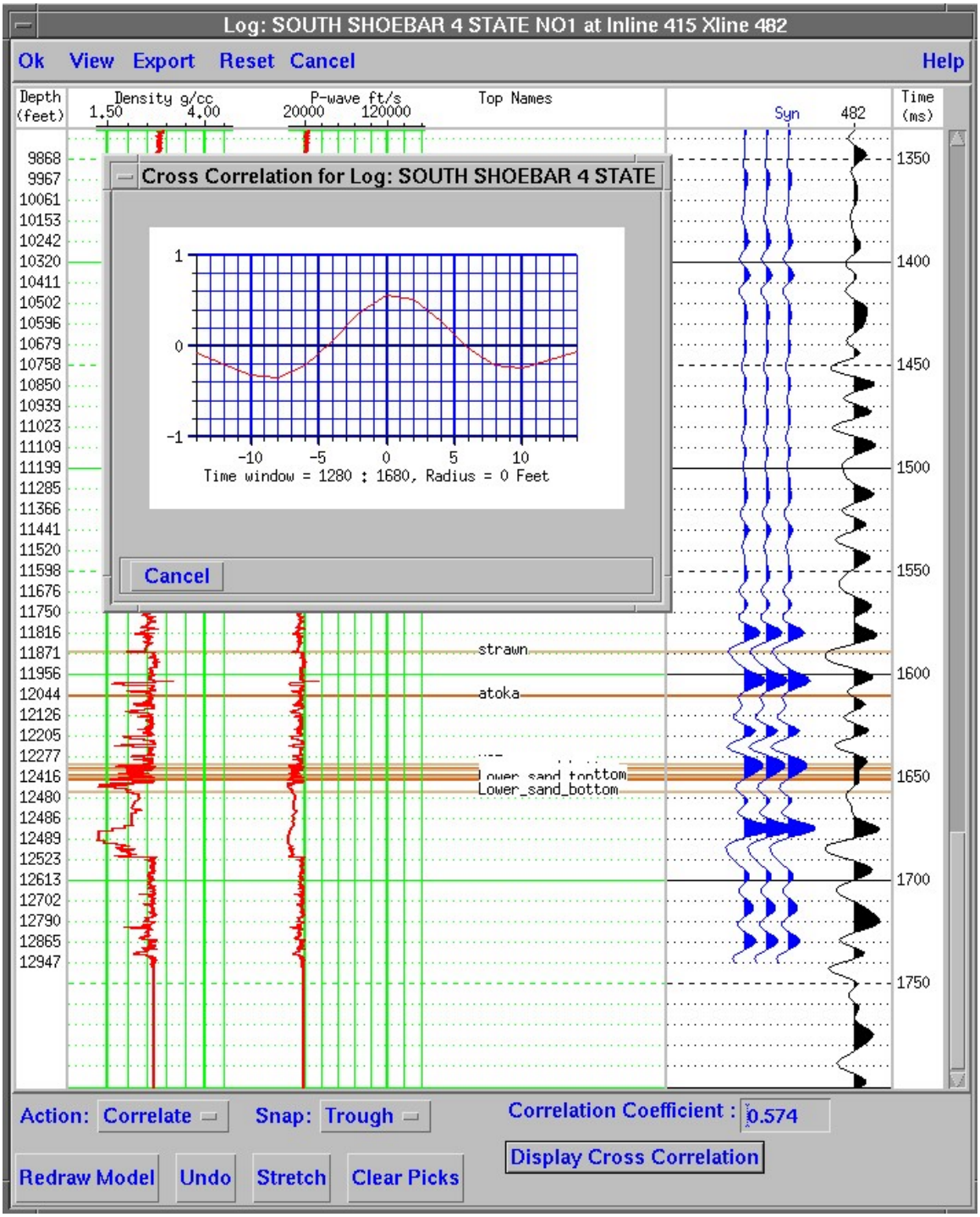

Figure A 2-7: Synthetic seismogram for SHOEBAR4 STATE 1

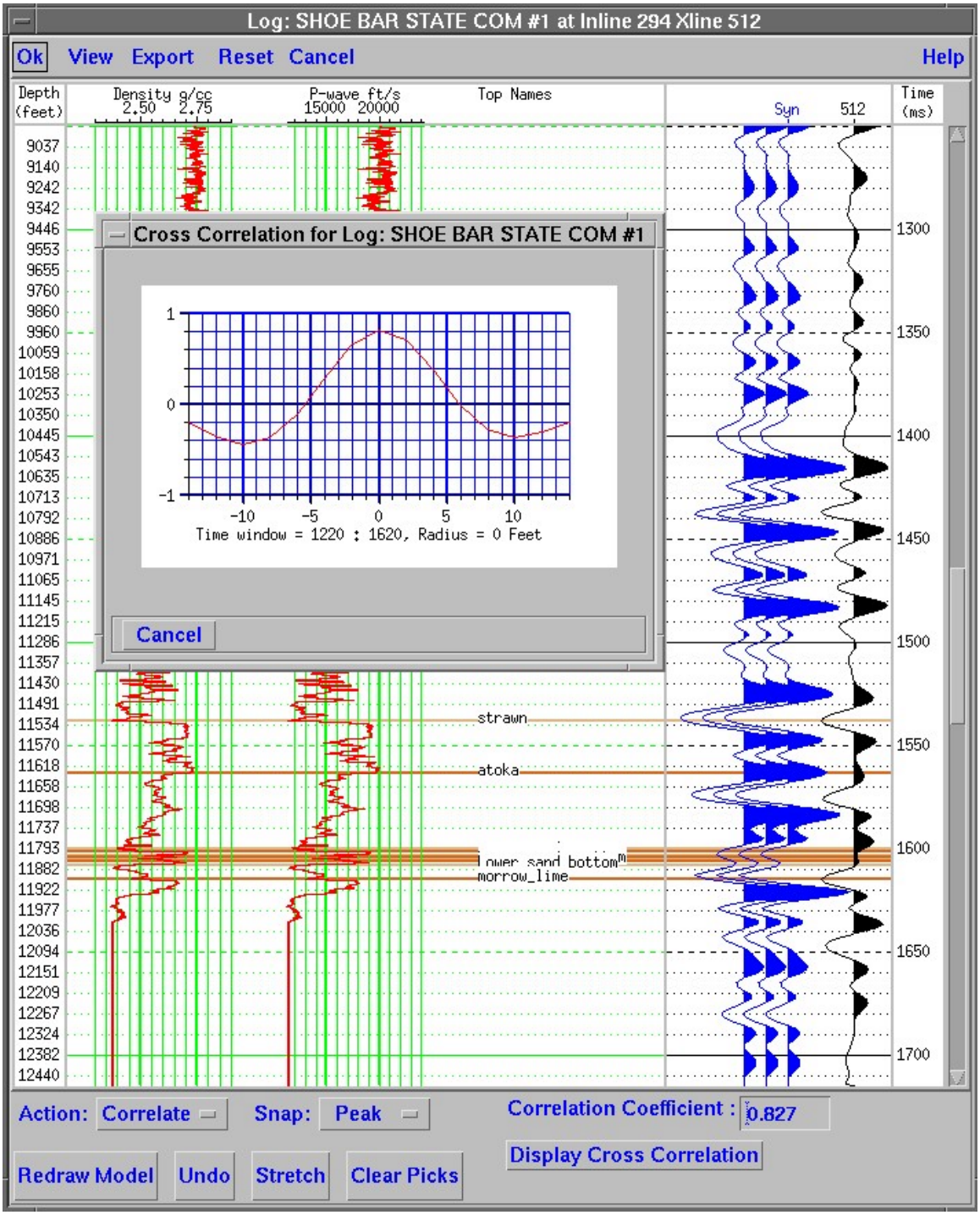

Figure A 2-8: Synthetic seismogram for SHOEBAR STATE COM1

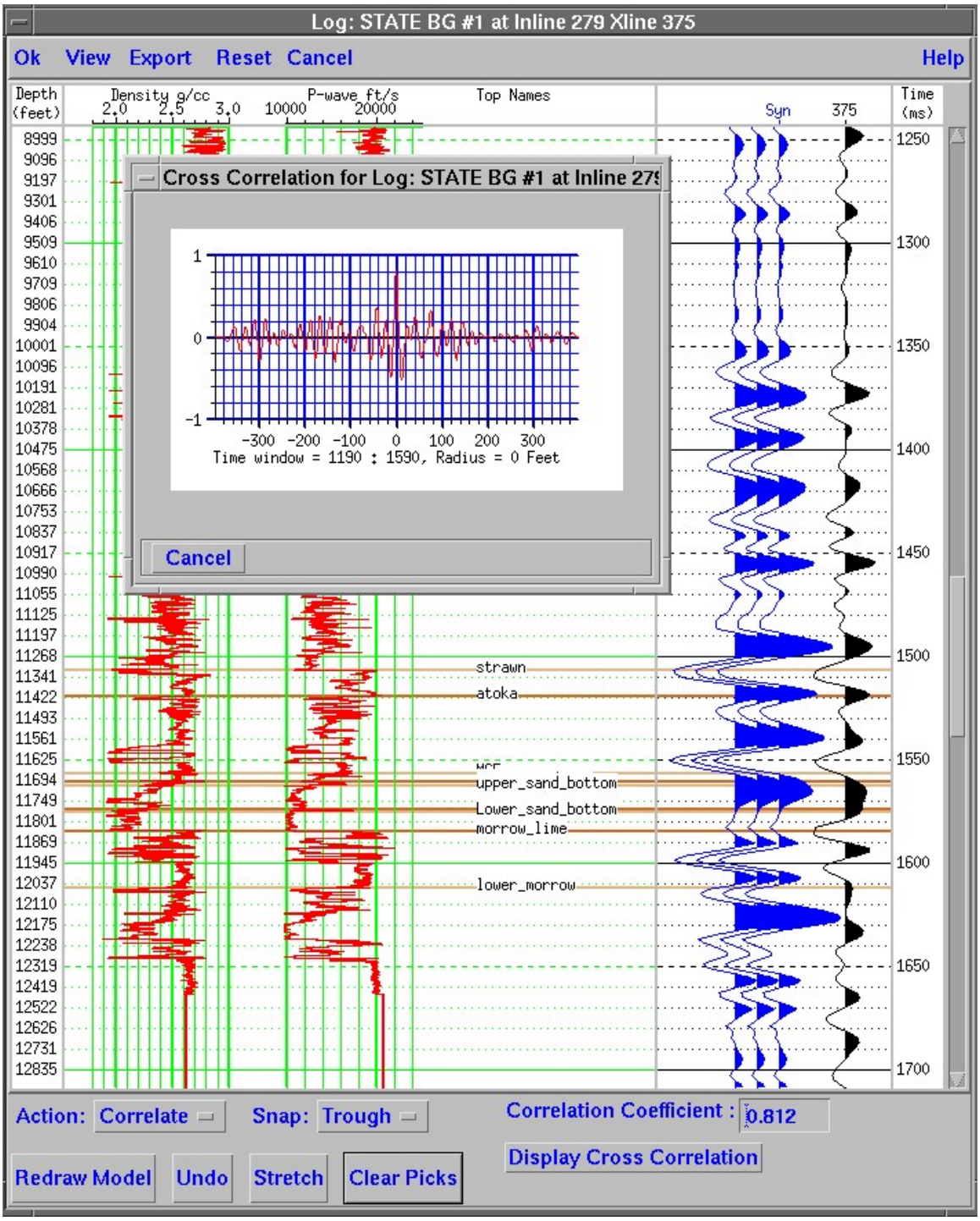

Figure A 2-9: Synthetic seismogram for STATE BG1

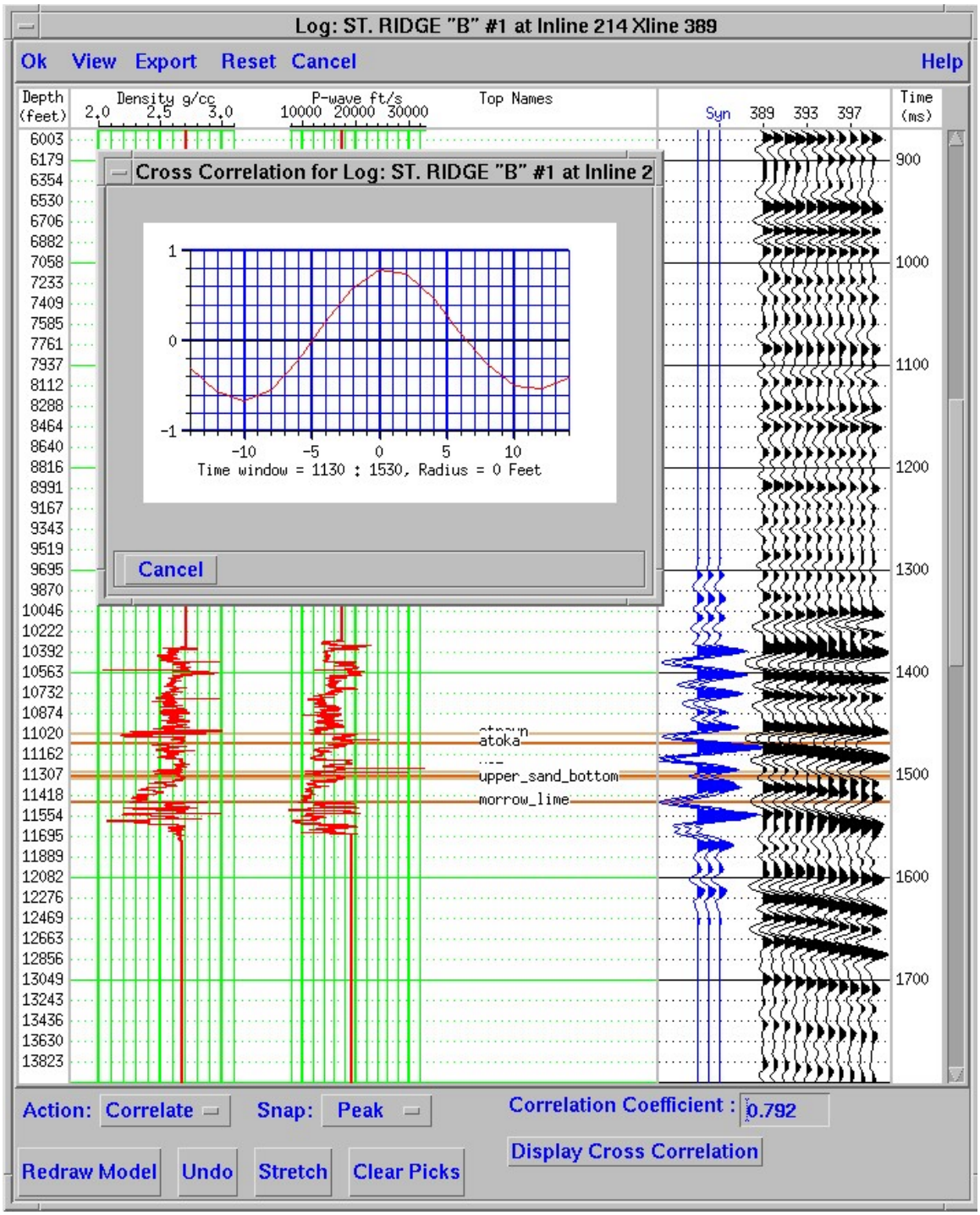

Figure A 2-10: Synthetic seismogram for STATE RIDGE NO1

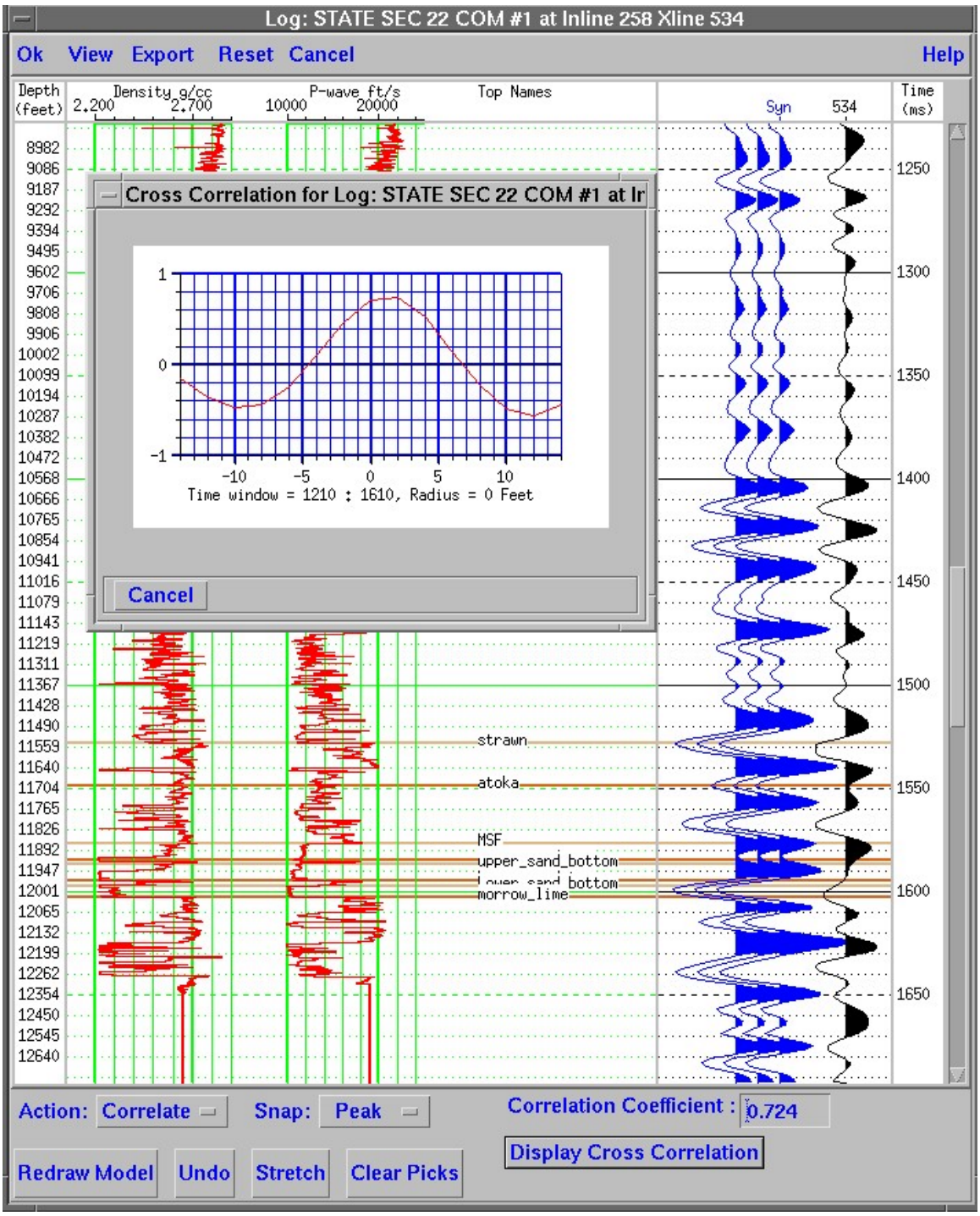

Figure A 2-11: Synthetic seismogram for STATE SEC22 COM1

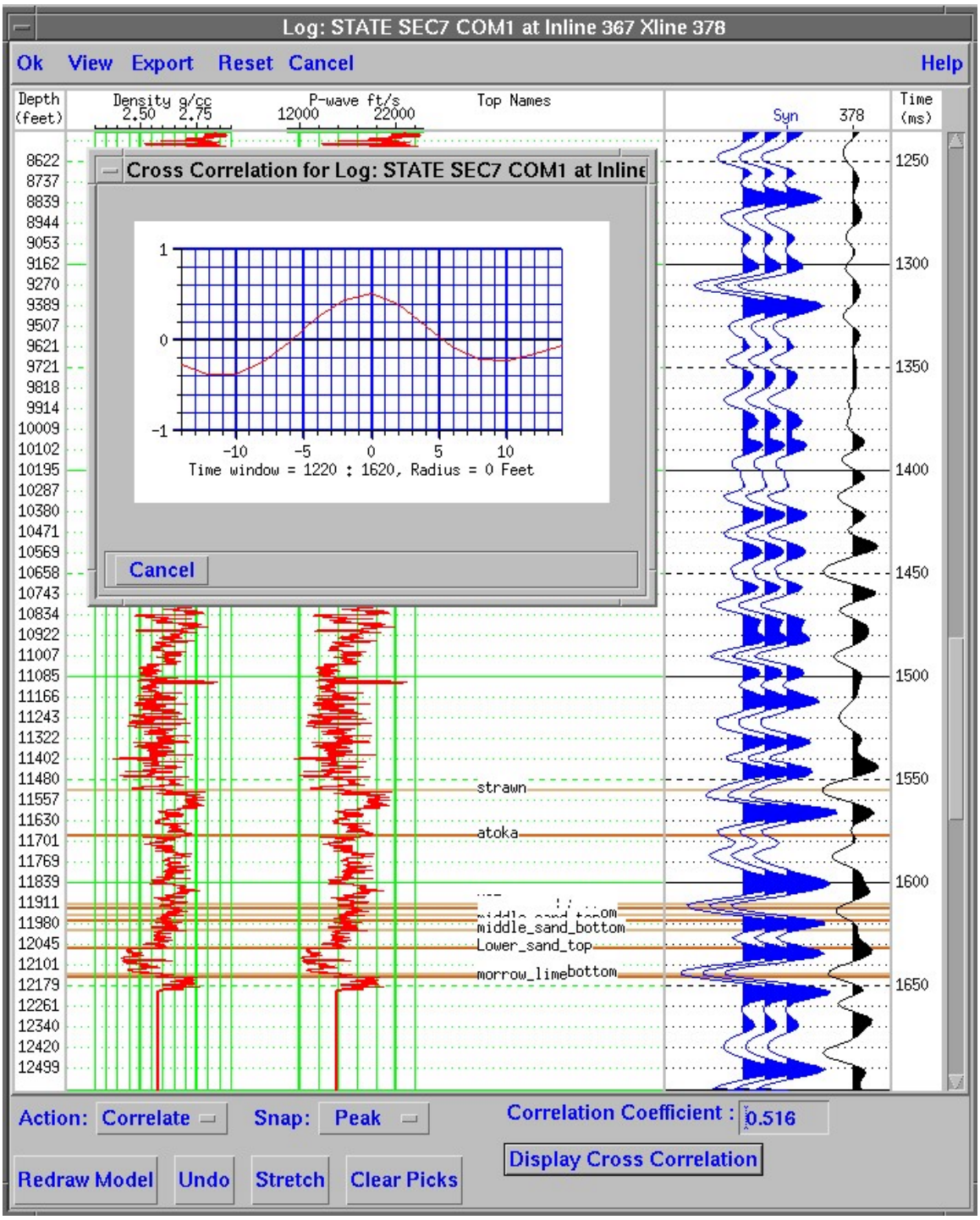

Figure A 2-12: Synthetic seismogram for STATE SECTION 7 COM1

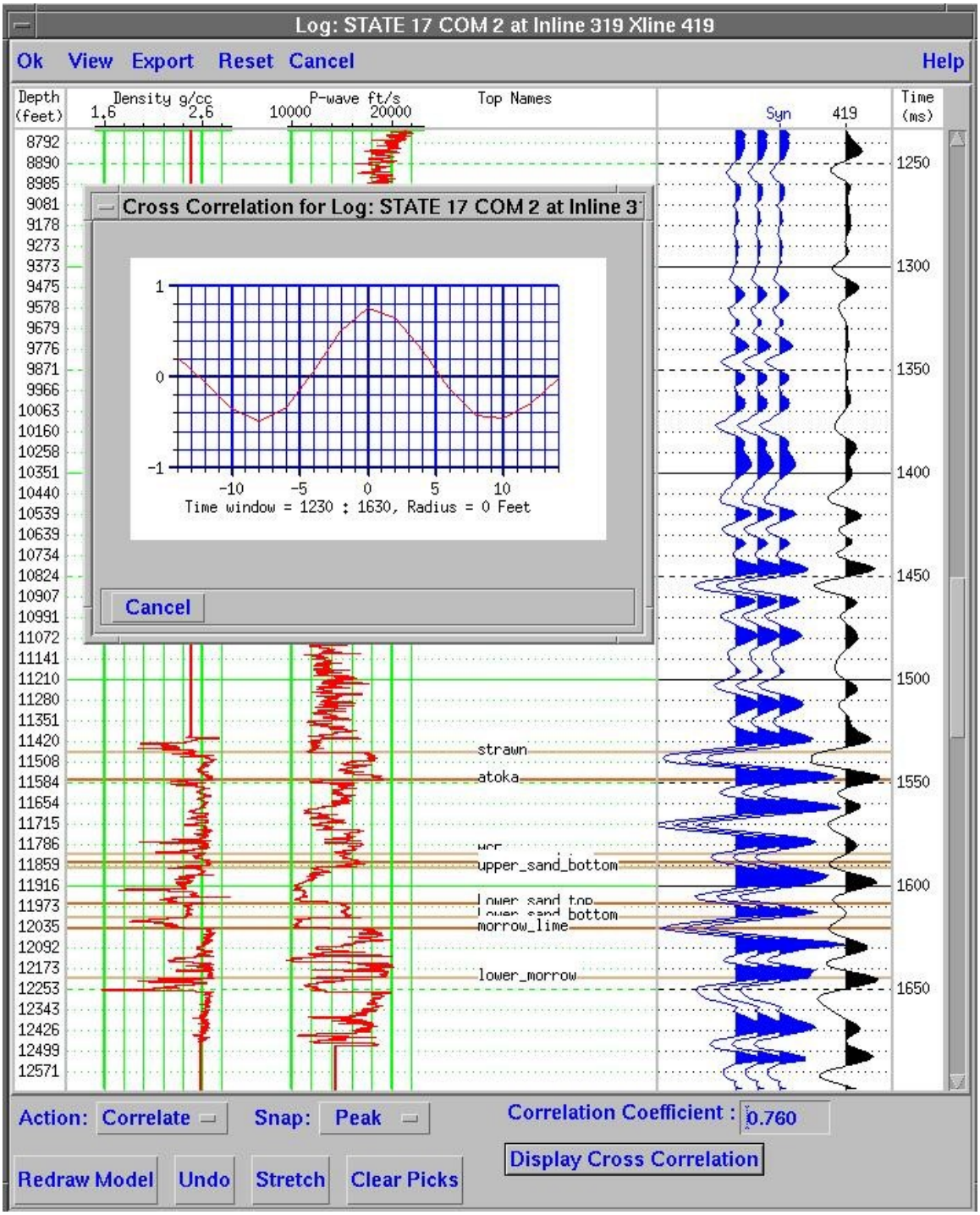

Figure A 2-13: Synthetic seismogram for STATE 17 COM2

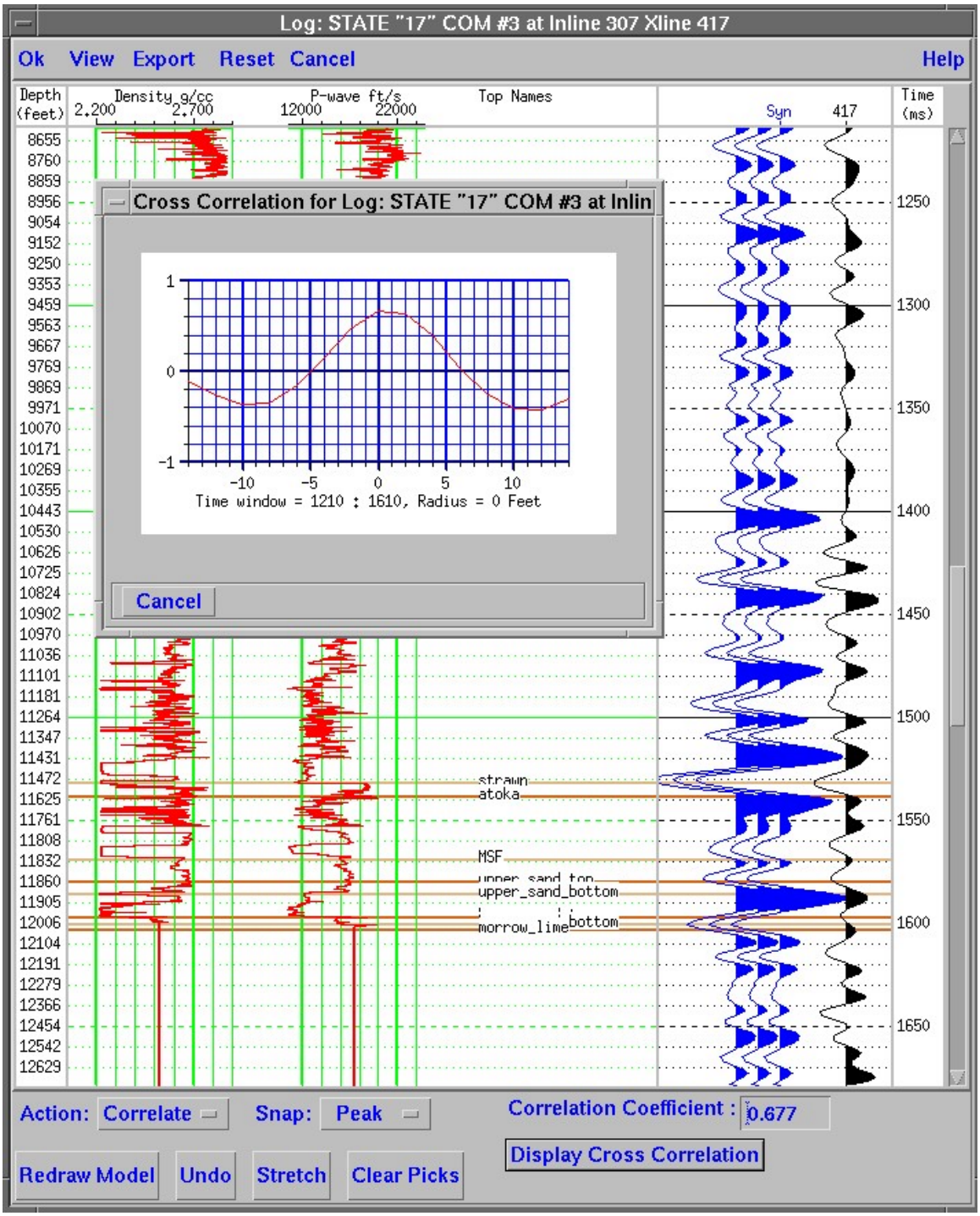

Figure A 2-14: Synthetic seismogram for STATE17 COM3

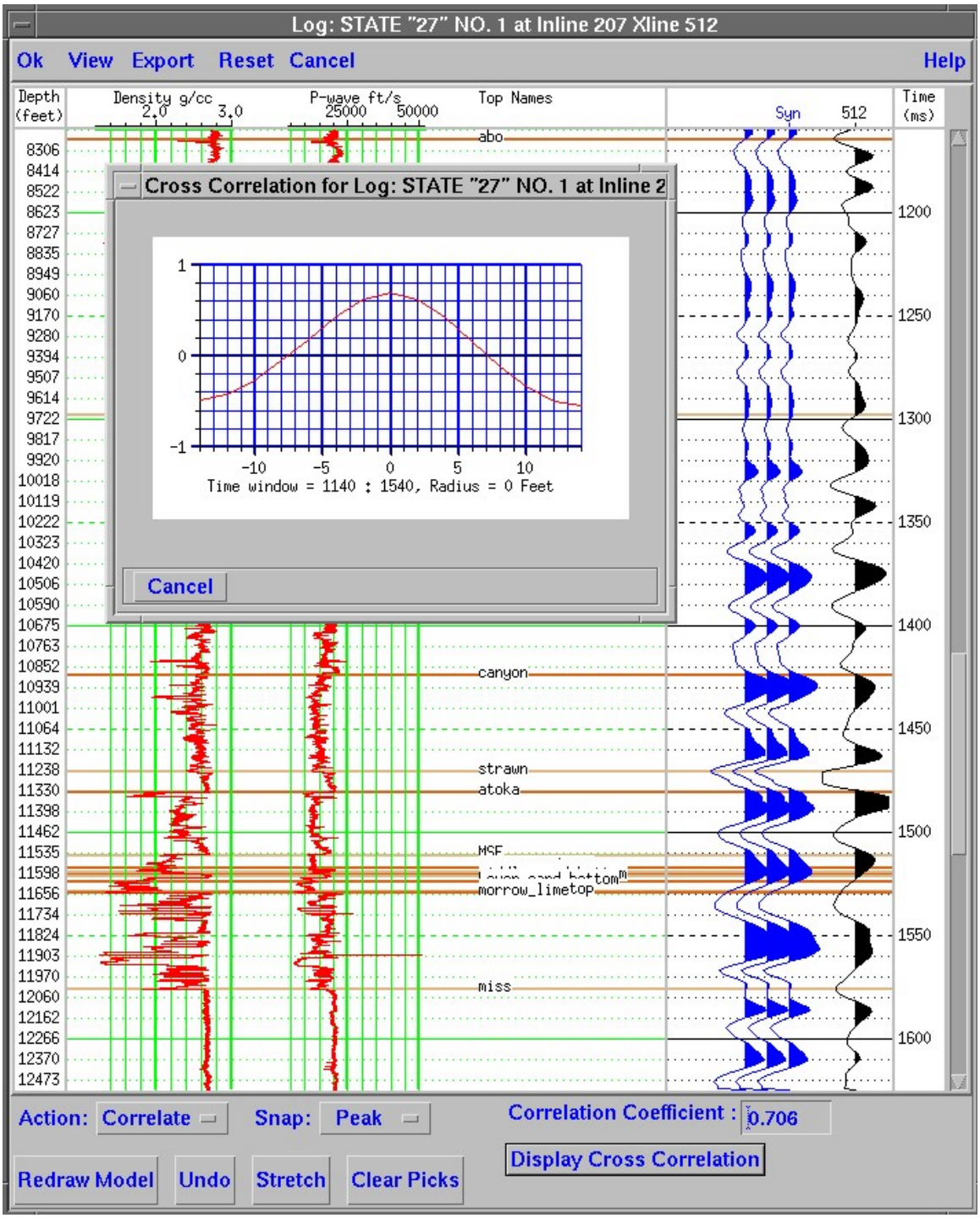

Figure A 2-15: Synthetic seismogram for STATE 27 NO1

APPENDIX 3: ATTRIUBUTE ANALYSIS

Coherency analysis

Coherency analysis, which is termed "FScan attribute" on the Landmark software, processes and measures lateral data similarity/dissimilarity through correlation and semblance techniques (Bahorich and Farmer, 1995). Figure A3-1 illustrates the concept of coherency analysis (Landmark manual), which measuring similarity/dissimilarity of wavelet in trace to trace locally. The result of coherency analysis reveals the subtle stratigraphic and structural changes, which can not be revealed on the conventional amplitude data (Bahorich and Farmer, 1995). More than 20 time slices were generated by coherency analysis in order to examine series of lateral channel migrations. Also flattened Morrow Formation that was picked on the seismic data was flattened to 1700ms as a datum and for removing paleostructural effects. Figures A3-2 to A3-21 show a series of time slices that depict lower Atoka Formation channel system and their migration across the area of focused study.

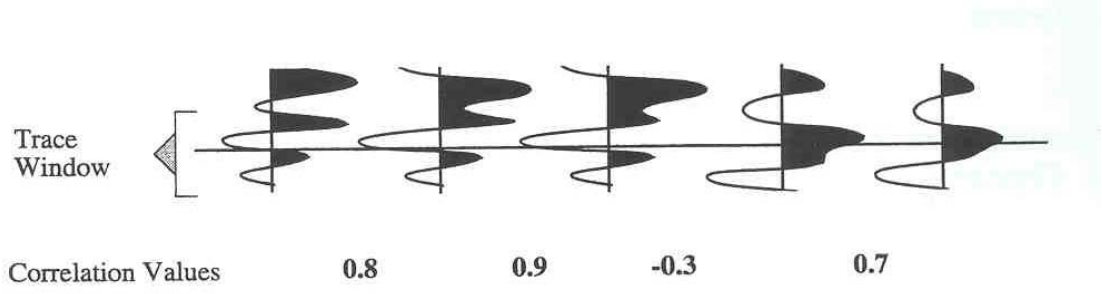

Figure A 3-1: Concepts of the coherency analysis. Coherency analysis searches the similarity or dissimilarity of wave-shape within a time interval.

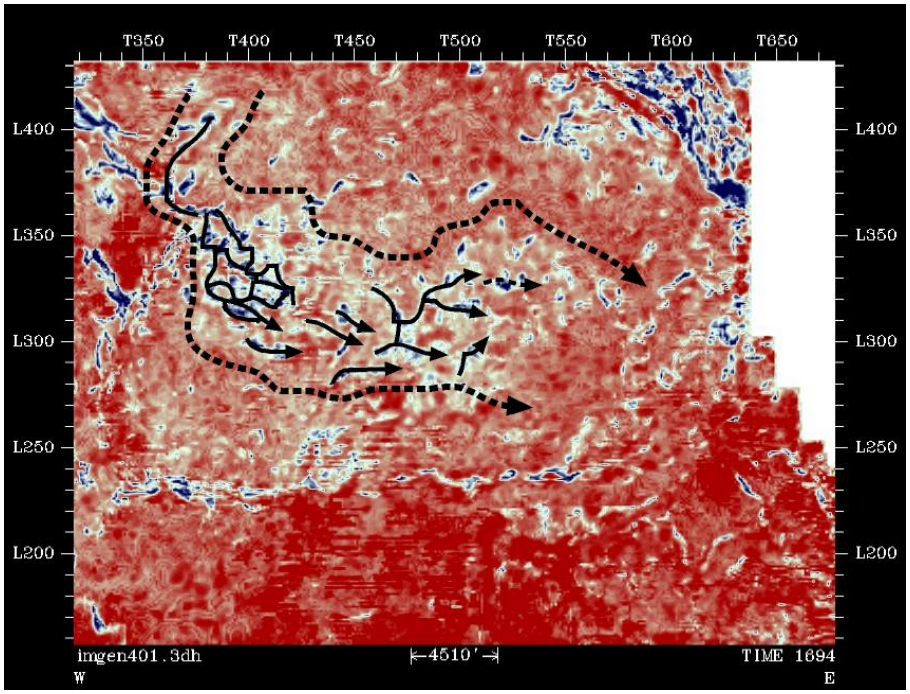

Figure A 3-2 Coherency analysis at 6ms (1694ms from the Morrow Formation that was flattened to 1700ms).

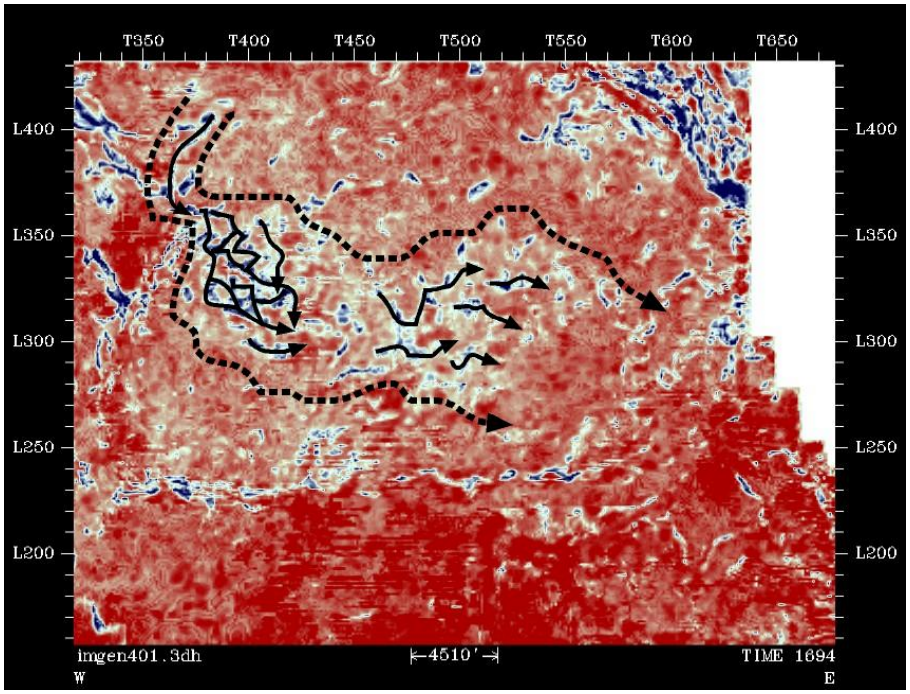

Figure A 3-3 Coherency analysis at 8ms (1692ms from the Morrow Formation that was flattened to 1700ms).

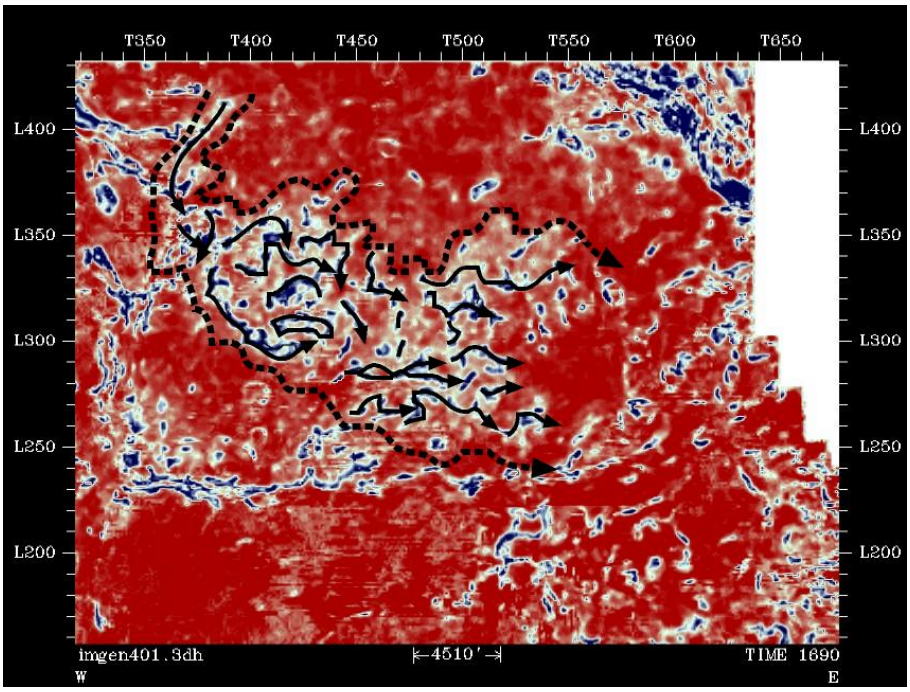

Figure A 3-4 Coherency analysis at 10ms (1690ms from the Morrow Formation that was flattened to 1700ms).

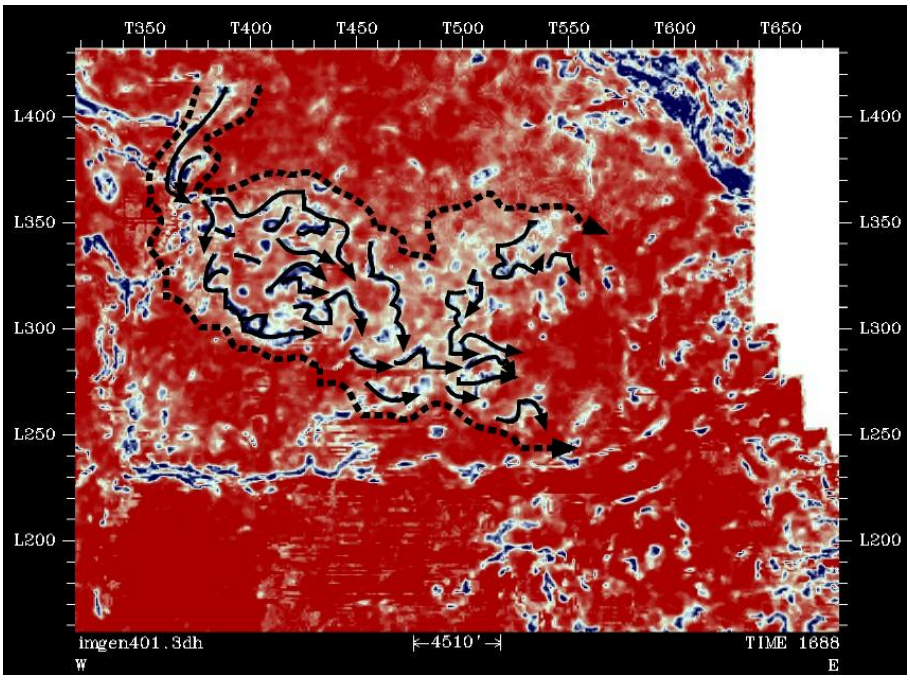

Figure A 3-5 Coherency analysis at 12ms (1688ms from the Morrow Formation that was flattened to 1700ms).

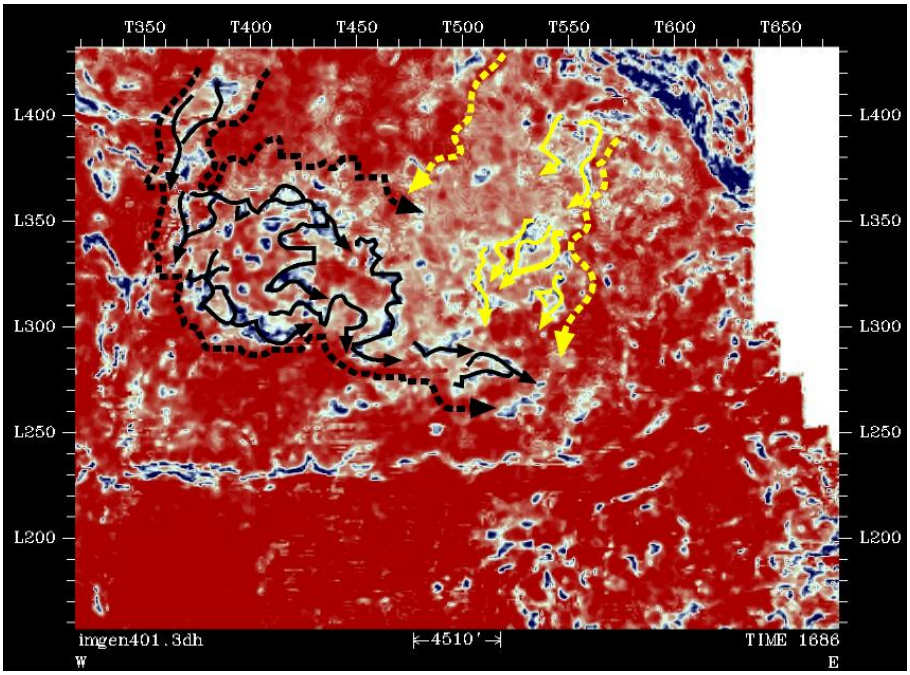

Figure A 3-6 Coherency analysis at 14ms (1686ms from the Morrow Formation that was flattened to 1700ms).

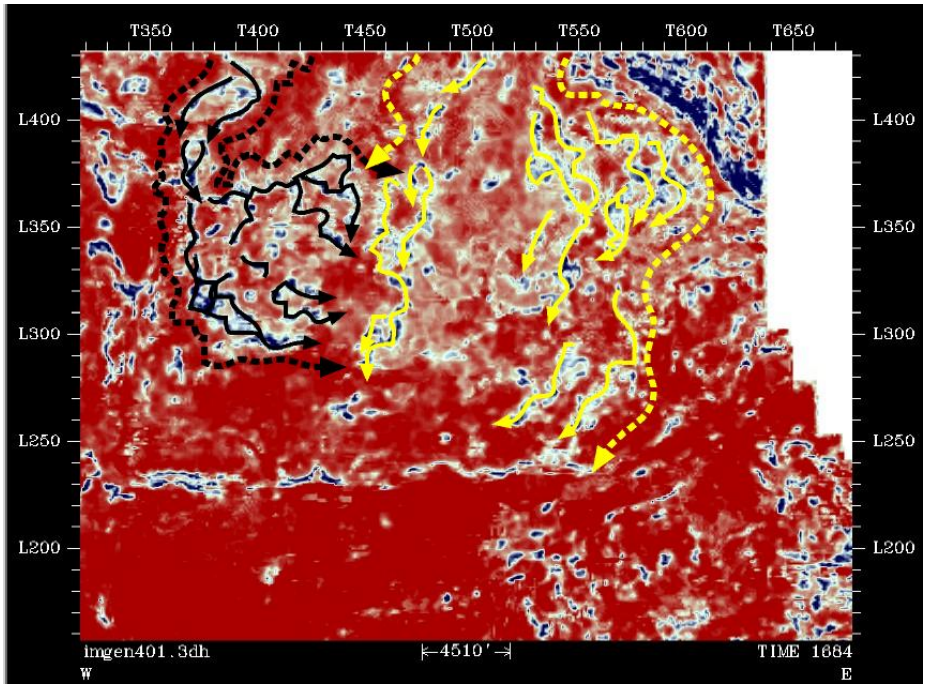

Figure A 3-7 Coherency analysis at 16ms (1684ms from the Morrow Formation that was flattened to 1700ms).

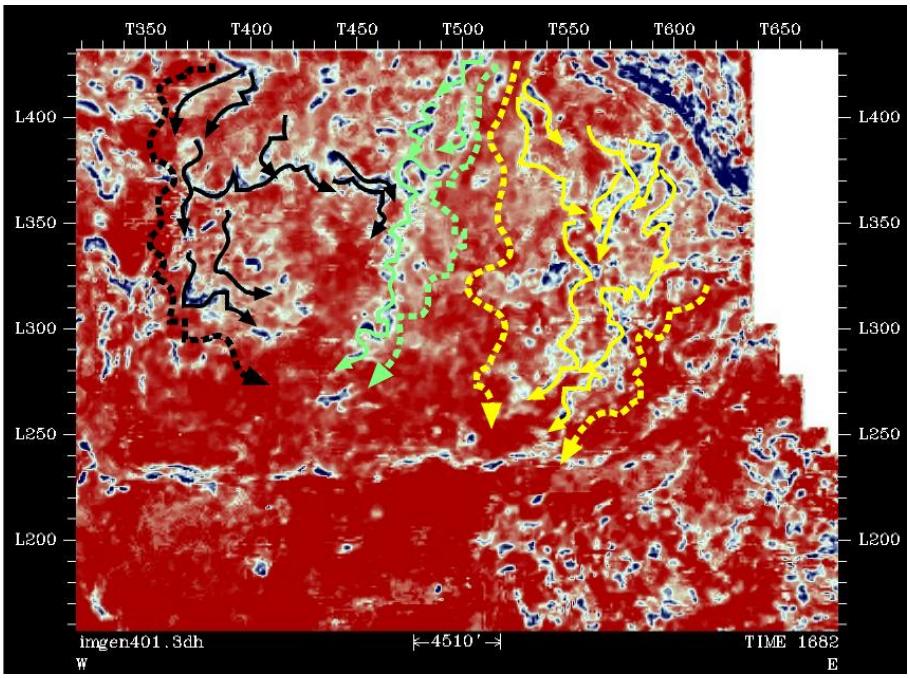

Figure A 3-8 Coherency analysis at 18ms (1682ms from the Morrow Formation that was flattened to 1700ms).

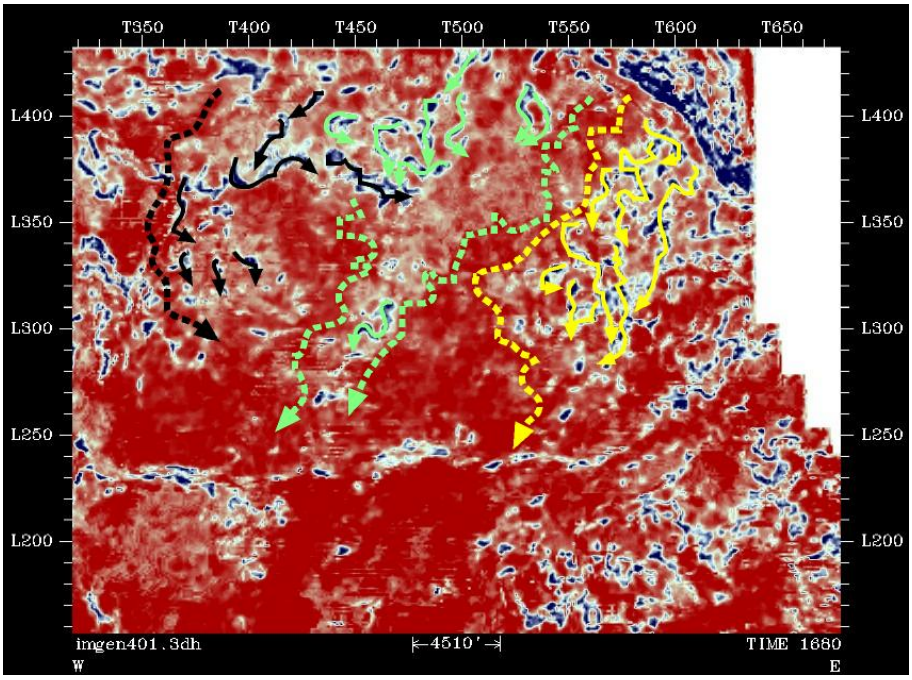

Figure A 3-9 Coherency analysis at 20ms (1680ms from the Morrow Formation that was flattened to 1700ms).

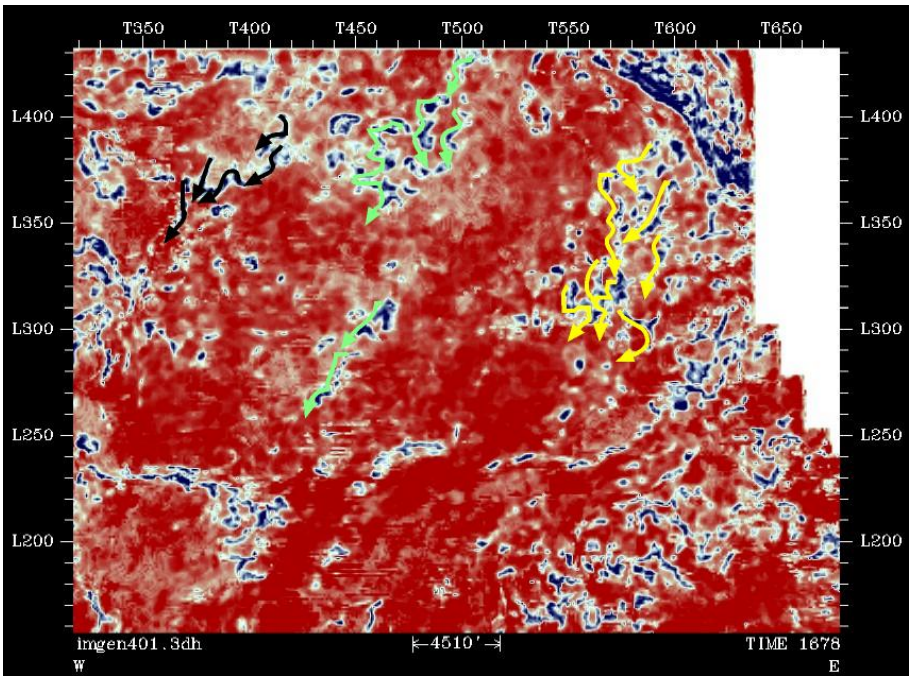

Figure A 3-10 Coherency analysis at 22ms (1678ms from the Morrow Formation that was flattened to 1700ms).

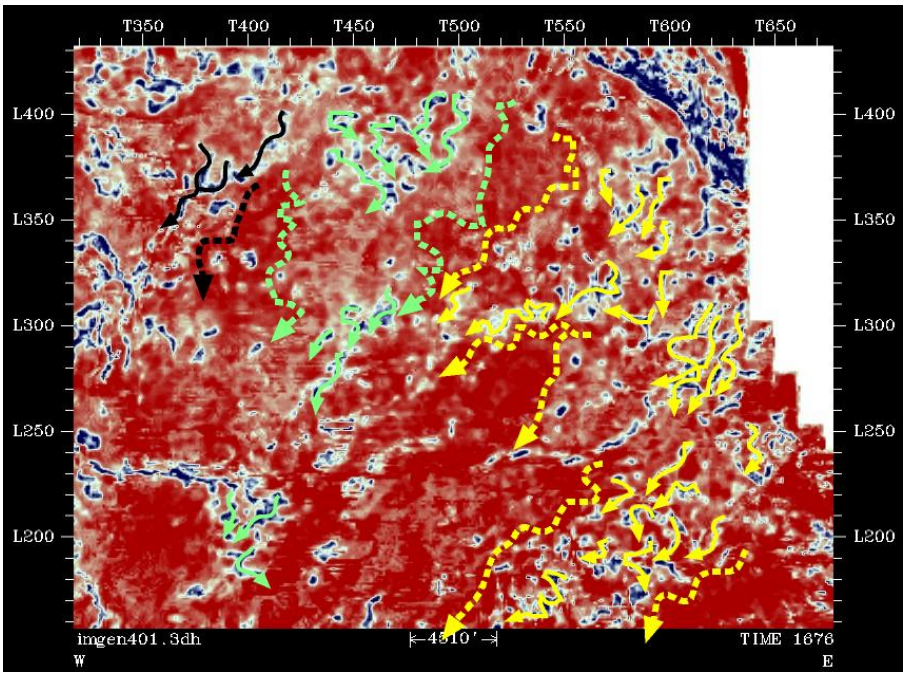

Figure A 3-11 Coherency analysis at 24ms (1676ms from the Morrow Formation that was flattened to 1700ms).

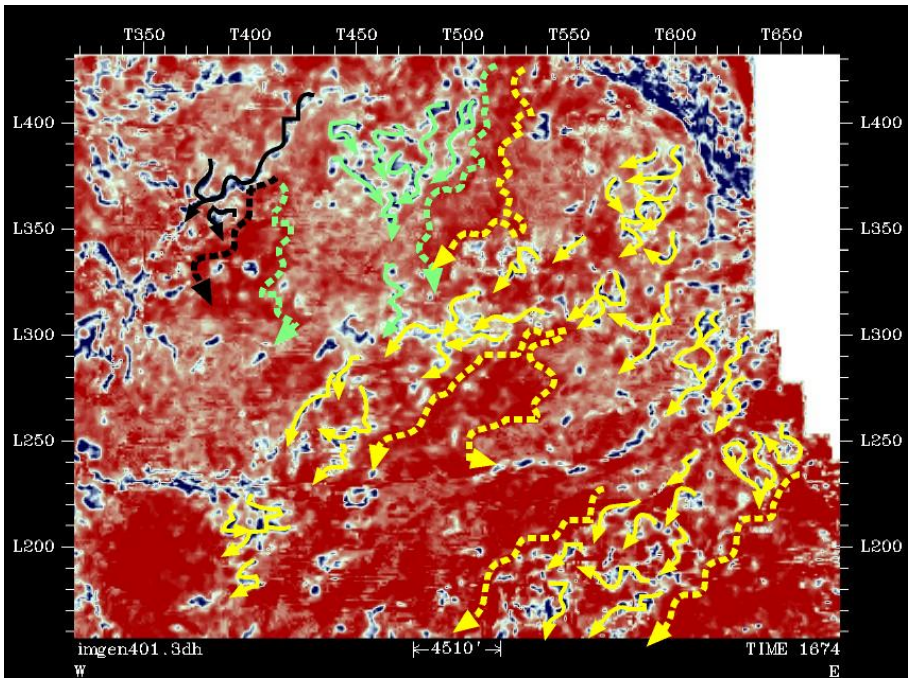

Figure A 3-12 Coherency analysis at 26ms (1674ms from the Morrow Formation that was flattened to 1700ms).

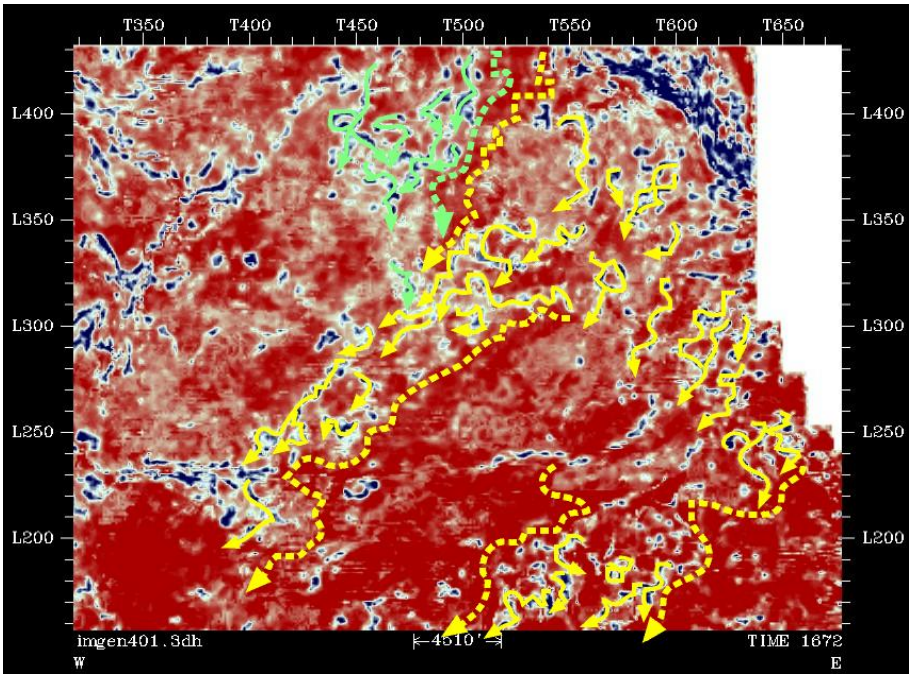

Figure A 3-13 Coherency analysis at 28ms (1672ms from the Morrow Formation that was flattened to 1700ms).

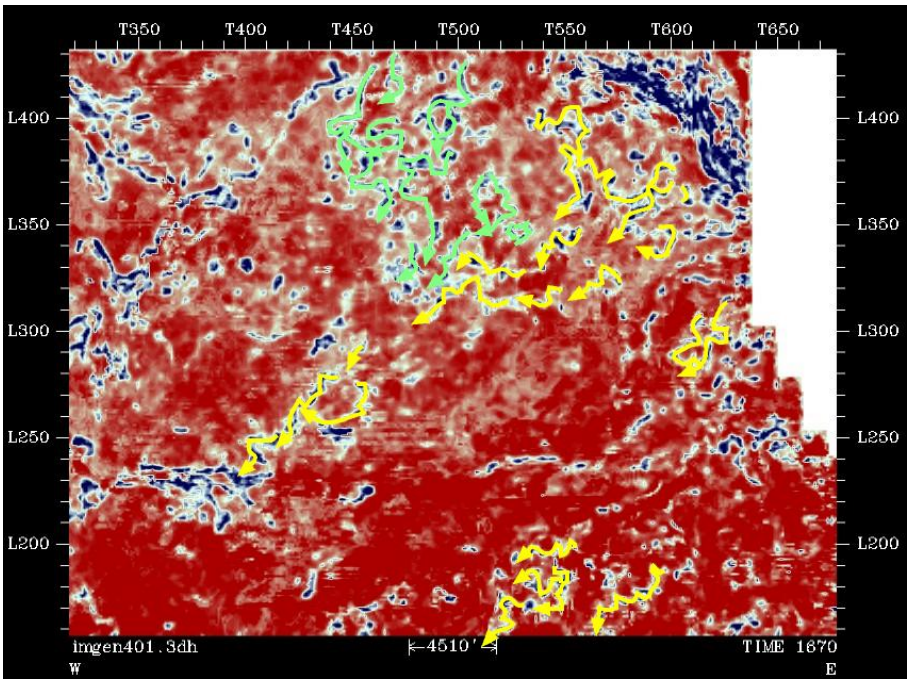

Figure A 3-14 Coherency analysis at 30ms (1670ms from the Morrow Formation that was flattened to 1700ms).

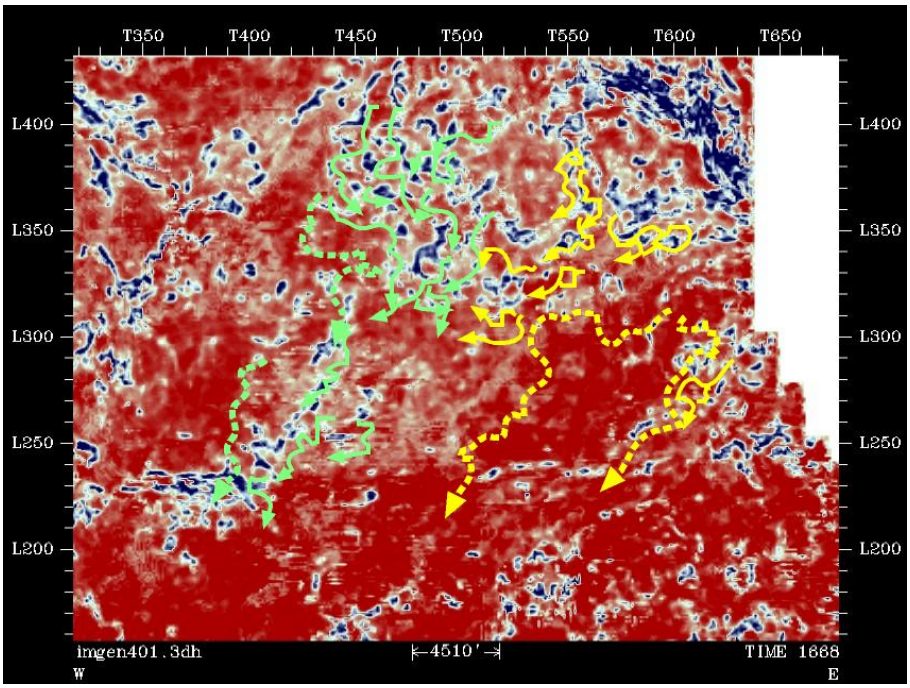

Figure A 3-15 Coherency analysis at 32ms (1668ms from the Morrow Formation that was flattened to 1700ms).

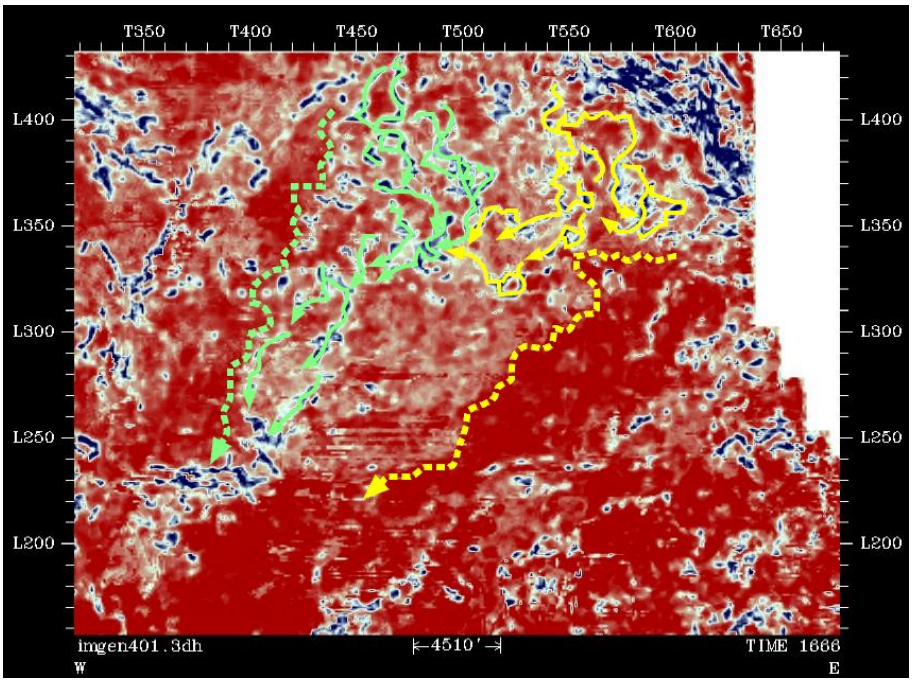

Figure A 3-16 Coherency analysis at 34ms (1666ms from the Morrow Formation that was flattened to 1700ms).

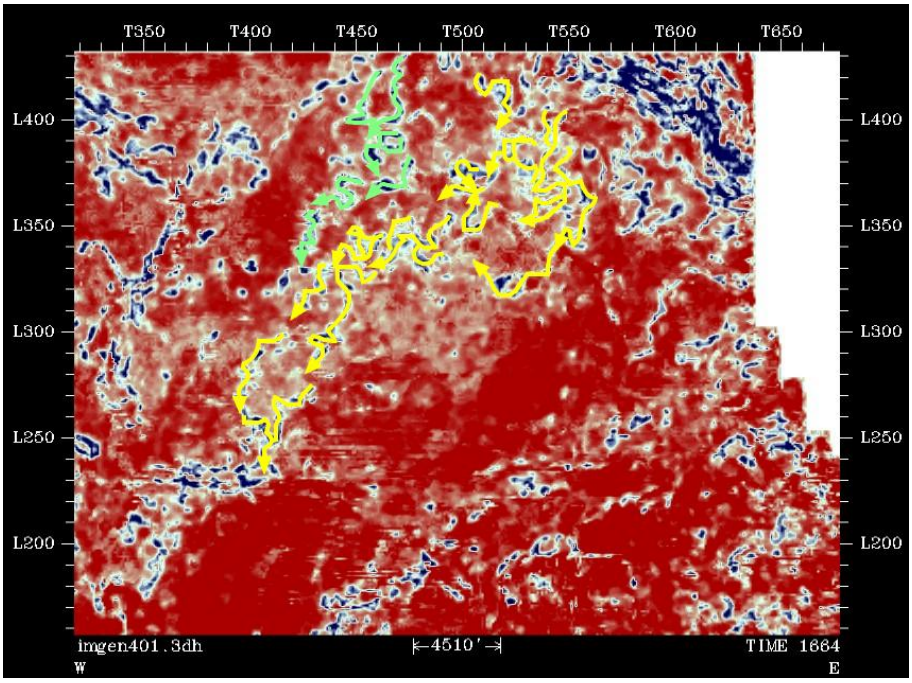

Figure A 3-17 Coherency analysis at 36ms (1664ms from the Morrow Formation that was flattened to 1700ms).

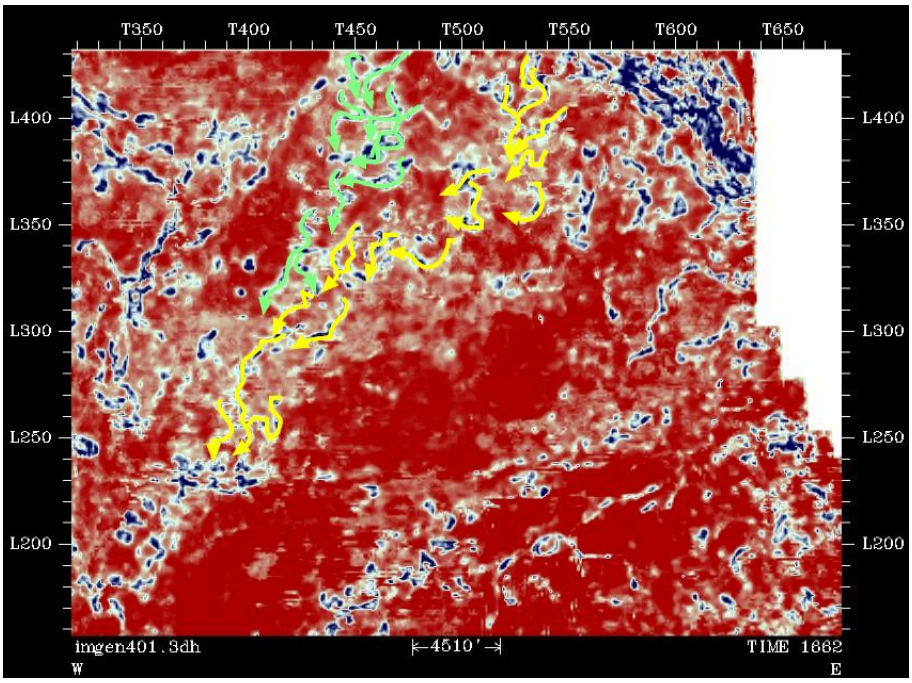

Figure A 3-18 Coherency analysis at 38ms (1662ms from the Morrow Formation that was flattened to 1700ms).

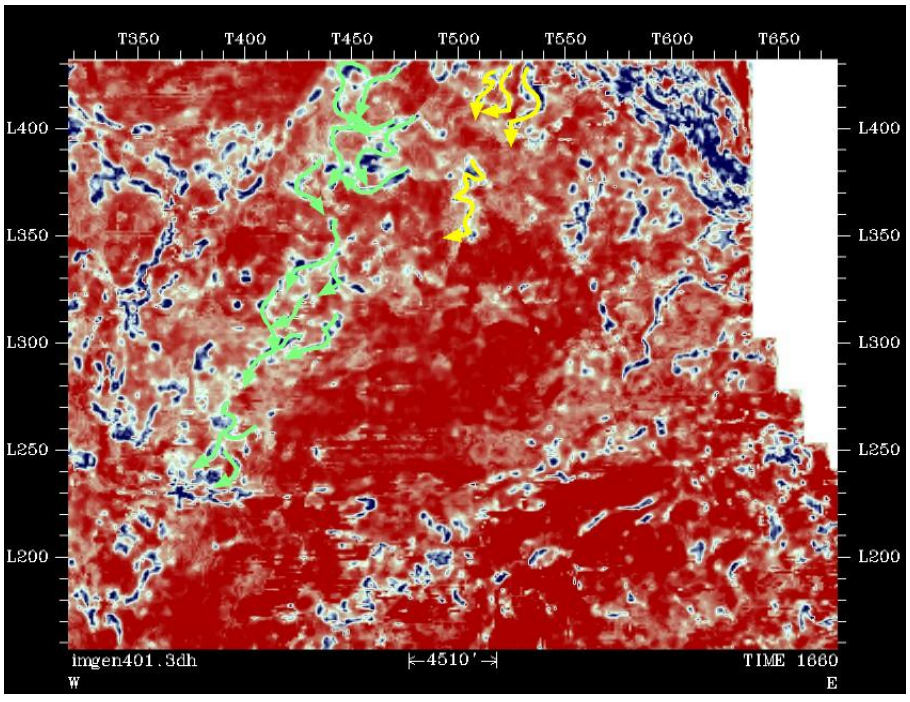

Figure A 3-19 Coherency analysis at 40ms (1660ms from the Morrow Formation that was flattened to 1700ms).

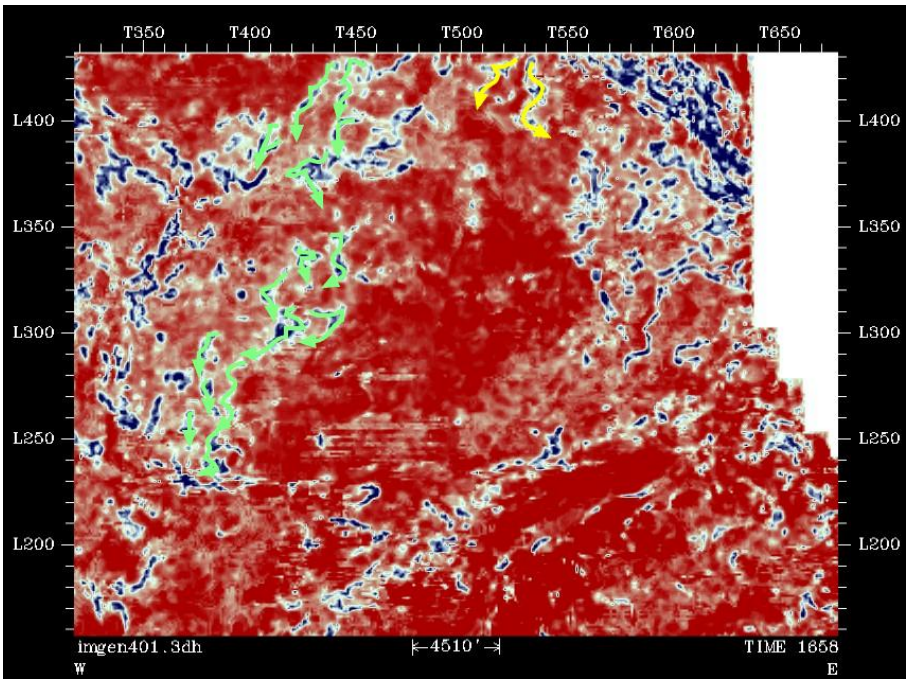

Figure A 3-20 Coherency analysis at 42ms (1658ms from the Morrow Formation that was flattened to 1700ms).

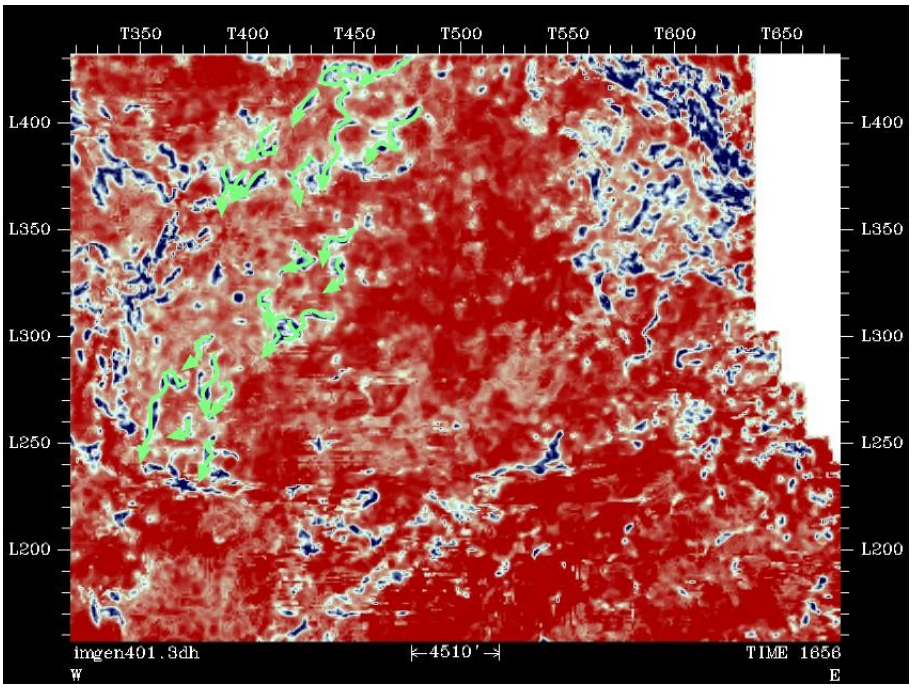

Figure A 3-21 Coherency analysis at 44ms (1656ms from the Morrow Formation that was flattened to 1700ms).

Single/Multi attribute analysis

Introduction

Seismic attributes may describe a physical property distribution, potentially correlative to log properties. Such relationships between log and seismic properties may assist in prediction of physical properties (density, porosity, velocity and so on) in inter well areas. In order to examine the attributes, such as amplitude, frequency and phase, to predict a relationship between log-derived physical properties and seismic attributes, a volume-based single attribute study was performed to find the relationship between each attribute and porosity related to the lower Atoka sandstone. Then volume-based multi-attribute study was performed to attempt to predict porosity of lower Atoka sandstone (Pearson, 1999 and Leiphart, 2000).

Results - Single attribute analysis

Single attribute analysis was performed on 11 wells using Emerge - Hampson-Russell software. The lower Atoka sand interval was used as an analysis window using synthetic seismograms because it is relatively thicker and has better log availability than the upper sand interval. Table A 3-1 describes the result of a single attribute analysis from the highest to next twenty single attribute correlations.

Target	Attribute	Error	Correlation
Sqrt(Porosity)	Second Derivative Instantaneous amplitude	0.067666	0.417732
Porosity	Second Derivative Instantaneous amplitude	0.067798	0.515295
Log(Porosity)	Second Derivative Instantaneous amplitude	0.070132	0.31774
Porosity	Derivative Instantaneous Amplitude	0.072987	0.385721
Sqrt(Porosity)	Derivative Instantaneous Amplitude	0.073229	0.371395
(Porosity)**2	Second Derivative Instantaneous amplitude	0.073686	0.672466
Log(Porosity)	Derivative Instantaneous Amplitude	0.074584	0.349368
Porosity	Cosine Instantaneous Phase	0.074657	0.330736
Porosity	Derivative	0.074887	0.322341
Sqrt(Porosity)	Cosine Instantaneous Phase	0.075137	0.306871
Sqrt(Porosity)	Derivative	0.075412	0.299336
Porosity	Integrate	0.076362	-0.261259
Porosity	Raw Seismic	0.076589	0.250421
Porosity	Amplitude Weighted Cosine Phase	0.0766	0.249876
Log(Porosity)	Cosine Instantaneous Phase	0.076714	0.270535
Porosity	Amplitude Envelope	0.076722	-0.243788
Sqrt(Porosity)	Integrate	0.076873	-0.277613
Log(Porosity)	Derivative	0.077064	0.262314
Sqrt(Porosity)	Raw Seismic	0.077165	0.247268
Sqrt(Porosity)	Amplitude Weighted Cosine Phase	0.077176	0.246689

Table A3-1: The result of single attribute analysis of the Lower sand

Interpretation

The results of single attribute analysis show only weak correlation between porosity and second derivative instantaneous amplitude. There is no correlation between porosity and frequency, or porosity and phase. The results of single attribute analysis are very poor.

Multi-attribute analysis

In order to obtain more porosity prediction power, multi-attribute analysis was performed. Twelve attributes were extracted from the seismic data volume. Table A3-2 describes the result of multi-attribute analysis. Additionally, six attributes were selected as the optimizing combination of attribute for prediction of porosity based on the analysis

of the validation error. Figure A3-22 presents the selected 6 attributes based on the validation analysis and the cross validation plot.

Number of Attribute	Traget	Final Attribute	Error
1	Sqrt(porosity)	Second Derivative Instantaneous Amplitude	0.061233
2	Sqrt(porosity)	Amplitude Envelope	0.048791
3	Sqrt(porosity)	Average Frequency	0.043397
4	Sqrt(porosity)	Derivative	0.041078
5	Sqrt(porosity)	Apparent Polarity	0.039283
6	Sqrt(porosity)	Amplitude Weighted Cosine Phase	0.03765
7	Sqrt(porosity)	Integrate	0.035725
8	Sqrt(porosity)	Integrated Absolute Amplitude	0.033965
9	Sqrt(porosity)	Instantaneous Frequency	0.031516
10	Sqrt(porosity)	Amplitude weighted Frequency	0.029564
11	Sqrt(porosity)	Amplitude Weighted Phase	0.023089
12	Sqrt(porosity)	Dominant Frequency	0.018368

Table A3-2: Result of multi-attribute analysis

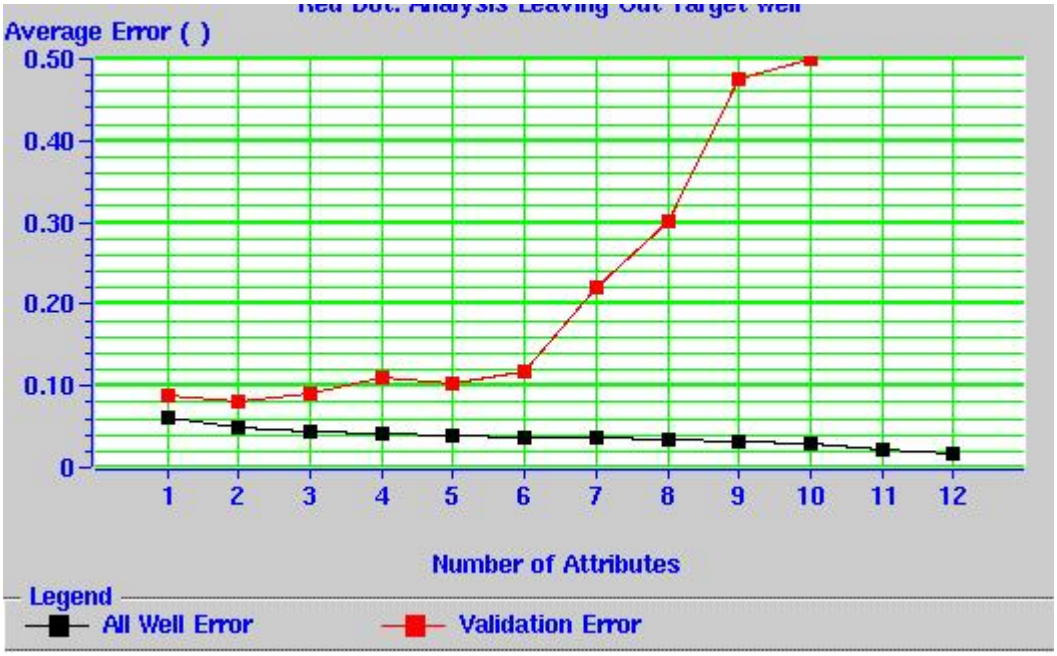

Figure A3-22: Validation analysis and the cross validation plot

The result of the multi-attribute analysis was obtained using linear regression multi-attribute analysis, and the linear regression equation can be defined as

$$\phi(t) = \quad w0 + A1w1(t) + A2w2 + A3w3 + A4w4 + A5w5 + A6w6 + A7w7$$

Where ϕ is porosity, An is the attribute, Wn is the weight applied to the attribute, and t is time. Figure A4-23 shows the result of the linear regression multi-attribute analysis by cross-plot of the data. The correlation coefficient of the linear regression is 0.868425 with an average error of 3.7 % (porosity unit).

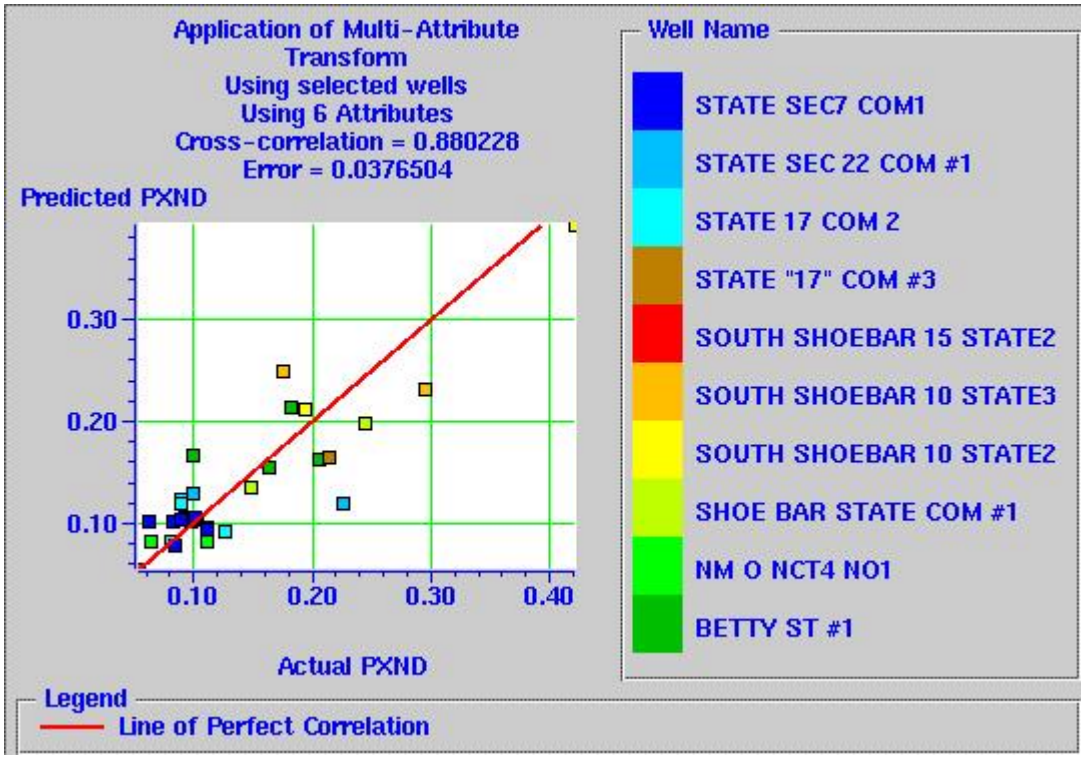

Figure A3-23: The result of the linear regression multi-attribute analysis by cross-plot of the data

Interpretation

Multi-attribute analysis approach improved the power of the porosity prediction as compared with single attribute analysis. It appears that 0.87 of correlation coefficient of the linear regression with an average error of 3.7% is enough power to predict porosity distribution in inter well areas. However, the porosity volume created as a result of multi attribute analysis demonstrates a geologically unreasonable result. This result could be due to the small data sample (small analysis window).